

# **Spatio-temporal dynamics of glycolysis in an open spatial reactor**

## **Dissertation**

zur Erlangung des akademischen Grades

**doctor rerum naturalium  
(Dr. rer. nat.)**

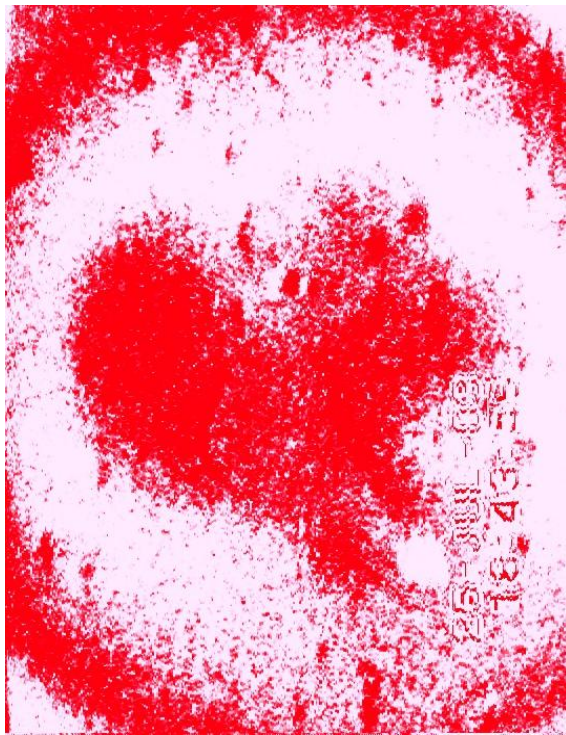
von: M.Sc. Satenik Vermeer (geb. Bagyan)  
geb. am: 26. Februar 1979  
in: Yerevan, Armenien

genehmigt durch die Fakultät für Verfahrens- und Systemtechnik  
der Otto-von-Guericke-Universität Magdeburg

Gutachter: Prof. Dr. rer. nat. habil. Helmut Weiß  
Jun.- Prof. Dr. rer. nat. habil. Marcus Hauser

eingereicht am: 27. Juni 2008

Promotionskolloquium am: 12. Dezember 2008



*In addition to all the glycolytic patterns investigated in this thesis more exotic structures may also be generated every now and then. For example, heart-shaped patterns.*

# Contents

<b>Contents</b> .....	<b>iii</b>
<b>Zusammenfassung</b> .....	<b>vi</b>
<b>Summary</b> .....	<b>viii</b>
<b>Abbreviations</b> .....	<b>x</b>
<b>1 Introduction and motivation</b> .....	<b>1</b>
1.1 Tasks of the study .....	4
<b>2 Fundamentals</b> .....	<b>5</b>
2.1 Basic concepts of spatio-temporal pattern formation .....	5
2.1.1 Spatially extended excitable media.....	7
2.1.1.1 Wave properties .....	7
2.1.2 Spatially extended oscillatory media .....	9
2.2 Glycolysis .....	12
2.3 Glycolytic oscillations .....	14
2.4 Non-linear reaction step in glycolysis .....	14
2.4.1 Allosteric regulation .....	15
2.5 Models of glycolysis .....	17
2.5.1 The Goldbeter model .....	18
2.5.2 The Selkov model .....	20
2.5.3 Glycolytic waves.....	21
<b>3 Materials and Methods</b> .....	<b>22</b>
3.1 Methods .....	22
3.1.1 Growth of yeast cells .....	22
3.1.1.1 Preparation of media for preculture and main culture .....	22
3.1.1.2 Preparation of the preculture.....	24
3.1.1.3 Preparation of the main culture.....	25
3.1.2 Preparation of yeast extract.....	25
3.1.3 Concentration and dilution of yeast extract .....	27
3.1.4 Methods for protein determination .....	27
3.1.4.1 The Warburg-Christian method .....	28
3.1.4.2 The Lowry method.....	29

---

3.1.5	Determination of metabolite concentration by the end-point method .....	30
3.1.6	Karhunen-Loève decomposition .....	35
3.2	Materials .....	38
3.3	Experimental set up .....	38
3.3.1	The open spatial reactor .....	38
3.3.2	Gel fixation of yeast extract .....	39
3.3.3	Experimental procedure .....	40
3.3.4	Optical set up .....	41
3.3.5	Tools for image analysis .....	42
3.4	Optimization of experimental conditions .....	43
3.4.1	Selection of the gel .....	44
3.4.2	Selection of the membrane .....	45
3.4.2.1	Test of membrane permeability .....	45
3.4.2.2	Calibration of NADH fluorescence in the open spatial reactor .....	47
<b>4</b>	<b>Results .....</b>	<b>51</b>
4.1	Temporal dynamics of glycolysis in an open spatial reactor .....	51
4.1.1	Glycolytic oscillations .....	51
4.1.2	Effect of adenine nucleotides on glycolytic oscillations .....	51
4.1.3	Effect of the protein concentration on the duration of oscillations .....	56
4.2	Formation of glycolytic patterns in an open spatial reactor .....	58
4.2.1	Temporal development of spatial patterns .....	58
4.2.2	Effect of the protein concentration on the spatio-temporal dynamics of glycolysis .....	60
4.2.3	Analysis of the wave dynamics .....	65
4.2.4	Phase waves and reaction diffusion waves .....	69
4.2.5	Dispersion relation at different protein concentrations .....	71
4.3	Analysis of spatio-temporal dynamics of glycolytic patterns .....	74
4.3.1	Analysis of spatio-temporal turbulence at high protein concentrations .....	74
4.3.2	Desynchronisation of spatial patterns at low protein concentrations .....	77
4.3.2.1	Transition from inwardly propagating patterns to outwardly propagating spirals .....	77

---

4.3.2.2	Analysis of the coherence of the patterns by the KL decomposition.....	80
4.3.2.3	Separation of spatial scales during interval 3 .....	83
<b>5</b>	<b>Discussion .....</b>	<b>88</b>
5.1	Impact of the feedback regulation of PFK.....	88
5.2	Effect of the protein concentration on the spatio-temporal patterns.....	92
5.2.1	Inwardly propagating target waves.....	94
5.2.1.1	Desynchronization of the inwardly propagation waves .....	95
5.2.2	Segmented waves and “bubbles” .....	100
5.2.3	Different types of waves: Phase waves or Reaction-Diffusion waves?.....	102
	<b>Outlook .....</b>	<b>104</b>
	<b>Appendix A.....</b>	<b>105</b>
A.1	IDL program for construction of time-space plots ( <i>timespaceplot_freedirection_v6</i> ) .....	105
A.2	IDL program for image enhancement ( <i>contrast_imgs</i> ) .....	110
	<b>References.....</b>	<b>121</b>
	<b>Acknowledgement.....</b>	<b>131</b>
	<b>Curriculum Vitae.....</b>	<b>133</b>

## Zusammenfassung

Die glykolytische Spaltung von Zucker ist der wichtigste Schritt zur Energieerzeugung in lebenden Zellen. Bei diesem Prozess können nichtlineare, oszillatorische Reaktionskinetiken entstehen, welche durch die autokatalytische Reaktion der Phosphofruktokinase (PFK) vermittelt werden. In der hier vorgestellten Arbeit wurde die Entstehung von raum-zeitlichen Mustern bei der Glykolyse des Hefeextrakts mit Hilfe eines offenen räumlichen Reaktors untersucht. Dabei wurde der Hefeextrakt in einem Agarose-Gel fixiert und der Reaktor kontinuierlich mit essentiellen Metaboliten und Salzen versorgt.

Zeitliche Oszillationen der Glykolyse wurden durch die Zugabe von Trehalose, einem Vorläufer des Substrats der Glykolyse, induziert. Durch die sorgfältige Auswahl der Bedingungen, konnten Oszillationen von mehr als 12 Stunden Dauer erreicht werden. Diese Dauer ließ sich durch Erhöhung der Proteinkonzentration auf 40 Stunden verlängern. Das richtige Verhältnis zwischen ATP-verbrauchenden und ATP-produzierenden Reaktionen ist eine notwendige Grundvoraussetzung für die Initiierung und das Aufrechterhalten von Oszillationen. Eine wichtige Funktion zur Erhaltung dieses Gleichgewichts übernimmt dabei die Adenylatkinase-Reaktion, welche die Umwandlung von zwei ADP-Molekülen in je ein ATP und ein AMP-Moleküle katalysiert. Diese Adeninenukleotide vermitteln eine positive und negative Rückkopplung der Phosphofruktokinase-Reaktion. Die unterschiedlichen Adenine-nukleotide bestimmen auch den energetischen Status von fast jeder Zelle. Die Ergebnisse dieser Arbeit zeigen, dass das Enzym Phosphofruktokinase in der Lage ist, verschiedene energetische Zustände in stationäre oder periodische Dynamiken des gesamten glykolytischen Pfads zu übersetzen. Somit kann die Phosphofruktokinase einen Beitrag zur biologischen Informationsverarbeitung liefern, zum Beispiel in Form der Frequenzkodierung.

Die Entstehung von glykolytischen Oszillationen steht im Zusammenhang mit der Erzeugung von NADH-Konzentrationswellen. Die Dynamiken dieser Wellen wurden in der vorliegenden Arbeit für verschiedene Proteinkonzentrationen des Hefeextrakts untersucht. Die Variation der Proteinkonzentration zwischen 23 mg/ml und 91 mg/ml hat einen starken Einfluss sowohl auf den Typ der Wellen als auch auf deren

Ausbreitungsdynamik. Unter diesen Wellenformen finden sich Muster, die bisher noch nicht in einem biologischen System gezeigt werden konnten. Es sind einwärts propagierende Wellen, segmentierende Wellen oder punktförmige Wellen, welche bei niedrigen, mittleren oder höheren Proteinkonzentrationen auftreten. Jeder Typ dieser Wellen ist durch eine bestimmte Ausbreitungsgeschwindigkeit und Wellendicke charakterisiert. Dabei ist die Periode der Wellen für alle Typen ähnlich. Bisher konnten die Entstehungen derartiger "exotischer" Mustern nur in der Belousov-Zhabotinsky Reaktion in Wasser-Öl Mikroemulsionen gezeigt werden. Die hier vorgestellten Ergebnisse zeigen, dass auch in biologischen Systemen eine Vielzahl von unterschiedlichen Mustern entstehen kann, wenn sich die Proteinkonzentration ändert. Diese Erkenntnis könnte eine wichtige Bedeutung für biologische Systeme mit räumlichen Gradienten von Proteinen haben.

Während der ersten zwei Stunden des Experiments, mit niedrigen Proteinkonzentrationen, bildet der Hefeextrakt im Gel mit der Nahrungslösung ein Gleichgewicht aus, wodurch ein stabiles Fließgleichgewicht entsteht. Während dieses Überganges entstehen drei verschiedene Muster: einwärts propagierende konzentrische Wellen in der ersten Phase, das heißt während der Equilibrierung des Geles; auswärts propagierende spiral- oder kreisförmige Wellen während der dritten Phase, das heißt, im Fließgleichgewichtszustand; und mehr komplexe Muster während des Übergangs zwischen den beiden Phasen. Um diesen Übergang zu analysieren und die dominanten räumlichen Strukturen zu identifizieren, wurde die Dynamik der raum-zeitlichen Muster mit Hilfe der Karhunen-Loève-Zerlegung untersucht. Die Analyse zeigt, dass der Übergang von den einwärts propagierenden konzentrischen Wellen zu den auswärts propagierenden Spiralwellen durch Desynchronisation ausgelöst wird. Während dieses Überganges tritt Desynchronisation allerdings nur bei räumlichen Skalen, die größer als 6 mm sind, auf. Darunter liegt immer noch Synchronisation vor. In der ersten Phase tritt hingegen keine Desynchronisation auf. Derartige raum-zeitliche Synchronisations- bzw. Desynchronisationsprozesse können eine wichtige funktionale Bedeutung für biologische Systeme haben.

## Summary

Glycolytic degradation of sugar is the primary pathway for the generation of energy in living cells and shows non-linear, oscillatory reaction kinetics, which is mediated by the autocatalytic reaction of the phosphofructokinase. In the present dissertation, the formation of spatio-temporal patterns during glycolysis in a yeast extract has been investigated in an open spatial reactor. The yeast extract was fixed in a gel and the reactor was continuously supplied with non-recycling metabolites and salts.

Temporal oscillations of glycolysis were induced by feeding the yeast extract with trehalose, a precursor of the substrate of glycolysis. Under appropriate conditions, sustained oscillations persist for more than 12 hours and can be further prolonged up to 40 hours at higher protein concentrations. The proper balance between ATP-consuming and ATP-producing reactions that allow for a negative feedback of the phosphofructokinase-catalysed reaction is a necessary prerequisite for the generation and maintenance of oscillations. An important function for maintaining this balance could be attributed to the adenylate kinase reaction, which catalyzes the conversion of two ADP molecules into one ATP molecule and one molecule of AMP. These different adenine nucleotides determine the energetic status of nearly every cell. The results of this work demonstrate that the enzyme phosphofructokinase can translate different energetic states into either stationary or oscillatory dynamics of the whole glycolytic pathway. Thus, the phosphofructokinase may contribute to biological information processing, e.g. via frequency encoding.

The emergence of glycolytic oscillations is associated with the generation of travelling NADH concentration waves. The dynamics of these waves were studied at different protein concentrations in the yeast extract. Variations in the protein concentration between 23 mg/ml and 91 mg/ml strongly affected the type waves as well as their propagation dynamics. Among these waves are patterns, which so far have not been reported in biological systems. These are inwardly propagating waves, segmented and dot-shaped waves, which occur at low, intermediate and high protein concentrations, respectively. Each of these waves is characterized by a distinct propagation velocity and wave thickness. However, the period of the waves is similar for all types.



So far, the formation of these novel patterns has only been reported for the Belousov-Zhabotinsky reaction in water-oil microemulsions. The present results demonstrate that also in biological systems a multitude of different patterns can arise when the protein concentration is changed. This may have important impacts for biological systems with spatial gradients of the protein.

During the first 2 hours of the experiment with low protein concentration, the yeast extract in the gel comes into equilibrium with the feeding solution. Thereafter a stable stationary state is maintained. This process is associated with the occurrence of 3 different types of patterns: inwardly propagating target waves in the first phase, i.e. during equilibration; outwardly propagating spiral or circular waves during the third phase, i.e. at stationary state conditions; and more complex patterns during the transition between these two phases. To elucidate the mechanisms leading to the transition from ordered to complex behaviour and to identify the dominant spatial structures, the dynamics of these spatio-temporal patterns were analysed by Karhunen-Loève decomposition. The analysis demonstrates that the transition from inwardly propagating target waves to outwardly moving spiral waves is accompanied by desynchronization and loss of spatial coherence. This desynchronization is space dependent. At spatial scales larger than 6 mm the local glycolytic oscillators become desynchronized, whereas at smaller scales they are still synchronized. In contrast, the patterns remain synchronized in the first phase independently of the spatial scales. Such spatio-temporal synchronization/desynchronization processes may have important functional meaning for biological systems.

## Abbreviations

ACA	Acetaldehyde
ADH	Alcohol dehydrogenase
ADP	Adenosine diphosphate
AK	Adenylate kinase
ALD	Aldolase
AMP	Adenosine monophosphate
AOT	Aerosol sodium bis (2-ethylhexyl) sulfosuccinate
ATP	Adenosine triphosphate
ATPase	Adenosine triphosphatase
BSA	Bovine serum albumin
BZ	Belousov-Zhabotinsky (reaction)
cAMP	Cyclic adenosine monophosphate
CGLE	Complex Ginzburg-Landau equation
CIMA	Chlorite-iodide-malonic acid (reaction)
CSTR	Continuous-flow stirred tank reactor
DAP	Dihydroxyacetone phosphate
DHAP	Dihydroxyacetone phosphate
DPG	1,3-Disphosphoglycerate
ENO	Enolase
Eq.	Equation
EtOH	Ethanol
FBP	Fructose-1,6-diphosphate
F-2,6-BP	Fructose-2,6-biposphate
FDP	Fructose-1,6-diphosphate
F-6-P	Fructose-6-phosphate
GAP	Glyceraldehyde-3-phosphate
GAPDH	Glyceraldehyde-3-phosphate dehydrogenase
GDH	Glycerol-3-phosphate dehydrogenase
Glc	Glucose
G-6-P	Glucose-6-phosphate

---

G6PDH	Glucose-6-phosphate dehydrogenase
HK	Hexokinase
KL	Karhunen-Loève
LDH	Lactate dehydrogenase
MK	Myokinase
MOPS	3-Morpholinopropanesulfonic acid
MW	Molecular weight
NAD <sup>+</sup>	Nicotinamide adenine dinucleotide (oxidized form)
NADH	Nicotinamide adenine dinucleotide (reduced form)
NADPH	Nicotinamide adenine dinucleotide phosphate
NAD(P)H	NADH+NADPH
OG	Optical glass
PDC	Pyruvate decarboxylase
PEP	Phosphoenolpyruvat
PFK	Phosphofructokinase
PGI	Phosphoglucose isomerase
2PG	2-phosphoglycerate
3PG	3-phosphoglycerate
6PG	6-Phosphogluconate
PGK	Phosphoglycerate kinase
PGM	Phosphoglycerate mutase
P <sub>i</sub>	Inorganic phosphate
PK	Pyruvate kinase
Pyr	Pyruvate
QG	Quartz glass
TIM	Triose-phosphate isomerase

# 1 Introduction and motivation

Pattern formation is a fascinating phenomenon widely observed in nature [1]. Many examples of pattern formation occur in physical, chemical, and biological systems far from thermodynamic equilibrium [2-8]. Since these patterns can be formed spontaneously due to the internal dynamics of the system, the process of pattern formation is also called self-organisation.

The necessary conditions for the generation of self-organisation are: the presence of non-linear dynamics, such as an autocatalytic step, coupled with transport, and far from equilibrium conditions [9;10]. Modern research on pattern formation is often associated with the paper by Turing [11]. He investigated the chemical basis of morphogenesis; with the help of a mathematical model, he showed that diffusion and interaction of two substances are sufficient to create spatio-temporal patterns under appropriate boundary conditions. Thus, the coupling of non-linear kinetics with diffusion may lead to spatial differentiation.

Substantial information about the dynamics and basic principles for the generation of spatio-temporal patterns has been obtained from investigations of chemical systems, mainly from the Belousov–Zhabotinsky (BZ) reaction [12-14].

However, travelling reaction-diffusion waves have also been reported from many different biological systems, e.g. calcium waves in frog oocytes [15], spreading depression waves in the cortex [16] and the retina [17], cAMP waves in cell layers of slime mould *Dictyostelium discoideum* [18;19], NAD(P)H waves in yeast extract [20;21] and in neutrophils [22]. Most of these waves exhibit the characteristic propagating dynamics of reaction-diffusion waves. In spite of the difference of specific mechanisms, which lead to the formation of the reaction-diffusion waves in biological, chemical, and physical systems, the basic principles of wave generation in all of these systems are very similar: namely, they are based on the interplay of non-linear reaction kinetics with transport processes.

In biological systems, reaction-diffusion waves may encode information, which can act at different hierarchical levels of cellular organization, e.g. cell migration, signal transduction between the cells, and coordination of the cellular processes. It is believed

that these waves may have an important impact in the biological information processing [23-25].

In order to unravel possible biological functions of reaction-diffusion waves, it is necessary to investigate the mechanisms of self-organisation. A well studied experimental example of biochemical self-organisation is the oscillatory glycolytic degradation of sugar in a yeast extract. Glycolysis plays a central role for the energy metabolism in nearly all living cells, and it is also involved in the regulation and coordination of cellular metabolism. Glycolytic oscillations are observed in many different cells and cell extracts. However, most of the knowledge about the temporal dynamics of glycolysis comes from experiments with yeast, both from cells [26-28] and organelle-free extracts [29;30]. Glycolytic waves have so far only been observed in yeast extracts [20;21].

The central role of glycolysis in cellular metabolism suggests various possible functions of glycolytic oscillations and waves. Indeed, experimental results indicate an interaction between glycolytic oscillations and the control of insulin secretion in pancreatic  $\beta$ -cells [31-34]. Also the immune response of neutrophil cells may involve the formation of travelling glycolytic NADPH waves [22;25]. It has been suggested that the propagation dynamics of these waves can translate the metabolic state of the cell into signals that co-ordinate the immune response of the cells [21;25].

The present thesis is focused on the study of spatio-temporal dynamics of glycolysis in yeast extracts. A necessary prerequisite for a precise investigation of such a system under nonequilibrium conditions is to have it operating in an open reactor. Several groups have studied the temporal dynamics of glycolysis in continuous-flow stirred tank reactors (CSTR) with yeast cells [35], yeast extract [36;37], or purified glycolytic enzymes [38;39]. However, these studies did not take the formation of spatial patterns into account, which have so far only been investigated under batch conditions [20;21].

The study of sustained spatio-temporal patterns is only possible in an open spatial reactor. Standard reactors of this type consist of a diffusive layer in contact with the contents of a CSTR. The former, often a disc of hydrogel, prevents any hydrodynamic flow but allows the coupling of reaction and diffusion within the gel. Permanent nonequilibrium conditions are ensured in the gel by diffusive exchange of matter

between the CSTR and the gel. Such open spatial reactors have been used to investigate travelling waves in the Belousov-Zhabotinsky (BZ) reaction [40;41] or stationary patterns in the Chlorite-iodide-malonic acid (CIMA) reaction [42-44]. In this thesis, such a reactor was used for the first time in the investigation of spatio-temporal dynamics of glycolytic waves.

This thesis is organized as follows. In section 2, the basic concepts of reaction-diffusion systems and non-linear dynamics in glycolysis are introduced. Two kinetic models describing temporal dynamics of glycolysis, namely, the Goldbeter and Selkov models, are presented. In section 3, the materials and methods as well as construction and optimization of an open spatial reactor for the investigation of glycolytic oscillations and waves are described. Section 4 includes the results of the temporal and spatial dynamics of yeast extract in the open spatial reactor, and it is divided into three parts. In the first part, the temporal dynamics of glycolysis is investigated. An effect of the adenine nucleotides on the glycolytic oscillations is shown, and the conditions are established to obtain sustained oscillations. The second part deals with the spatial dynamics of glycolysis at different protein concentrations in the yeast extract. The third part of the results is focused on the analysis of the spatial desynchronization of the wave dynamics by Karhunen-Loève decomposition. As example of spatial desynchronization, the transition from inwardly propagating target waves to outwardly propagating target waves and spirals is analyzed. The last two sections present the discussion of the key results of this thesis, as well as future perspectives.

## 1.1 Tasks of the study

Glycolytic degradation of sugar in a yeast extract was chosen as a model system for investigation of the spatio-temporal dynamics of glycolysis. The first task of this thesis was to optimize and establish conditions for the generation of glycolytic oscillations and waves in an open spatial reactor. With the help of such a reactor, it is possible to investigate spatio-temporal pattern formation in a yeast extract under far from equilibrium conditions.

This system has the advantage that the origin of spatio-temporal patterns can be investigated in detail and the complexity of the yeast extract can be changed. For example, different factors in the feeding solutions can be changed, leading to different metabolic states in the yeast extract. On the other hand, the dynamics of the yeast extract can also be changed by varying the protein concentration in the yeast extract.

One important aim of this work was to study the impact of feedback regulation of phosphofructokinase (PFK) on the dynamics of glycolysis by varying the adenine nucleotide composition in the feeding solution. Another task was to prove the effect of the protein concentration on the wave dynamics. These investigations should provide information about the local and global system properties of the yeast extract as a function of the metabolic components. For example, synchronization/desynchronization processes may occur at different metabolic states. Additionally, different types of wave patterns may form when the network complexity of the yeast extract is changed.

These results will provide new insights into the regulation of glycolytic oscillations and waves, thereby implying indications for their biological functions.

## 2 Fundamentals

### 2.1 Basic concepts of spatio-temporal pattern formation

For reaction-diffusion systems it is possible and convenient to establish the connection between the observed patterns and the temporal dynamics of the system without diffusion. Two main types of pattern-forming or so-called active media are described in this thesis: excitable and oscillatory. Many features of general pattern-forming active media could be discussed using a system of differential equations:

$$\begin{aligned}\frac{\partial u}{\partial t} &= \frac{1}{\epsilon} f(u, v) + D_u \nabla^2 u \\ \frac{\partial v}{\partial t} &= g(u, v) + D_v \nabla^2 v,\end{aligned}\tag{2.1}$$

where,  $u$  and  $v$  are two dynamic variables. In the dynamical systems theory the variable  $u$  is called the activator<sup>1</sup> and the variable  $v$  is called the inhibitor.  $D_u$  and  $D_v$  are the diffusion coefficients for  $u$  and  $v$ , respectively;  $\nabla^2$  is the Laplacian operator. The functions  $f(u, v)$  and  $g(u, v)$  account for the kinetics of the reaction system, and the parameter  $0 < \epsilon \ll 1$  accounts for the markedly different characteristic timescales of  $u$  and  $v$  variables, so that  $u$  changes much more rapidly than  $v$ .

The temporal dynamics of the two variables  $u$  and  $v$  without diffusion terms are best represented in the phase diagram. There are two special functions on the phase plane, so-called nullclines, on which the rate of change of each variable is zero. Figure 2.1a shows the nullclines of  $f(u, v) = 0$  ( $\dot{u}$ -nullcline) and the  $g(u, v) = 0$  ( $\dot{v}$ -nullcline), when the reaction terms  $f(u, v)$  and  $g(u, v)$  are cubic and linear functions, respectively. The  $\dot{u}$ -nullcline, ( $\partial u / \partial t = 0$ ) has a characteristic S-shape, while the  $\dot{v}$ -nullcline ( $\partial v / \partial t = 0$ ) is simply a straight line (Figure 2.1). The intersections of the two nullclines determine the stationary state of the system.

By means of the nullclines, active media can be classified as excitable (Figure 2.1a) and oscillatory (Figure 2.1c) (see e.g. [45]). In addition, stationary or multistable solutions can also be obtained (not show in Figure 2.1).

---

<sup>1</sup> Note that in this nomenclature the activator drives the system out of its present dynamic state, while the inhibitor tends to stabilize it. It is therefore evident that the terms “activator” and “inhibitor” as used in the dynamical system theory differ from the terms “activator” and “inhibitor” as known from enzyme kinetics.



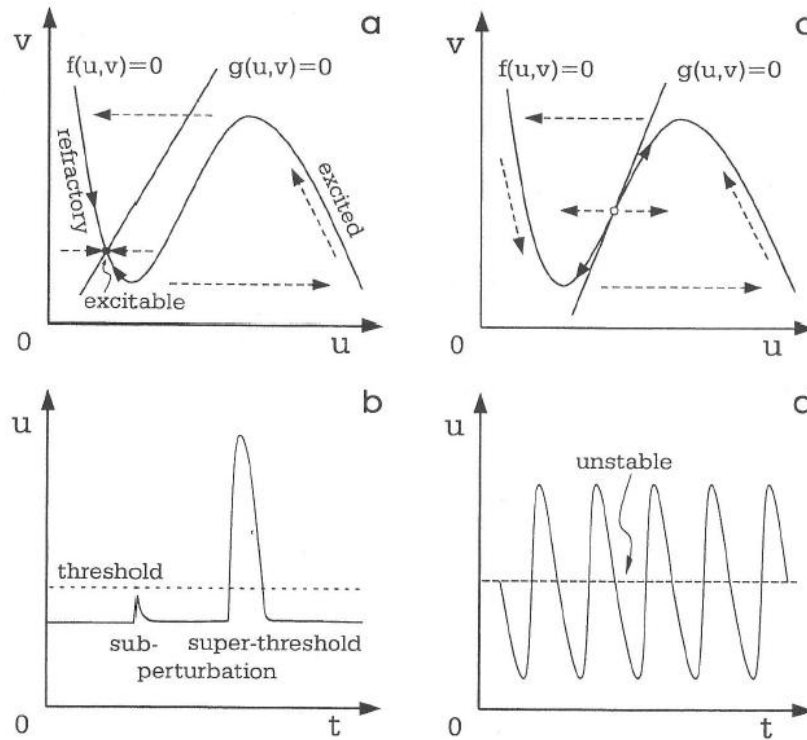


**Figure 2.1:** Phase diagram of the local dynamics of  $u$  and  $v$  variables in an excitable medium (a) and in an oscillatory medium (c). The temporal evolution of perturbations in the excitable and oscillatory medium is shown in (b) and (d), respectively. The solid lines in (a) and (b) denote the nullclines of  $f(u, v) = 0$  and  $g(u, v) = 0$  as indicated. The intersection point indicates the stationary state of the system, which is stable (filled circle) in the case of excitable media (a) and unstable (open circle) for the oscillatory media (c). The arrows indicate the trajectory of the system following a perturbation. From [46].

An excitable medium is characterized by having a stable stationary state. The stationary state intersection point lies slightly to the left of the minimum in the  $\dot{u}$ -nullcline as shown in Figure 2.1a. If  $u$  variable increases due to some perturbation to values that remain on the left of the middle branch of the  $\dot{u}$ -nullcline, the system returns quickly to the stationary state (Figure 2.1a). If the perturbation takes the system across the middle branch of the  $\dot{u}$ -nullcline, the system becomes stimulated and jumps to the right-hand branch of the  $\dot{u}$ -nullcline. This state of the system is called excited state. The system performs a large amplitude excursion into the phase space before returning to the original stationary state. The trajectory of the system following the perturbation is indicated by the dashed arrows in Figure 2.1a. The large excursion is a typical property

of excitability, where the stationary state is stable to small perturbations, but perturbations above a certain threshold will lead to large amplitude excitations before returning to the stationary state (see Figure 2.1b). Whilst the system is moving from the maximum of the right-hand branch to the left-hand branch of the  $\dot{u}$ -nullcline and down the left-hand branch, the system is insensitive to the further perturbations. This state is called refractory state, and is characterized by the high concentration of the inhibitor  $v$ . As the system approaches the stationary state it regains its excitability and becomes ready for the next excitation.

In the case of the oscillatory media, the intersection point of the nullclines lies in the middle branch of the  $\dot{u}$ -nullcline (Figure 2.1c). This fixed point is unstable and any perturbation of the system points away from the stationary state (Figure 2.1c). At no time the system can jump “back” to the middle branch, and so the stationary state is never approached. Instead there is continuous cycling in the phase space around the closed loop indicated with the dashed arrows in Figure 2.1c. This loop describes the trajectory of oscillations and is called limit cycle. In this case, both,  $u$  and  $v$  variables oscillate (Figure 2.1d).

### 2.1.1 Spatially extended excitable media

In spatially extended systems, the coupling of the local dynamics with diffusive transport leads to the formation of spatial patterns. In the case of excitable media, stationary patterns or travelling waves can be observed, depending on the magnitude of the diffusion coefficients of the activator ( $u$ ) and inhibitor ( $v$ ) (Eq. (2.1)). If the diffusion coefficients are roughly of the same order of magnitude, travelling concentration waves, such as concentric (also called target), spiral-shaped waves, or more complex patterns, like scroll waves in three dimensions, can be found [47]. If the diffusion coefficient of the inhibitor ( $v$ ) is sufficiently larger than that of the activator ( $u$ ), stationary patterns, as for example Turing structures, may be formed [4;42-44].

#### 2.1.1.1 Wave properties

In spatially extended excitable media, travelling reaction-diffusion waves often occur as circular-shaped waves. If circular-shaped waves are broken, their open ends curl up forming a pair of counter-rotating spirals. Travelling excitation waves show mutual annihilation upon collision, due to their excitable nature.

### Dispersion relation

A characteristic property of the travelling excitation waves, also called trigger waves, is their propagation velocity. The wave velocity is determined by kinetic and transport parameters of the system. However, in a strict sense, this is valid only for a solitary planar wave. A more common situation is the generation of target patterns, i.e. wave trains consisting of several concentric waves that originate from a common centre. The velocity of these waves is also influenced by the precursor waves, so that the decrease of the spatial distance from the precursor wave leads to the decrease of the wave velocity. The dependence of wave velocity on the source frequency, or equivalently, the period or wavelength of the target pattern is known as the dispersion relation.

The most common type of the dispersion relation is monotonic, where the wave velocity increases monotonously with increasing wavelength and approaches a constant value at high wavelengths (Figure 2.2a). This dispersion relation is characteristic for many excitable media [10;48-50] and is therefore referred to as normal dispersion.

If there are deviations from monotonic dispersion behaviour, the dispersion relation is called anomalous [51;52]. In this case the domains with negative slopes can be found. Examples of the anomalous dispersion relation are shown in Figure 2.2b and Figure 2.2c.

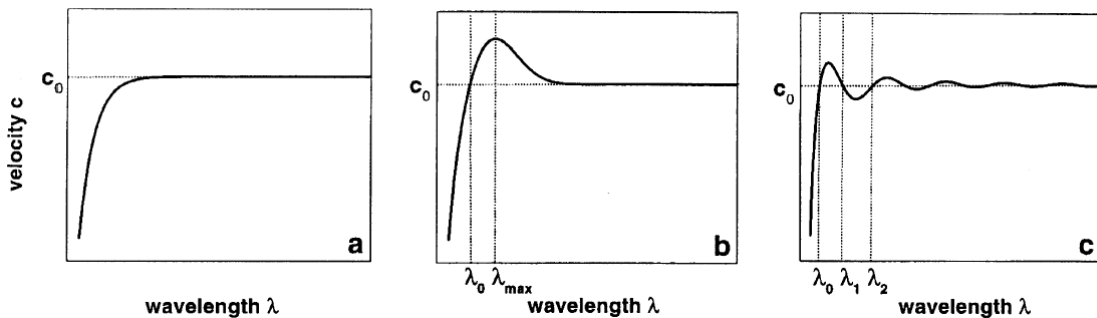


**Figure 2.2:** Schematic illustration of three qualitatively different types of dispersion curves for trigger waves: (a) normal, (b) non-monotonic non-oscillatory, and (c) oscillatory.  $c_0$  is the velocity of the single solitary wave. From [51].

At normal dispersion, the first wave propagates through the excitable medium with the maximum possible velocity ( $c_0$ ) (Figure 2.2a). The medium in the wake of the first wave is refractory (i.e. contains a high concentration of inhibitor), and it takes some time until the excitable state will be recovered. Therefore, the velocity of the subsequent wave depends on the spatial distance from the previous wave, e.g. wavelength of the waves. When the distance between two waves is small, the subsequent wave propagates into the refractory zone and consequently slows down. Only for sufficiently large spacing the velocity of consecutive wave front becomes independent from the previous wave. In general the shortest possible wavelength corresponds to the absolute refractory period, where the inhibitor concentration is too high for the generation of new waves.

### Curvature effect

Another important parameter which influences the propagation velocity of travelling excitation waves is the wave curvature. It has been shown theoretically [10;53] and experimentally [54] that the velocity of circular-shaped waves depends on the curvature of the wave front. An increase of the curvature leads to a decrease of the velocity. This relationship can be expressed by the eikonal equation:

$$N = c - \kappa D, \quad (2.2)$$

where,  $N$  is the normal velocity of the curved wave front,  $c$  is the velocity of a planar wave front,  $\kappa$  is the curvature,  $D$  is the diffusion coefficient of the activator species ( $u$ ). If the curvature  $\kappa = 1/R$  becomes too high, i.e., if radius  $R$  is too small, the velocity may become zero, that is, the wave does not propagate anymore. This critical radius  $R_{cr.}$  for initiation of waves can be determined by setting  $N = 0$  in Eq. (2.2):

$$R_{cr.} = \frac{D}{c}. \quad (2.3)$$

This means that propagation of waves cannot take place at and below the critical radius of waves.

### **2.1.2 Spatially extended oscillatory media**

An oscillatory medium consists of elements that perform stable limit-cycle oscillations, with weak interactions between the neighbours. If the oscillatory phase between any two subsequent elements is non-zero, and a constant phase shift in the initial phase of

oscillations is established, this results in a time-dependent activity pattern, which looks like propagating waves. These waves are known as phase waves [55], also called kinematic waves [56], or pseudowaves [57]. The velocity of these waves is inversely proportional to the steepness of the phase gradient and increases with the decrease of the concentration gradients. Such waves do not involve diffusion.

In a spatially extended oscillatory medium, both trigger and phase waves can be formed, depending on the system parameters [55;56]. In the experiments phase waves and trigger waves often look very similar and cannot be easily distinguished one from another. One possibility for distinguishing between these patterns is their dispersion relation [58]. Figure 2.3 illustrates the dispersion relation of phase waves (solid line) and trigger waves (dashed line). Up to a certain value of the wavelength ( $\lambda_i$ ), phase and trigger waves have roughly the same dispersion (Figure 2.3, inflection point I). When the wavelength increases further, the velocity of phase waves grows infinitely with increasing wavelength, whereas the velocity of trigger waves shows normal dispersion, approaching a constant value  $c_0$  [59].

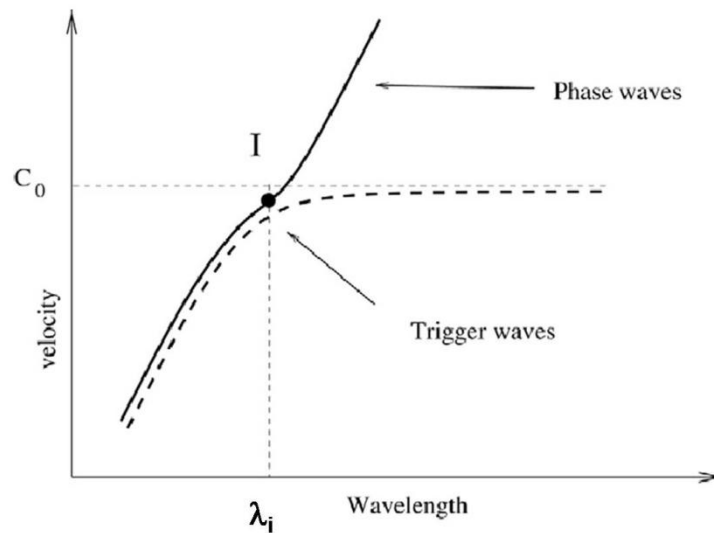


**Figure 2.3:** Dispersion relation of phase and trigger waves. The solid line represents the dispersion curve of phase waves and the dashed line represents the dispersion curve of trigger waves. The velocity of phase and trigger waves coincide up to a critical wavelength  $\lambda_i$ .  $I$  denotes the inflection point, which separates phase waves from trigger waves.  $c_0$  is the velocity of the single solitary excitation pulse. From [59].

Nonuniform phase distribution and phase waves can play significant roles in the formation of various wave patterns. Recently, the formation of a new type of target and spiral waves, which propagate inwardly (i.e. towards the source), have been observed in an oscillatory medium [60] (Figure 2.3c). The condition for the occurrence of these waves is that the frequency of the bulk oscillations is larger than the frequency of the inwardly propagating waves and spirals [60;61]. The essential difference between inwardly propagating spirals (Figure 2.3b) and outwardly propagating, so-called “normal” spirals (Figure 2.3a) is the sign of the selected group and phase velocity of the

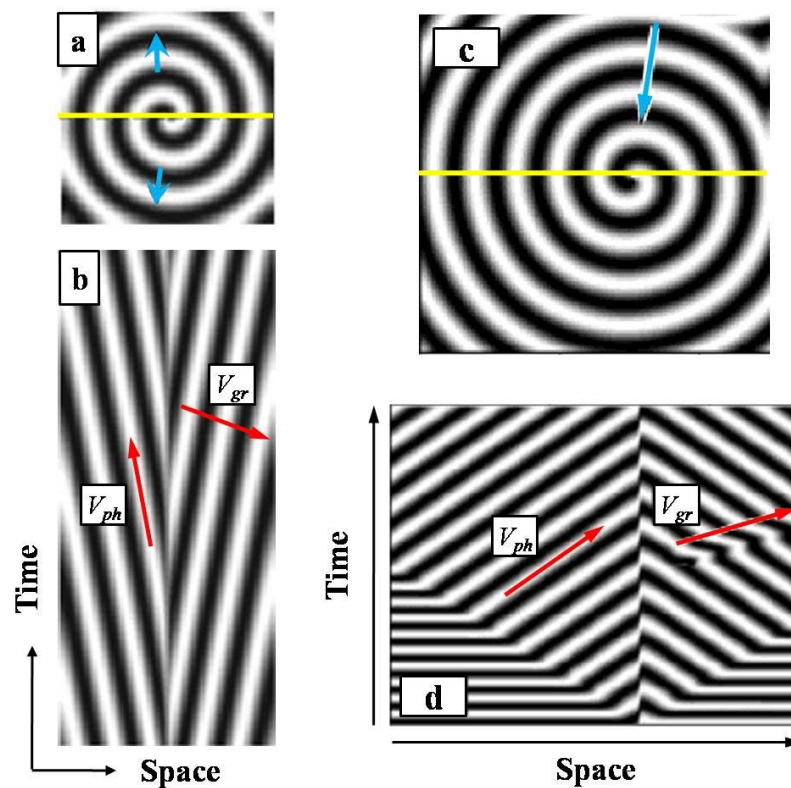
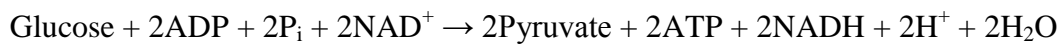


**Figure 2.4:** Schematic illustration of the phase and group velocities. (a) and (b) outwardly rotating so-called “normal” spiral and its evolution in time, respectively. (c) and (d) inwardly rotating spiral and its evolution in time, respectively. The yellow lines in (a) and (c) mark the image lines along which the time evolution in (b) and (d) is plotted. The red arrows in (b) and (d) indicate the directions of phase and group velocities. In both cases, “normal” spirals and inwardly propagating spirals, the group velocity ( $V_{gr.}$ ) points away from the spiral core. The distinction between “normal” spirals and inwardly propagating spirals comes only from the sign of the phase velocity ( $V_{ph.}$ ), which points toward the core for inwardly propagating spirals (d) and away from the core for “normal” spirals (b). Figures (a) and (b) are from [62], and (c) and (d) from [63].

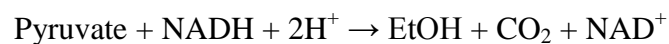
travelling waves emanating from the core region. The phase velocity is defined as  $V_{ph.} = \frac{\omega}{k}$  (where  $\omega$  and  $k$  are wave frequency and wave number, respectively), and characterizes the velocity at which the positions of waves maxima move. Typically, the wave velocity observed from the experiments corresponds to the phase velocity. The group velocity is defined as  $V_{gr.} = \frac{\Delta\omega}{\Delta k}$ , and determines the velocity at which small perturbations propagate through the medium (Figure 2.3d) [64;65]. For the inwardly propagating spirals, the phase velocity points towards and the group velocity away from the spiral core (Figure 2.3d), whereas for the “normal” spirals, phase and group velocities point in the same direction, i.e. away from the core (Figure 2.3b) [63].

## 2.2 Glycolysis

Glycolysis is the primary pathway for generation of energy in almost all living cells. It converts the chemical energy of sugars into biologically available energy in the form of adenosine triphosphate (ATP). Glycolysis is catalyzed by a series of enzymes, which transform a sugar into the key metabolite pyruvate, yielding two moles of ATP per mol of glucose:



Under anaerobic oxidation of glucose, the NADH is re-oxidized by fermentation of pyruvate in order to maintain the homeostasis of the cells. In yeast, this fermentation leads to the formation of ethanol and  $\text{CO}_2$ :



The overall reaction steps, i.e. the metabolic cascade of yeast glycolysis under anaerobic conditions, are presented in Figure 2.5.

Under aerobic conditions, pyruvate is degraded further in order to provide energy for the cells. This degradation takes place in the mitochondria, where pyruvate is oxidized primarily by  $\text{NAD}^+$  in the citric acid cycle. The NADH from this oxidation is oxidized by oxygen in the electron transport chain, finally producing ATP.

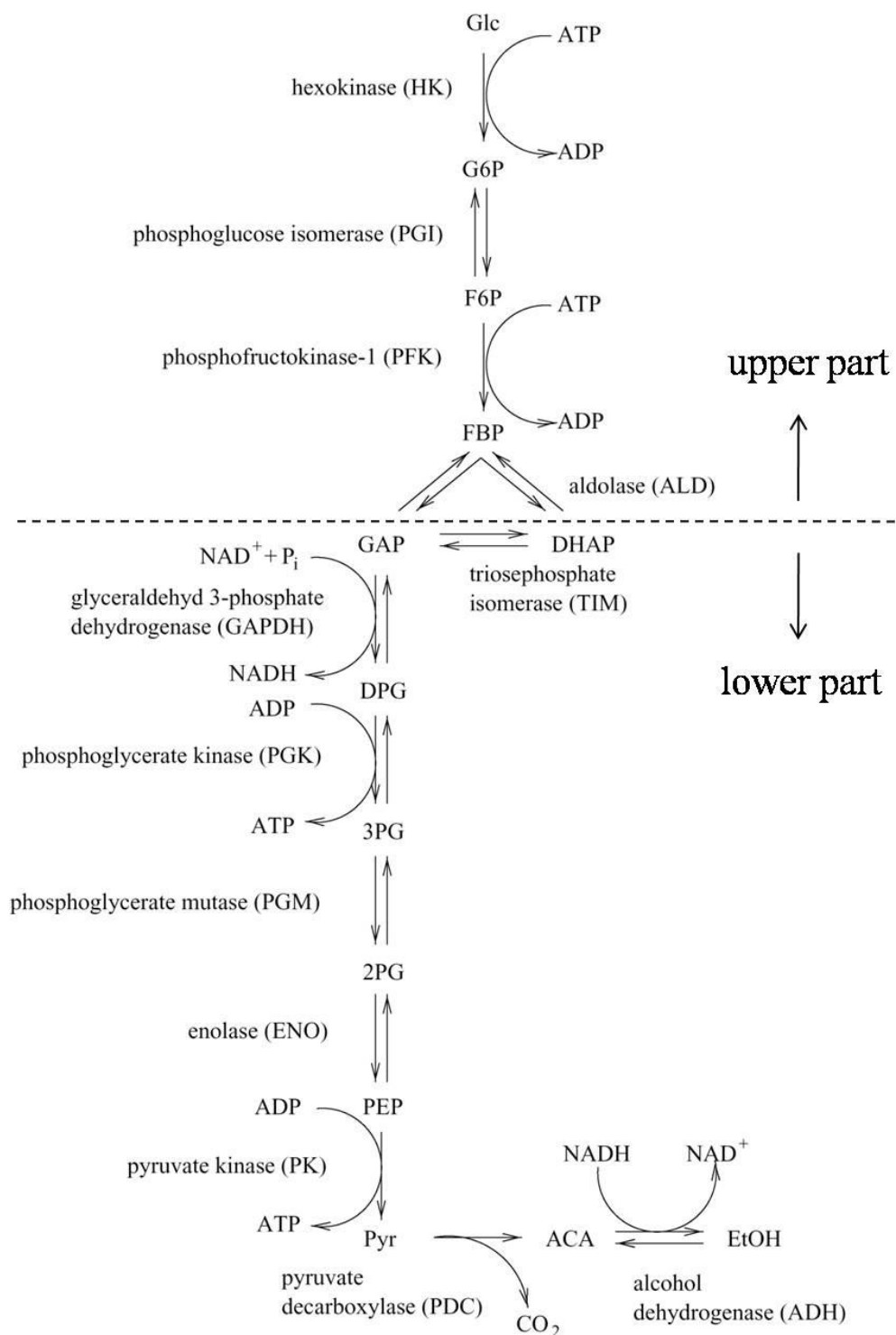


**Figure 2.5:** Overall enzymatic reactions of glycolysis in yeast under anaerobic conditions. For simplification glycolysis can be divided into two parts: the upper part, where the sugar is phosphorylated ( $C_6$ -carbohydrates) and the lower part, starting from glyceraldehyde-3-phosphate (GAP). In the upper part, two molecules of ATP are consumed, whereas in the lower part four molecules of ATP are produced. In total, two moles of ATP are formed from one mole of glucose. From [66].



### 2.3 Glycolytic oscillations

Glycolytic oscillations have been intensively studied since the early sixties of the last century. The first observation of oscillatory behaviour in glycolysis dates back to 1957, when Duysens and Ames<sup>z</sup> studied the fluorescence of some glycolytic intermediates in yeast, and reported that one of these intermediates underwent damped oscillations [67]. Oscillations of the NADH concentration in intact yeast cells were then described by Chance and co-workers in 1964 [27]. Shortly thereafter glycolytic oscillations were also demonstrated in cell-free yeast extract [29;30]. Recently, glycolytic oscillations have also been observed in the isolated single yeast cells [68]. Besides yeast, glycolytic oscillations have been observed in many other types of cells and cell extracts, e.g. in smooth muscle cell extract [69], skeletal muscle cell extract [70], heart cells [71], tumour cells [72], and pancreatic  $\beta$ -cells [32;33].

Experiments with yeast extract at constant glucose supply demonstrate that glycolytic oscillations can be observed only at certain supply rates of glucose into glycolysis. For yeast extract, this rate is in the range of 40 mM/h to 120 mM/h [73]. These conditions can be achieved by a permanent supply of glucose, or by using trehalose as a substrate for glycolysis [74]. Trehalose is transformed into two molecules of glucose by the enzyme trehalase at a low, constant rate, providing a constant input of glucose during glycolysis. It was shown that all glycolytic intermediates oscillate with the same frequency, but with different phases. This phenomenon was observed for yeast cells [26;28] as well as for yeast extract [75]. The frequency of oscillations depends on the rate of substrate supply, temperature, pH, and enzyme concentration. It was shown that an increase in the phosphate ( $P_i$ ) and decrease in the enzyme concentration [76], as well as a decrease of the temperature lengthened the period of the oscillations [77;78].

### 2.4 Non-linear reaction step in glycolysis

Glycolysis exhibits non-linear reaction kinetics by means of an autocatalytic reaction step. This autocatalytic step is catalyzed by the enzyme phosphofructokinase (PFK) via positive and negative feedback regulation. The adenine nucleotides serve as important effectors of PFK with adenosine triphosphate (ATP), which acts as inhibitor<sup>2</sup> (and substrate) of PFK, and adenosine mophosphate (AMP) and adenosine diphosphate

---

<sup>2</sup> Note that the terms activator and inhibitor are used in the sense of enzyme kinetics.

(ADP) both acting as activators of PFK [28]. The allosteric regulation and the cooperativity of the PFK are the kinetic bases that drive the system into the oscillatory state [79].

The oscillatory function of PFK has also been demonstrated by experiments, where the yeast extract was continuously supplied with a substrate of glycolysis [73]. It has been shown that the periodic behaviour in glycolysis can still be observed when glucose-6-phosphate (G-6-P) or fructose-6-phosphate (F-6-P) is used as a glycolytic substrate instead of glucose. However, when the PFK step is bypassed and the metabolites further down the glycolytic pathway (Figure 2.5) are used as glycolytic substrates, no oscillations could be observed.

The control of PFK by adenine nucleotides represents a way in which the energy metabolism responds to the adenylate energy charge [80]. The adenylate energy charge, which is defined as a ratio of concentrations ( $\frac{[ATP] + 0.5[ADP]}{[ATP] + [ADP] + [AMP]}$ ), provides a measure of the energetic resources of the cell. The energy charge increases from zero up to unity as adenylates transform from AMP into ADP, and finally into ATP. At high energy charge, the relative abundance of ATP causes the energy-yielding glycolytic pathway to become reduced in activity. As a consequence, PFK becomes inhibited. Conversely, high ADP or AMP levels signal that the energy charge is low and that flux through glycolysis should be increased. In this case, the signal results in activation of PFK.

#### 2.4.1 Allosteric regulation

The PFK belongs to the group of regulatory proteins that are known as allosteric enzymes. These enzymes possess multiple subunits that carry catalytic sites specific for the substrate and regulatory sites where an activator or inhibitor may bind. This allows for a modulation of the enzyme activity.

An essential property of allosteric enzymes is their cooperativity: the subunits forming the protein interact in such a manner that the binding of an effector or of the substrate to one of the sites facilitates (positive cooperativity) or impedes (negative cooperativity) the binding of the substrate to the remaining free sites. These properties are responsible for the sigmoidal kinetic curves obtained for the majority of allosteric enzymes in the most common case, namely positive cooperativity. In contrast to Michaelis-Menten enzymes, which have hyperbolic kinetic curves, allosteric enzymes,

due to their sigmoidal kinetics, possess an enhanced sensitivity towards variations in the concentration of an effector or of the substrate.

Several models have been developed to describe the mechanism of allosteric regulation of enzyme activity [81;82]. The simplest model for accounting the effect of allosteric activators and inhibitors is the concerted model of Monod-Wyman-Changeux [82]. According to this model, allosteric enzymes exist in two different forms, in the T (tense) form, which has a low affinity and in the R (relaxed) form, which has a high affinity for the substrate. The transition between these two conformational forms is concerted, i.e. binding of substrate leads to a simultaneous transition of all subunits of the enzyme from the T form into the R form. Hybrids such as TR are forbidden. This simultaneous conformational changes cause a drastic alteration in an enzyme activity.

The principle of allosteric regulation of the PFK can be explained based on the concerted model [82]. PFK is a tetrameric enzyme [83], which is allosterically activated by ADP, AMP, and its product FDP, and is allosterically inhibited by its substrate ATP (Figure 2.6).

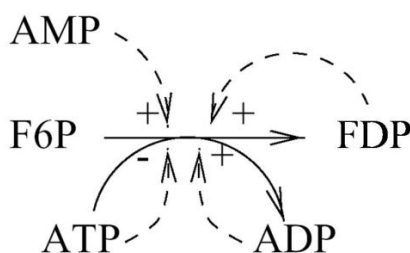


**Figure 2.6:** Reaction catalyzed by the enzyme PFK. The figure illustrates the allosteric regulation of PFK by positive and negative effectors. From [66].

ATP is both substrate and inhibitor of PFK (Figure 2.6). Each subunit of the PFK contains two binding sites for ATP, one for binding of ATP as a substrate, and the other for binding of ATP as an inhibitor. As a substrate, ATP binds to the catalytic site of PFK, independently of the conformation of the enzyme, whereas as an inhibitor, ATP binds to the regulatory site of PFK preferentially in the T form. Conversely, allosteric activators of PFK (AMP or ADP) bind to the regulatory site preferentially in the R form. Consequently, ATP shifts the R→T conformational equilibrium towards the T form, whereas AMP or ADP shifts it towards the R form. The second substrate, F-6-P,

binds to the PFK enzyme primarily in the R form. The result is that high concentrations of AMP or ADP favour the binding of F-6-P to the PFK, whereas high concentrations of ATP decrease the binding of F-6-P to the PFK.

Figure 2.7 illustrates the influence of an activator and an inhibitor on the PFK activity. An activator (ADP or AMP) shifts the substrate-concentration curve to lower substrate (F-6-P) concentrations and consequently increases the activity of the PFK. The inhibitor (ATP) shifts it towards higher substrate (F-6-P) concentrations, so that higher concentrations of substrate are required to activate the PFK (Figure 2.7).

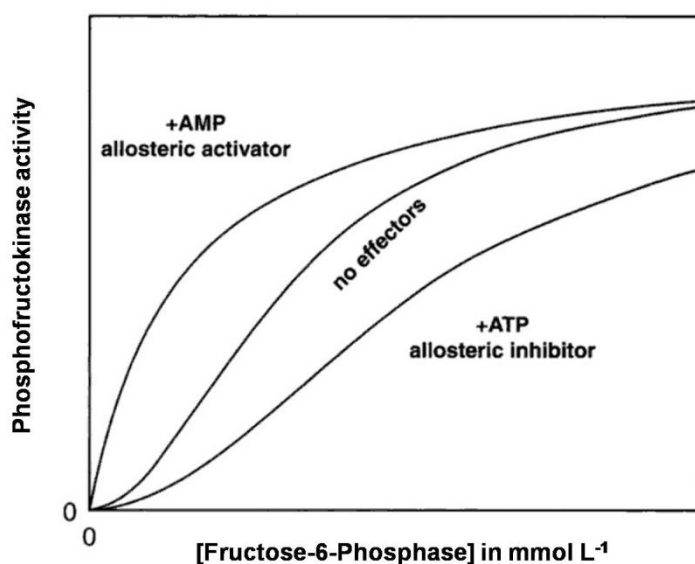


**Figure 2.7:** The influence of an activator and inhibitor on the PFK activity. The middle curve is observed in the absence of activator and inhibitor. In the presence of activator (AMP) this curve is shifted to low F-6-P concentrations, whereas in the presence of an inhibitor (ATP) it is shifted to higher F-6-P concentrations. From [84].

## 2.5 Models of glycolysis

The first model for glycolytic oscillations was proposed by Higgins in 1964 [85]. It is based on the activation of the enzyme PFK by its product fructose-1,6-diphosphate (FDP). This model, however, produced damped oscillations. A second model was suggested a few years later by Selkov [86]. In this model, a similar autocatalytic regulation of PFK was considered, which leads to sustained oscillations of the limit

cycle type. This model gives good qualitative description of the basic dynamic properties of the PFK reaction. However, due to its simplicity some of the important properties observed in the experiments, as for example, the existence of two critical values of the substrate supply rate, cannot be explained by means of this model.

An improved model for glycolytic oscillations was later proposed by Goldbeter [79], and it is focused on the cooperativity and allosteric regulation of PFK, where product activation occurs via ADP. This allosteric model yields better agreement with the experimental data both qualitatively and quantitatively.

Later, detailed models, including all relevant or possibly all glycolytic steps and intermediates, were proposed [36;37;87].

In the next two sections, two of the widely used models for describing the dynamics of glycolytic oscillations, namely the Goldbeter [79] and Selkov models [86], will be shortly reviewed.

### 2.5.1 The Goldbeter model

The Goldbeter model considers the PFK reaction and its regulation via the product ADP as the key step of oscillatory glycolysis [79;88]. According to this model, the enzyme PFK can exist in two different forms, either in the active R or in the inactive T form. These conformational forms differ in their affinity for the substrate and/or in their catalytic activity. Following the concept of Monod-Wyman-Changeux [82], the transition between the two conformational forms is taken as concerted. The reaction product ADP is the activator, as it binds exclusively to the most active, R form, of the enzyme. The conformational ratio of enzyme in the T and R forms in the absence of ligand is given by the allosteric constant  $L$  ( $L=[T]/[R]$ ) [82]. The openness of the system is assured by the supply of the substrate  $S$  at a constant influx rate, and the removal of the product  $P$  (ADP) at a rate proportional to its concentration.

Based on these assumptions, a two variable model of the substrate and the product was proposed, which is schematically shown in Figure 2.8.

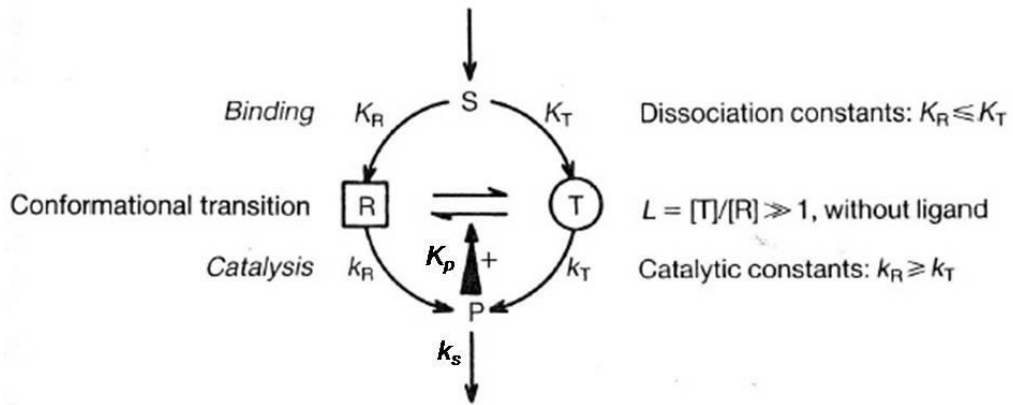


**Figure 2.8:** Schematic model of allosteric regulation of PFK enzyme. The PFK can exist in two different conformational forms, R and T, which differ in their affinity for the substrate and/or in their catalytic activity. The transition between the two forms is concerned. The product P is an activator of the PFK. It binds to the R form of the enzyme and thereby shifts the conformational equilibrium from the T to the R form. The system is open as the substrate S is continuously supplied at the constant rate and the product P is removed at the rate proportional to its concentration. From [2].

The Goldbeter model [79;88] can be expressed in the following dimensionless form:

$$\frac{d\alpha}{dt} = v - \sigma\phi = f(\alpha, \gamma) \quad (2.4)$$

$$\frac{d\gamma}{dt} = q\sigma\phi - k_s\gamma = g(\alpha, \gamma), \quad (2.5)$$

where,  $\alpha$  corresponds to the dimensionless substrate concentration ( $[S]/K_R$ ), and  $\gamma$  to the dimensionless product concentration ( $[P]/K_P$ ).  $K_R$  and  $K_P$  denote the dissociation constants for binding of the substrate and the product to the R form;  $v$  and  $\sigma$  are the substrate input rate and the maximal enzyme reaction rate, divided by  $K_R$ ;  $q = K_R/K_P$ ;  $\phi$  is the rate function, which describes the allosteric regulation of the enzyme. In the case when the enzyme is a  $n$ -mer the rate function  $\phi$  can be expressed in the general form [88]:

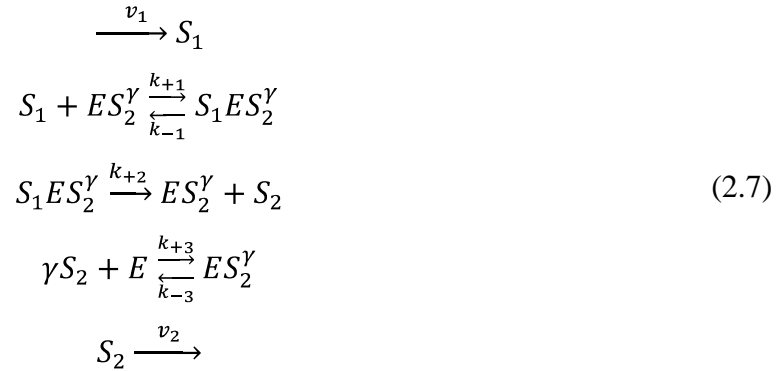
$$\phi = \frac{\alpha(1 + \alpha)^{n-1}(1 + \gamma)^n}{L + (1 + \alpha)^n(1 + \gamma)^n}, \quad (2.6)$$

where  $n = 4$ , since the PFK is a tetrameric enzyme [83], i.e. contains four subunits.

Extension of this model to two-dimensional reaction-diffusion processes predicts the appearance of travelling waves in the yeast extract [89].

### 2.5.2 The Selkov model

The Selkov model is a simple kinetic model which also describes the PFK reaction. However, in contrast to the Goldbeter model it does not account for the allosteric nature of the PFK explicitly. This model is based on the regulation of the PFK reaction, where the enzyme is inhibited by the substrate (ATP) and activated by the product (ADP) [86], according to the following scheme:



Here, the substrate  $S_1$  (ATP), that is supplied at a constant rate  $v_1$ , is irreversibly converted to the product  $S_2$  (ADP), which is irreversibly removed at the rate  $v_2$ . The free enzyme (PFK)  $E$  becomes activated by forming the  $\gamma S_2$  complex ( $\gamma$  is the number of  $S_2$  molecules required for the regulation of the enzyme).

The following three conditions should be satisfied [86]:  $\gamma > 1$ ;  $\frac{k_{+1}}{s_1}$ ,  $k_{-1}$ ,  $k_{+2}$ ,  $\frac{k_{+3}}{s_2^\gamma}$ ,  $k_{-3} \gg 1$ ,  $\frac{s_1}{e_o}$ ,  $\frac{s_2}{e_o} \gg 1$ , where  $e_o \equiv E + ES_2^\gamma + S_1ES_2^\gamma$ . Additionally, since glycolytic oscillations occur at very low glycolytic flux, it can be assumed that the substrate supply rate  $v_1$  is  $\ll 1$ . Under these conditions and taking into account the kinetic scheme (2.7), the Selkov model can be expressed in the following dimensionless form:

$$\frac{dx}{d\tau} = 1 - xy^\gamma \tag{2.8}$$

$$\frac{dy}{d\tau} = \alpha y(xy^{\gamma-1} - 1), \tag{2.9}$$

where,  $x$  and  $y$  correspond to the substrate and product, respectively, and are defined as:  $x = v_1^{\gamma-1} \chi_2^{-\gamma} \sigma_1$  and  $y = v_1^{\gamma-1} \chi_2 \sigma_2$ . The variables  $\alpha$  and  $\tau$  are given as  $\alpha = \alpha_2 v_1^{-\gamma} \chi_2^{\gamma+1}$  and  $\tau = v_1^{\gamma} \chi_2^{-\gamma} \theta$ . Here,  $\sigma_1$  and  $\sigma_2$  are the relative concentrations of the substrate and product, respectively;  $v_1$  is the relative supply rate;  $\alpha_2$  is the relative enzyme-product affinity;  $\theta$  is the dimensionless time;  $\chi_2$  is a product of rate constants and the total enzyme concentration  $e_0$ .

### 2.5.3 Glycolytic waves

When the excitable reaction system is coupled to diffusion, oscillatory glycolysis is associated with the formation of travelling reaction-diffusion waves. Using an extended version of the Goldbeter model, the occurrence of spatial patterns in glycolysis was predicted before experimental data were available [89]. Travelling NADH and proton concentration waves in a yeast extract have been observed experimentally by Mair and Müller [20]. They showed that these waves exhibit all properties of chemical reaction-diffusion systems, e.g. mutual annihilation and formation of spiral-shaped waves. The propagation velocity and front width of NADH waves were determined as 5  $\mu\text{m/s}$  and 0.7 mm, respectively, which is in a good agreement with the predicted wave velocity from the model simulations [89].

Controlled initiation of NADH concentration waves by local injection of fructose-2,6-biphosphate (F-2,6-BP), the strong activator of PFK, indicated the crucial role of the PFK enzyme in the control of the dynamics of these patterns. This result confirmed the validity of the theoretical assumption, underlying the Goldbeter model, namely the important impact of PFK enzyme for glycolysis, and hence also for wave generation [89]. Further investigations of NADH waves provided a first study on the dispersion of these waves [21]. Recently, the dynamics of NADH waves were studied by applying spatial temperature gradients to the yeast extract by means of a Peltier element [77]. So far, all studies on wave propagation in a yeast extract were performed under batch conditions.



## 3 Materials and Methods

### 3.1 Methods

#### 3.1.1 Growth of yeast cells

All experiments were performed with a cell-free yeast extract. The yeast extract was prepared from yeast cells, which were grown under aerobic conditions from agar slants of the yeast *Saccharomyces carlsbergensis* (ATCC 9080).

Since the yeast cells on the agar slants are stored at 4 °C and thus located in the passive state, it is necessary to first adapt these cells to the growth conditions in order to obtain more controlled and reproducible fermentation. To this purpose, the yeast cells were grown in two-step cultures [90]. At first, the yeast from the agar slant was grown in a small-volume preculture, in order to increase the growth rate of cells. Subsequently, for conduction of the final growth of yeast cells, a large-volume main culture was inoculated with a defined amount of yeast cells from the preculture.

##### 3.1.1.1 Preparation of media for preculture and main culture

The media for preculture and main culture were prepared together from stock solutions (Table 3.1) as described in Table 3.2. After the consecutive addition of the substances of Table 3.2 (except for glucose and vitamins), the medium was filled up with distilled water to 4500 ml, and the pH of the medium was adjusted to 5.5 with KOH pellets. Then the medium was filled with distilled water to a total volume of 8871 ml and well mixed. Finally, the medium was split into the 240 ml preculture medium and 8630 ml main culture medium. The medium for the preculture was transferred into a 1000 ml shaking flask and the medium for the main culture was poured into a fermenter. In order to prevent foam formation during growth of the yeast cells in the fermenter, 1 ml of Antifoam 289 (Sigma) was added to the main culture.

The medium for the main culture was sterilized for 1h and the medium for the preculture and glucose solution for 20 min in an autoclave at 120 °C (Table 3.3). The solution of vitamins was sterilized at room temperature by mechanical filtration through a sterile filter (Sartorius, pore size: 0.2 µm) under a clean bench.

**Table 3.1:** Stock solutions for yeast culture medium

<b>Salt A</b>	(NH <sub>4</sub> ) <sub>2</sub> SO <sub>4</sub>	<u>Mass/200 ml</u> 18.75 g
	KH <sub>2</sub> PO <sub>4</sub>	5.5 g
	KCl	4.25 g
	MgSO <sub>4</sub> x 7H <sub>2</sub> O	1.25 g
<b>Salt B</b>	CaCl <sub>2</sub> x 2H <sub>2</sub> O	<u>Mass/50 ml</u> 0.85 g
<b>Trace elements</b>	FeCl <sub>3</sub> x 6H <sub>2</sub> O	<u>Mass/50 ml</u> 125 mg
	MnSO <sub>4</sub> x 7H <sub>2</sub> O	125 mg
	(1 drop of 2N HCl)	
<b>Vitamins</b>	Pyridoxine /HCl	<u>Mass/50 ml</u> 12.5 mg
	Thiamine	12.5 mg
	Biotin (12.5 mg in 0.07 ml 1mM KOH + 0.93 ml absolute ethanol)	0.1 ml
	Ca-Pantothenate	175 mg
	Myo-Inositol	500 mg
<b>Citric acid</b>	Citric acid (pH 5, with KOH pellets)	<u>Mass/500 ml</u> 31.52 g
<b>Casein Hydrolysate</b>	Casein Hydrolysate (acid)	<u>Mass/375 ml</u> 37.5 g
<b>Glucose</b>	Glucose (heat up to ~ 40 °C for dissolution)	<u>Mass/400 ml</u> 200 g
<b>Tryptophan</b>	L-Tryptophan in 2N KOH	1.638 g in 1 ml 2N KOH

**Table 3.2:** Preculture and main culture media for growth of yeast cells

Substances	Main culture (9000 ml)	Preculture (250 ml)
Yeast extract	9 g	0.25 g
Salt A	180 ml	5 ml
Trace elements	9 ml	0.25 ml
Citric acid	450 ml	12.5 ml
Casein Hydrolysate	360 ml	10 ml
Salt B	45 ml	1.25
Tryptophan in KOH	1.62 g	0.045
pH 5.5 with KOH pellets		
Glucose	360 ml	10 ml
Vitamins	9 ml	0.25 ml

**Table 3.3:** Specification of the sterilization parameters

	Duration	Temperature
Preculture medium	20 min	120 °C
Main culture medium	60 min	120 °C
Glucose solution	20 min	120 °C
Vitamins		Sterile filtration (0.2 µm pore size) at room temperature

### 3.1.1.2 Preparation of the preculture

10 ml of sterile glucose solution and 0.25 ml of sterile vitamin solution (Table 3.2) were added to the preculture medium under the clean bench. Afterwards, the preculture was inoculated (approximately one inoculation loop) with the yeast *Saccharomyces carlsbergensis* from agar slants under the clean bench. The preculture was incubated in a rotary shaker at 28 °C for 18 h under constant shaking (170 rpm). This culture serves as the inoculum for the main culture.

### 3.1.1.3 Preparation of the main culture

360 ml of sterile glucose solution and 9 ml of sterile vitamin solution (Table 3.2) were added to the main culture medium. Finally, the main culture of 9000 ml volume in the fermenter was inoculated with 0.25 million precultured cells per ml. In order to determine the amount of preculture containing 0.25 million cells, the number of cells in the preculture was counted after 17.5 h of growth by using a Thoma chamber. When the number of cells in 1 ml of the preculture is determined, the required amount of the preculture for inoculation of the main culture can be calculated as follows,

$$V_{\text{prec.}} = \frac{0.25 \left[ \frac{\text{million}}{\text{ml}} \right] \times V_{\text{main culture}} [\text{ml}]}{Q [\text{million/ml}]} ; \quad (3.1)$$

where,  $V_{\text{prec.}}$  is the volume of preculture required for inoculation of the main culture, 0.25 million cells/ml is the quantity of cells used for the inoculation of the main culture,  $V_{\text{main culture}}$  is the total volume of the main culture, which is 9000 ml, and  $Q$  is the number of cells in 1 ml of preculture.

The main culture was grown for 16 h at 28 °C under constant mixing at 550 rpm/min and continuous air supply at 700 l/h.

### 3.1.2 Preparation of yeast extract

The cells were harvested at the beginning of the stationary phase (see Figure 3.1), when the glucose concentration in the medium was approaching zero. In order to determine this time point, after 16 h of growth, 20 ml of the main culture were taken out from the fermenter and centrifuged at  $10000 \times g$  for 5 min at 21 °C in a Avanti J-20 centrifuge (Beckmann, JA 20 rotor). The concentration of glucose was measured in the supernatant by using a coupled enzymatic determination method (for recipe see section 3.1.5). When the glucose concentration in the fermenter was below 0.1 mM, the fermentation was stopped and the cells were harvested by centrifugation at  $5000 \times g$  for 6 min at 4 °C in the Avanti J-20 centrifuge (Beckmann, JLA 8100 rotor). After centrifugation, the pellet was resedimented, washed, and centrifuged twice at  $5000 \times g$  for 6 min at 4 °C with cooled distilled water in the Avanti J-20 centrifuge (Beckmann, JLA 8100 rotor). After removal of the supernatant, the cell pellet was resuspended in 25 mM MOPS, 50 mM KCl, pH 6.5 buffer and kept on ice. The millilitre volume of the buffer added for

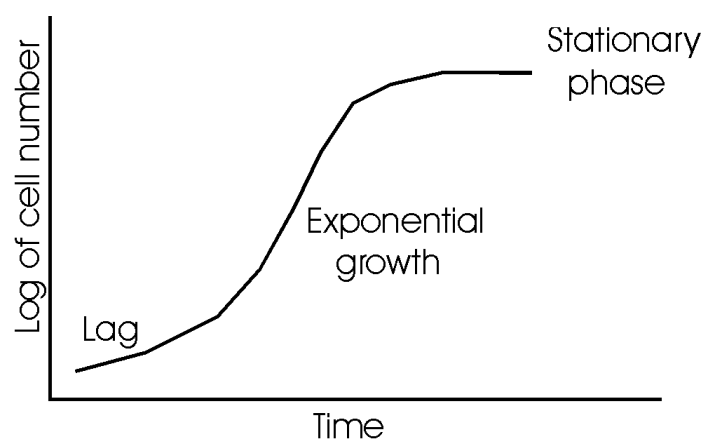


**Figure 3.1:** Growth curve of yeast. It shows different phases of yeast growth in a batch culture. The yeast cells were harvested at the beginning of the stationary phase. From [91].

resuspension of the cells corresponds to 1/10 of the cell weight in gram (e.g. for resuspension of 200 g of yeast cells 20 ml of the buffer is used). The cells were then ruptured by use of glass beads in a Braun – Melsungen cell homogenizer. For this, 10 ml of the cell suspension and 25 g of glass beads (diameter 0.45-0.5 mm, B. Braun Biothech International) were placed into a 50 ml Duran glass flask (precooled at 4 °C). The cell suspension in the Duran flask was then shaken 6 × 30 s at 4000 rpm. Throughout the homogenization process the cells were cooled to about 0 – 10 °C with liquid CO<sub>2</sub> using 10 s on/off cycles. All further steps were carried out at 4 °C. The broken cells were transferred into the centrifuge tubes and 1 ml of buffer (25 mM MOPS, 50 mM KCl pH 6.5) was used to wash the rest of the cells from the Duran flasks. The cell homogenate was immediately centrifuged twice (6000 × g and 10000 × g, respectively for 5 min at 4 °C) using the Avanti J-20 centrifuge (Beckmann, JLA 16250 rotor) to remove the glass beads before further differential centrifugation. The sediment with glass beads was removed and the resulting supernatant was then further centrifuged at 20000 × g for 30 min at 4 °C in the Avanti J-20 centrifuge (Beckmann, JA 20 rotor). Finally, to separate proteins and enzymes from mitochondria and organelles, the supernatant was centrifuged in a Beckmann Optima Le-80K ultracentrifuge (Ti 70 rotor) at 130000 × g for 1 h at 4 °C. After ultracentrifugation, the solution was separated in four differently coloured layers. A white layer on top of solution, containing mainly lipids, a transparent yellow layer, containing all proteins

and enzymes of the cytoplasm, a brown layer, containing organelles and a dark brown layer, containing mainly mitochondrial proteins. The yellow layer (second layer from top) was carefully removed with a Pasteur pipet and centrifuged a second time at  $130000 \times g$  for 1 h at 4 °C in the a Beckmann Optima Le-80K ultracentrifuge (Ti 70 rotor). The remaining yellow layer, which represents a yeast extract, was divided in aliquots of 1 ml and stored at -75 °C until later use. Under these conditions the extract maintained its activity for about one year.

### **3.1.3 Concentration and dilution of yeast extract**

The concentration of proteins in a yeast extract obtained from different preparations varied between 32 and 81 mg/ml, depending on the dilution of yeast extract during the preparation.

In order to obtain low protein concentrations, the yeast extract was diluted with buffer (25 mM MOPS, 50 mM KCl, pH 6.5) before use. For obtaining higher protein concentrations (higher as 81 mg/ml), the yeast extract was concentrated in a dialysis bag (Sartorius, Viva Spin 2, cellulose triacetate with molecular weight (MW) cut off 10 kD). For this purpose, the dialysis bag was first washed with distilled water twice for 5 min, at  $6000 \times g$  at 4 °C using the Avanti J-20 centrifuge (Beckmann, JA 20 rotor). Then, 1.5 - 1.8 ml of yeast extract were filled into the dialysis bag and centrifuged at  $6000 \times g$  for 40 min at 4 °C in the Avanti J-20 centrifuge (Beckmann, JA 20 rotor) to a final volume of 1.0 - 1.15 ml. After centrifugation, the concentrate was carefully mixed with a pipet and removed from the dialysis bag. The maximal concentration of yeast extract obtained by this procedure was 125 mg/ml.

### **3.1.4 Methods for protein determination**

In this thesis the protein content of yeast extract was measured; however, according to biochemical conventions, this is generally called protein concentration. Therefore, for the rest of the thesis the terminology protein concentration will be used.

Two different methods were used for determination of the protein concentration in the yeast extract. For a rough estimation of the protein concentration and of the quality of preparation, the Warburg-Christian method [92] was used.

In some experiments in an open spatial reactor, the protein concentration of yeast extract was varied. Hence, the determination of the protein concentration in these experiments requires a more accurate method. Therefore, the protein concentration was additionally determined by the Lowry procedure [93].

#### 3.1.4.1 The Warburg-Christian method

Most proteins exhibit an ultraviolet-light absorption maximum at 280 nm wavelength, due to the absorption of the tyrosine and tryptophan amino acids. Since the tyrosine and tryptophan content of various enzymes varies within narrow limits, the absorption peak at 280 nm is used as a rapid and fairly sensitive measure of protein concentration [94]. However, not only does protein absorb at 280 nm, but many other compounds also absorb in this wavelength. This includes nucleic acids that are one of the most common contaminants of protein preparations. The Warburg-Christian method [92] was developed to correct for nucleic acids contamination, leaving only the absorbance due to protein. Since nucleic acids absorb strongly at 260 nm while proteins do not, the method uses a correction factor calculated from the ratio of the absorbance at 280 nm to that at 260 nm. The Warburg-Christian method uses the  $A_{280}$  and  $A_{260}$  values to calculate protein concentrations.

At first, 2.8 ml of distilled water were filled into a quartz cuvette (optical length  $d=1$  cm) and the absorption was measured at 260 nm and 280 nm ( $A_1$ ). The protein concentration of yeast extract was diluted with distilled water to obtain the protein concentration in the range of the calibration curve. Then 0.2 ml of the diluted sample were added to the quartz cuvette and well mixed. The absorption of the sample was measured at 260 nm and 280 nm ( $A_2$ ). The measurement was conducted at room temperature. The protein concentration was calculated from

$$c = \frac{\Delta A \times V_{\text{total}} \times d}{V_{\text{sample}}} \times f_D \quad (3.2)$$

while  $\Delta A$  was determined according to the formula given by Warburg-Christian [92]:

$$\Delta A = 1.55 (A_2 - A_1)_{280\text{nm}} - 0.76 (A_2 - A_1)_{260\text{nm}}, \quad (3.3)$$

where,  $c$  is the protein concentration in mg/ml,  $A_1$  is the absorption of water and  $A_2$  is the absorption of sample,  $V_{\text{total}}$  is the total volume of the test solution (3 ml),  $V_{\text{sample}}$  is

the volume of the sample (0.2 ml),  $d$  is the length of the cuvette (1 cm), and  $f_D$  is the dilution factor. The coefficients 1.55 and 0.76 of Eq. (3.3) are based on the extinction coefficients of the crystalline yeast enolase and yeast nucleic acids [92].

#### 3.1.4.2 The Lowry method

The Lowry procedure is one of the widely used protein assays, which is sensitive down to about 0.01 mg of protein/ml [93]. The method is based on two colour forming reactions. Under alkaline conditions, the divalent copper ion forms a complex with peptide bonds in which it is reduced to a monovalent ion (Biuret reaction). Monovalent copper ion and the radical groups of tyrosine, tryptophan, and cysteine react with the Folin-Ciocalteu reagent to produce an unstable product that becomes reduced to molybdenum/tungsten blue (Folin-Ciocalteu reaction). The reactions result in an intensive blue color, which depends on the tyrosine and tryptophan content.

##### Reagent A:

1 ml water

0.5 ml of 0.08 M  $\text{CuSO}_4 \times 5\text{H}_2\text{O}$

0.5 ml of 0.174 M sodium potassium tartrate ( $\text{NaKC}_4\text{H}_4\text{O}_6 \times 4\text{H}_2\text{O}$ )

20 ml of 0.944 M  $\text{Na}_2\text{CO}_3$  in 0.5 N NaOH

Reagent A was prepared freshly before use.

##### Reagent B:

Folin-Ciocalteu phenol reagent (phosphomolybdic-phosphotungstic acid) from Sigma.

The Folin-Ciocalteu phenol reagent was diluted in distilled water to 1:14 before use.

##### Standards:

Each time the assay is performed, a calibration curve from a set of standards of known protein concentrations should be prepared. A stock solution of bovine serum albumin (BSA) containing 5 mg/ml protein in distilled water was used for preparation of the standards. The standards were prepared by diluting the stock solution of BSA with distilled water as described in Table 3.4. Each standard was prepared in triplicate.



Samples:

The samples with unknown protein concentration were diluted with two different dilution factors, to obtain the protein concentration in the range of the calibration curve. Each sample was prepared in triplicate.

**Table 3.4:** Preparation of the standards from 5 mg/ml BSA stock solution

Final concentration of proteins, $\mu\text{g/ml}$	0	25	50	100	150	200	250	300	350
BSA (5 mg/ml), $\mu\text{l}$	0	5	10	20	30	40	50	60	70
Water, $\mu\text{l}$	1000	995	990	980	970	960	950	940	930

Assay:

250  $\mu\text{l}$  of each standard and sample solution were pipeted into a clean, dry test tube. 250  $\mu\text{l}$  of Reagent A were added to each tube and immediately mixed using a vortex mixer. The solutions were incubated at room temperature for 10 min. Subsequently, 750  $\mu\text{l}$  of Reagent B were added to each solution tube and thoroughly mixed using a vortex mixer. This mixing step is critical for obtaining reproducible results. The samples were incubated at room temperature for 30 min. The content of each tube was transferred into the half-micro cuvettes (Brand, optical length  $d=1$  cm). The absorption of the standards was measured at 550 nm, starting from the lowest to the highest protein concentration. Then, the absorption of the samples was measured at the same wavelength. A calibration curve was prepared by plotting the absorbance of the standards versus their concentrations. The amount of protein present in the sample was then determined from the calibration curve by taking the dilution factor into consideration.

**3.1.5 Determination of metabolite concentration by the end-point method**

The concentration of glycolytic metabolites was determined by means of a coupled enzymatic determination analysis [94]. This analysis is based on coupling of an enzyme-catalysed reaction that uses the metabolite to be analysed as substrate, with an enzyme-catalysed  $\text{NAD}^+/\text{NADH}$  oxidation/reduction reaction. The NADH absorption is

measured at 340 nm before and after the addition of each of the enzymes. The concentration of the metabolite can be calculated according to the law of Lambert-Beer:

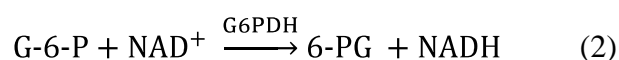
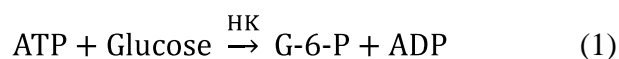
$$c = \frac{A \times V_{\text{total}}}{\varepsilon \times d \times V_{\text{probe}}}, \quad (3.4)$$

where,  $A$  is the absorption difference before and after the addition of enzyme,  $\varepsilon$  is the extinction coefficient of NADH at 340 nm ( $6.3 \times 10^3$  l/(mol $\times$ cm) [94]),  $d$  is the length of cuvette,  $V_{\text{total}}$  is the total volume of sample in the cuvette, and  $V_{\text{probe}}$  is the volume of the probe in the total sample.

The procedure of metabolite analysis is described for the determination of ATP and G-6-P.

### Determination of ATP and G-6-P:

#### Reaction:



#### Materials:

Substance	Concentration of stock solution	Volume
Triethanolamin buffer pH 7.6	0.1 M	2 ml
MgSO <sub>4</sub>	0.1 M	0.1 ml
NAD <sup>+</sup>	0.024 M	0.1 ml
Probe		0.05 ml
G6PDH (contains ~ 0.05% HK)	1000 Unit/ml	0.005 ml
Glucose	0.1 M	0.05 ml
HK	1500 Unit/ml	0.005 ml

#### Procedure:

Triethanolamin buffer, MgSO<sub>4</sub>, NAD<sup>+</sup>, and the probe were filled into the quartz (QG) or optical glass (OG) cuvette (Hellma, optical length  $d=1\text{cm}$ ) and well mixed. The cuvette was placed into the spectrophotometer and the absorption of NADH was measured at

340 nm. When the NADH absorption became constant, the first enzyme, Glucose-6-phosphate dehydrogenase (G6PDH), was added into the cuvette (reaction 2). The absorption of NADH increases and reaches the maximum when Glucose-6-Phosphate (G-6-P) present in the probe is converted into 6-Phosphogluconate (6-PG) (Figure 3.2). Since the conversion of 1 mol G-6-P yields 1 mol NADH (reaction 2), the difference in NADH absorption before and after addition of the enzyme G6PDH corresponds to the concentration of G-6-P and can be calculated by using the Eq. (3.4).

In order to determine the concentration of ATP in the probe, glucose<sup>3</sup> and the second enzyme Hexokinase (HK) were added to the assay mixture (reaction 1). Thereby, in the presence of glucose the ATP contained in the probe was converted to ADP and G-6-P (reaction 1), which was further converted to 6PG and NADH (reaction 2). This results in an increase of NADH absorption, which reaches its maximum when all ATP is consumed. In this case, the difference in NADH absorption corresponds to the ATP concentration.

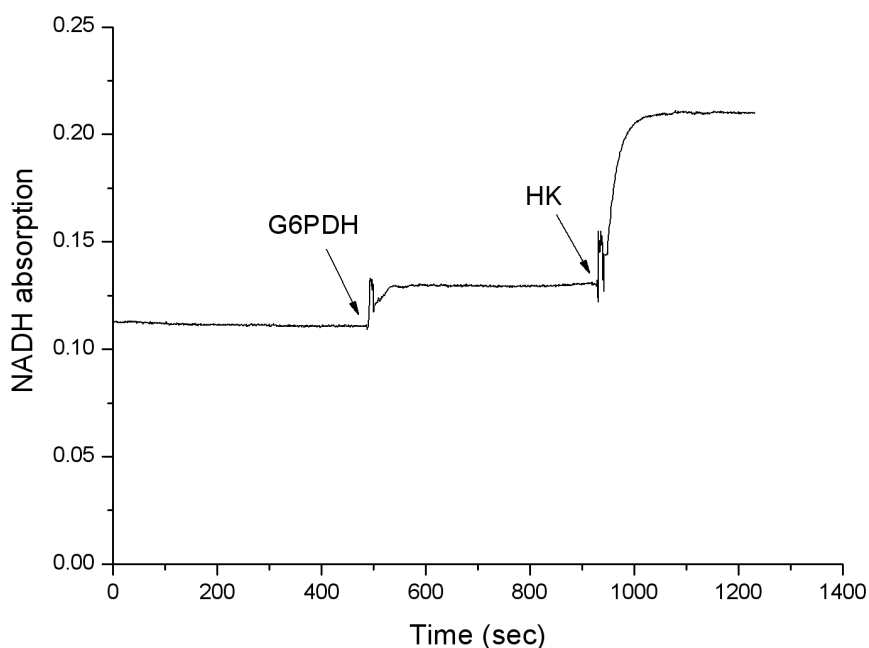


**Figure 3.2:** Development of NADH absorption during determination of ATP and G-6-P. NADH absorption was measured at 340 nm. The arrows correspond to the addition of enzymes G6PDH and HK into the cuvette. The difference in NADH concentration after addition of G6PDH and HK corresponds to the concentration of G6P and ATP, respectively.

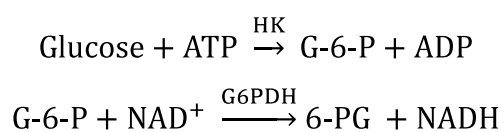
<sup>3</sup> Since the enzyme G6PDH contains HK (about 0.05%), glucose was added to the assay mixture after determination of the G-6-P in the probe.

If the concentration of the metabolites in the probe is too high ( $A > 0.7$ ), the metabolite will not be converted completely, because the substances of the assay (Glucose, NADH, etc.) are limited. In this case the analysis should be repeated with diluted probes.

The determination of all other metabolites was performed in an analogous way. The analysis of these metabolites is described below.

### **Determination of Glucose and G-6-P:**

#### Reaction:

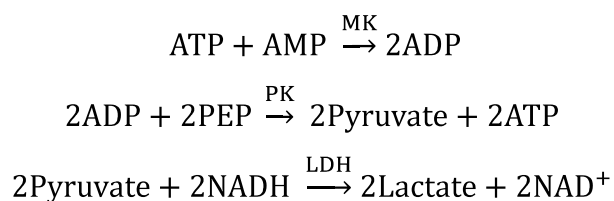


#### Materials:

Substance	Concentration of stock solution	Volume
Triethanolamin buffer pH 7.6	0.1 M	2 ml
MgSO <sub>4</sub>	0.1 M	0.1 ml
NAD <sup>+</sup>	0.024 M	0.1 ml
Probe		0.05 ml
G6PDH (contains ~ 0.05% HK)	1000 Unit/ml	0.005 ml
ATP	0.1 M	0.05 ml
HK	1500 Unit/ml	0.005 ml

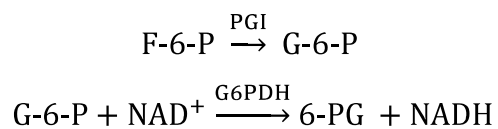
### **Determination of AMP, ADP, and Pyruvate:**

#### Reaction:

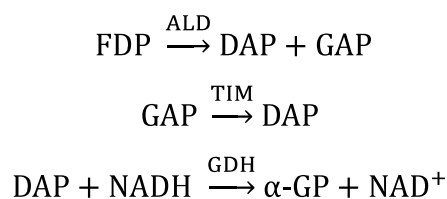


Materials:

Substance	Concentration of stock solution	Volume
Triethanolamin buffer pH 7.6	0.1 M	2 ml
MgSO <sub>4</sub>	0.1 M	0.1 ml
KCl	0.1 M	0.1 ml
NADH	0.01 M	0.05 ml
Probe		0.05 ml
LDH (contains ~ 0.001 % PK)	2750 Unit/ml	0.005 ml
PEP (contains ~ 3.14 % Pyruvate)	0.01 M	0.2 ml
PK	2000 Unit/ml	0.005 ml
MK	6630 Unit/ml	0.005 ml

**Determination of G-6-P and F-6-P:**Reaction:Materials:

Substance	Concentration of stock solution	Volume
Triethanolamin buffer pH 7.6	0.1 M	2 ml
MgSO <sub>4</sub>	0.1 M	0.1 ml
NAD <sup>+</sup>	0.024 M	0.1 ml
Probe		0.05 ml
G6PDH (contains ~ 0.05% HK)	1000 Unit/ml	0.005 ml
PGI	700 Unit/ml	0.005 ml

**Determination of DAP, GAP, and FDP:**Reaction:Materials:

Substance	Concentration of stock solution	Volume
Triethanolamin buffer pH 7.6	0.1 M	2 ml
NADH	0.01 M	0.05 ml
Probe		0.05 ml
GDH	360 Unit/ml	0.005 ml
TIM	10000 Unit/ml	0.005 ml
ALD	90 Unit/ml	0.005 ml

**3.1.6 Karhunen-Loève decomposition**

The Karhunen-Loève (KL) decomposition is a well-established method which allows one to find a minimal linear representation for a given data set that is optimal in the statistical sense [95]. It has been successfully exploited to characterize the catalytic CO oxidation on Pt surfaces [96] as well as for the local characterization of spatio-temporal chaos in a reaction diffusion system [97]. When applied to spatio-temporal data, it yields a separation of the dynamics into a set of static spatial modes and corresponding time-dependent amplitudes, which describe the temporal behaviour of the associated spatial mode. It is frequently used to obtain a low dimensional representation of experimental data, which might then allow for an interpretation of the data even in the case that a detailed model is either missing or too intricate.

To perform KL analysis of the spatio-temporal dynamics of glycolytic patterns, a *MatLab* program, written by Ronny Straube (Max-Planck-Institute Magdeburg, Group

of Systems Biology), was applied to a temporal sequence of two-dimensional video images.

The experiments yielded a set of  $t = 1 \dots n$  intensity images ( $\tilde{B}^t$ ) of dimension  $\dim x \times \dim y$ . In this representation, a particular image  $\tilde{B}^t$  is given by a matrix  $\tilde{B}_{ij}^t$  where the  $(i, j)$ -th entry denotes the grey value of the  $(i, j)$ -th pixel in the image  $\tilde{B}^t$ . Next, the time average of the image sequence was subtracted from each image:

$$B_{ij}^t = \tilde{B}_{ij}^t - \frac{1}{n} \sum_{k=1}^t \tilde{B}_{ij}^k, \quad 1 \leq i \leq \dim x, \quad 1 \leq j \leq \dim y,$$

where,  $\tilde{B}_{ij}^t$  are the original grey value images ( $\dim x \times \dim y$ ),  $B_{ij}^t$  are deviations from the mean value. As a result, the new data set  $B_{ij}^t$  has a vanishing mean value  $\langle B^t \rangle = 0$ .

For explicit calculations, it is convenient to represent each intensity image by a vector instead of a matrix. This can be done by reordering the matrix elements  $B_{ij}^t$  in the row major form; i.e. the rows of the image  $B^t$  are concatenated such that the matrix element  $B_{ij}^t$  is mapped to the vector component  $b_{(t)q}$ , where  $q$  is given by

$$q = j + (i - 1) \times \dim y \quad (3.5)$$

and the indices  $(i, j)$  range between  $1 \leq i \leq \dim x$  and  $1 \leq j \leq \dim y$ , respectively. As a result, one large matrix of dimension  $n \times (\dim x \times \dim y)$  is obtained from the initial set of  $n$  images  $B_{ij}^t$ . The corresponding matrix elements  $b_{(t)q}$  have the following form:

$$b_{(t)q} = \begin{pmatrix} 1st & image B_{ij}^1 \\ \vdots & \\ n-th & image B_{ij}^n \end{pmatrix}, \quad (3.6)$$

i.e. each row, labelled by the index  $t$ , corresponds to one of the original images ( $B^t$ ). The KL decomposition of the matrix  $b_{(t)q}$  can be obtained from its singular value decomposition

$$b_{(t)q} = \sum_{r,s} u_{(t)r} \lambda_{rs} v_{sq} \quad \text{or} \quad b = u \lambda v^T \quad (3.7)$$

as

$$b_{(t)q} = \sum_l a_l^t v_{lq} \quad \text{with} \quad a_l^t = \sum_r u_{(t)r} \lambda_{rl} \quad (3.8)$$

which yields the desired separation of the original data set into time-independent modes  $v_{(\cdot)l}$  and their corresponding time-dependent amplitudes  $a_l^t$ . In Eq. (3.7) the superscript  $(\cdot)^T$  denotes matrix transposition, whereas  $u$  and  $v$  are matrices of the left and right eigenvectors of  $b$ , and  $\lambda_{rl} = \lambda_r \delta_{rl}$  denotes a diagonal matrix containing the associated singular values of  $b$ . The right eigenvectors  $v$  are also eigenvectors of the covariance matrix

$$k_{qr} = \frac{1}{n-1} \sum_{t=1}^n b_{q(t)} b_{(t)r} \quad \text{or} \quad k = \frac{1}{n-1} b^T b, \quad (3.9)$$

that is

$$kv = \Lambda v \quad \text{with} \quad \Lambda = \frac{\lambda^2}{n-1}. \quad (3.10)$$

This relation defines the KL modes  $v$  in Eq. (3.8). i.e. they diagonalize the covariance matrix of the original data set. Note that each KL mode  $v_{(\cdot)l}$  can be rearranged into a matrix  $m_{ij}^l$  with the help of transformation (3.5). In terms of these matrices the original image sequence  $\tilde{B}_{ij}^t$  can be reconstructed from

$$\tilde{B}_{ij}^t = \frac{1}{n} \sum_{k=1}^n \tilde{B}_{ij}^k + \sum_l a_l^t m_{ij}^l. \quad (3.11)$$

The eigenvalues  $\Lambda_l$  in Eq. (3.10) are all positive and can be ordered as  $\Lambda_1 > \Lambda_2 > \dots > \Lambda_l > \dots > 0$ . Their magnitude is a measure for the variance of the original data set projected along the  $l$ -th KL mode since the coefficients  $a_l^t$  are on average uncorrelated, i.e.

$$\text{var}(a) = \frac{1}{n-1} \sum_t a_l^t a_m^t = \frac{\lambda_l^2}{n-1} \delta_{lm} = \Lambda_l \delta_{lm}. \quad (3.12)$$

Experimental data sets usually exhibit some degree of redundancy due to correlations among certain variables. Accordingly, the eigenvalue spectrum will decay towards higher mode numbers. In this case, the original images  $\tilde{B}_{ij}^t$  may well be reconstructed using only the first  $k$  modes  $l = 1 \dots k$ . The number of modes, which are used for reconstruction, is generally much smaller, than the total number of modes  $N$  of the covariance matrix. Only the modes with significantly high eigenvalues are used for reconstruction, since these modes reflect most of the correlations of the original data set.



A widely used measure to determine the number of modes for reconstruction is the fraction of the statistical variance that is captured by the first  $k$  KL modes:

$$V_k = \frac{\sum_{i=1}^k \Lambda_i}{\sum_{i=1}^n \Lambda_i}, \quad \frac{\Lambda_1}{\sum_{i=1}^n \Lambda_i} \leq V_k \leq 1. \quad (3.13)$$

For later reference, normalized eigenvalues  $\sigma_k$  are defined as:

$$\sigma_k = \frac{\Lambda_k}{\sum_{i=1}^n \Lambda_i}. \quad (3.14)$$

## 3.2 Materials

Enzymes, their substrates, and coenzymes were purchased from Roche. Antifoam 289 and agarose (Type IXA) were purchased from Sigma, casein hydrolysate and yeast extract from Oxoid, Folin-Ciocalteu's phenol reagent from Merck, and vitamins from Fluka. All other chemicals were purchased from Merck, Fluka, and Sigma at the highest purity available.

## 3.3 Experimental set up

### 3.3.1 The open spatial reactor

The open spatial reactor is made of two parts: the lower part is a continuous-flow stirred tank reactor (CSTR) in which solutions of substrates and co-factors for glycolysis are permanently supplied by means of a peristaltic pump (Figure 3.3) and constantly mixed by a magnetic stirrer. The upper part consists of a gel-fixed yeast extract. A set of two circular membranes is placed between the gel and the CSTR: a black nitrocellulose membrane with 0.8  $\mu\text{m}$  pore size from Millipore is tightly placed on a cellulose triacetate membrane, molecular weight (MW) cut off 10 kD, from Sartorius. The black membrane strongly reduces the fluorescence background from the slightly fluorescing white membrane and greatly improves the detection of the NADH-fluorescence from the yeast extract. The role of the membrane is not only to keep the enzymes within the gel but also to partly decouple the gel contents from the CSTR contents. The effective volume of the reactor (CSTR) is 3.2 ml.

In the experiments shown in section 4.1.2, an O-ring from rubber was additionally used to ensure that the membranes are tightly squeezed to the holder. This O-ring ( $23 \times$

1mm) was placed on the black nitrocellulose membrane (Figure 3.3). All other experiments were conducted without this O-ring.

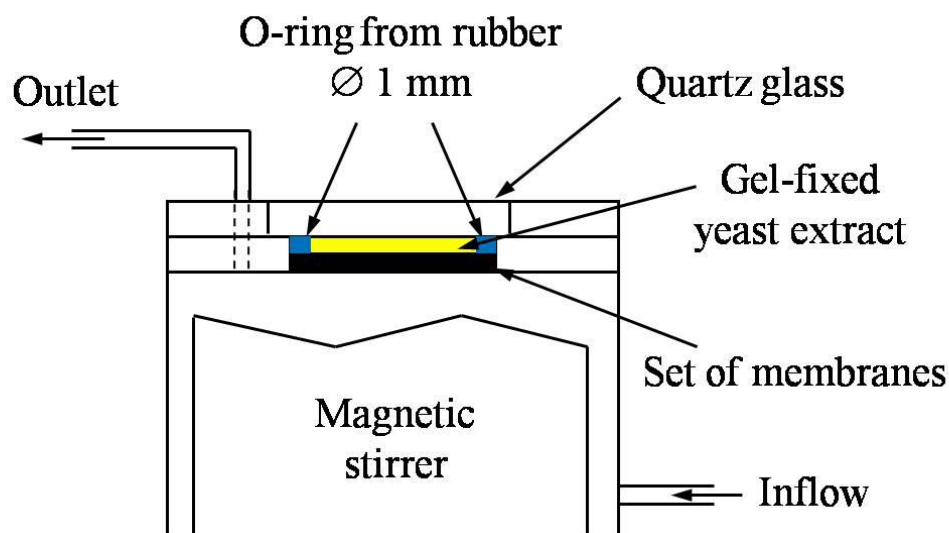


**Figure 3.3:** Schematic drawing of the open spatial reactor. The lower part of the reactor represents the CSTR with effective volume of 3.2 ml. The upper part of the reactor contains the gel-fixed yeast extract. The diameter and volume of the circular piece of gel are 24 mm and 590  $\mu\text{l}$ , respectively. An O-ring made from rubber with diameter 1 mm was placed on the upper membrane. This O-ring was used only for the experiments in section 4.1.2.

### 3.3.2 Gel fixation of yeast extract

0.35 ml of deionized water (conductivity  $\leq 0.056 \mu\text{S}\times\text{cm}$ ) was added to 21.45 mg of agarose (Type IXA from Sigma) and the mixture was heated for 5-7 min at 65 °C. The liquid solution of agarose was then placed in a water bath at 23 °C. At the same time 0.95 ml of yeast extract were also incubated at 23 °C. After 2-3 min, the yeast extract was carefully mixed with the agarose solution (end concentration of agarose: 1.65 % (w/v)). This mixture was then placed between two glass plates separated by 1.3 mm thick spacers. A 5 kg weight was placed on the upper glass plate (20 cm x 15 cm) for 15 min in order to obtain a flat surface of the gel. During this gelation process the temperature was kept at 0 °C by ice containers. Thereafter, a circular piece (diameter 24 mm) was cut out of the gel slide and placed on the black nitrocellulose membrane. The volume of the circular piece of gel was 590  $\mu\text{l}$ .

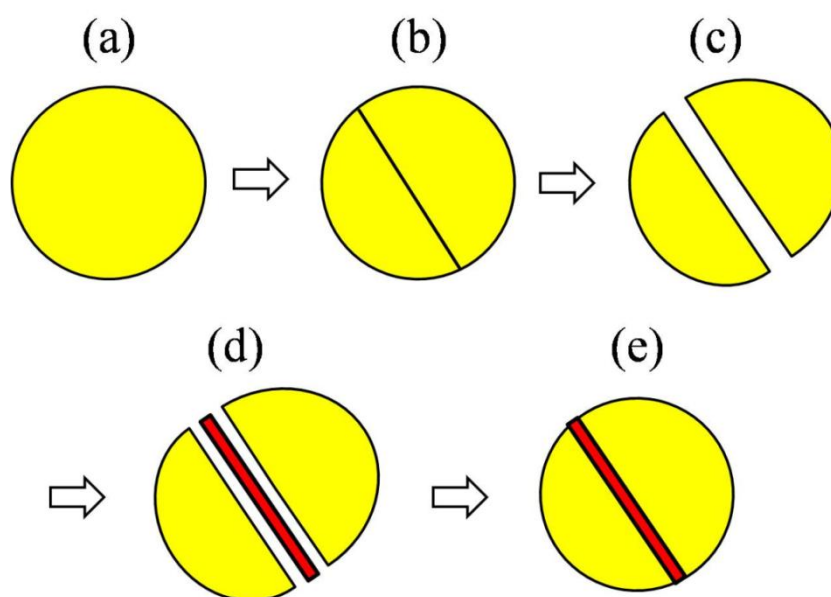


**Figure 3.4:** Scheme of the preparation of the gel with a diffusive barrier. (a) A circular piece of gel ( $\varnothing = 24$  mm). (b) and (c) The gel was cut and detached into two halves. (d) A segment made from rubber ( $\varnothing = 1$  mm and  $l = 37$  mm) was placed in-between the two gel pieces. (e) The gel separated by the barrier.

For the experiments with the diffusive barrier (section 4.2.4), the circular piece of gel was prepared from yeast extract and agarose as described above (Figure 3.4a). The gel was then cut into two halves (Figure 3.4b and c). A semicircle made from rubber with a diameter of 1 mm and length 37 mm was placed in-between these two gel pieces (Figure 3.4d). This gel (Figure 3.4e) was placed in the reactor and the experiment was started as usual.

### 3.3.3 Experimental procedure

Prior to the start of the experiments, the black nitrocellulose and the white cellulose triacetate membranes were soaked in deionized water for 2 h. The gel-fixed yeast extract was placed on top of the set of these two membranes and then transferred into the reactor. The upper face of the gel was pressed against a quartz window. Time zero of experiments is defined as the start of the supply of feeding solution to the CSTR. The flow rate and stirring rate were 6.2 ml/h and 500 rpm, respectively. The residence time in the reactor was 30 min. The temperature in the reservoir of the reactor was kept constant at 21 °C by a Cryostat (Lauda RM6).

The following solution was used (end concentrations in the total input flow) for feeding into the reactor: 0.6 mM ATP, 0.4 mM ADP, 0.8 mM NAD, 10 mM MOPS pH 6.5, 3 mM  $\text{MgCl}_2$ , 50 mM trehalose, 50 mM  $\text{KH}_2\text{PO}_4$  pH 6.5, 100 mM KCl. Derivations of this composition are indicated in the text.

### 3.3.4 Optical set up

The spatio-temporal dynamics of glycolysis in the yeast extract were monitored using the optical set up shown in Figure 3.5. White light from a Xenon lamp (Laser 2000) was passed through an UG-11 filter (broadband filter, centered around 340 nm) and the resulting light beam was reflected via a dichroic mirror (LINOS) to the yeast extract. Fluorescence light of NADH in the gel (460 nm) passed through the dichroic mirror to an intensified camera, containing a bialkali-photocathode (Corail, Optronis -SG). In order to reduce noise from reflecting light, a 460 nm long pass filter was placed directly in front of the camera objective. This optical set up is based on the principle of Köhler illumination [98]. It allows homogenous illumination of the area of interest and independent adjustment of the brightness and the size of the illuminated area.

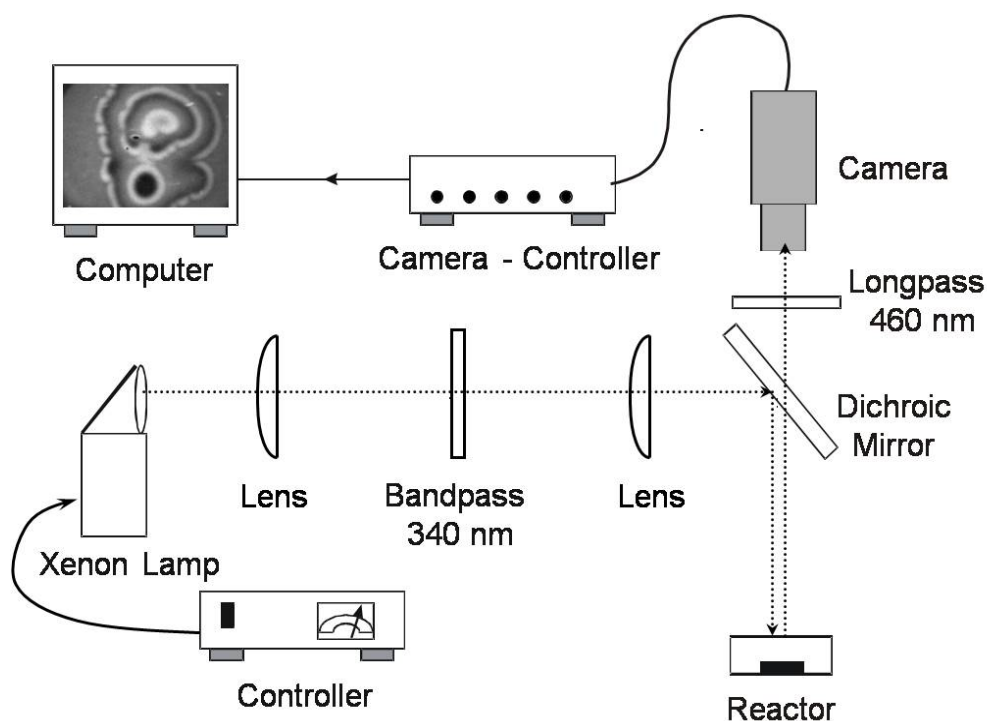


**Figure 3.5:** Schematic drawing of the optical set up for monitoring spatio-temporal patterns of NADH.

The camera output was connected to a frame grabber card (Data Translation DT 3155) in the computer. The analogue signal from the camera was grabbed by a frame grabber and digitized into \*.tif images by means of *Acquisition program* (Lab View) written by Ulrich Storb (Biophysics Group, Otto-von-Guericke University of Magdeburg). Every 10 images were averaged online to yield 1 image, which was stored as a final movie. After each experiment the length scale was calibrated with a millimetre paper.

The temporal dynamics of the system were studied by following the local changes of the NADH fluorescence in the gel. For this purpose, the grey levels of a selected small area (10 x 10 pixel = 0.22 mm x 0.22 mm) were averaged and the arithmetic mean of the grey levels was plotted as a function of time.

### 3.3.5 Tools for image analysis

The sequence of grabbed images was processed and analysed using an IDL (Interactive Data Language, Version 6.3) program written by Ulrich Storb and Chaiya Luengviriyaya (Biophysics Group, Otto-von-Guericke University of Magdeburg). The program *contrast\_img.pro* (Appendix A.1) was used to subtract the background and enhance the contrast of the original images. The background image was obtained by averaging each individual pixel of the sequence of images. The obtained background intensity was subtracted from the sequence of original images. Then, the contrast of the resulting images was increased by rescaling the histogram of grey values in the images to the range from 0 to 255 grey levels. This was performed by applying the following formula [99] to each pixel of a background subtracted image:

$$I_{ij} = 255 \frac{\check{I}_{ij} - I_{min}}{I_{max} + I_{min}}, \quad (3.15)$$

where,  $I_{ij}$  and  $\check{I}_{ij}$  are the original and rescaled grey levels of the pixel ( $ij$ ),  $I_{min}$  and  $I_{max}$  are the minimal and maximal values of grey level in the original image. The resulting images were stored as a new file and used for future analysis of the experiments.

Substantial information about the dynamics of spatio-temporal patterns was obtained from the time-space plots. The time-space plot was constructed from the sequence of enhanced images by using the program *timespaceplot\_freedirection\_v6.pro*

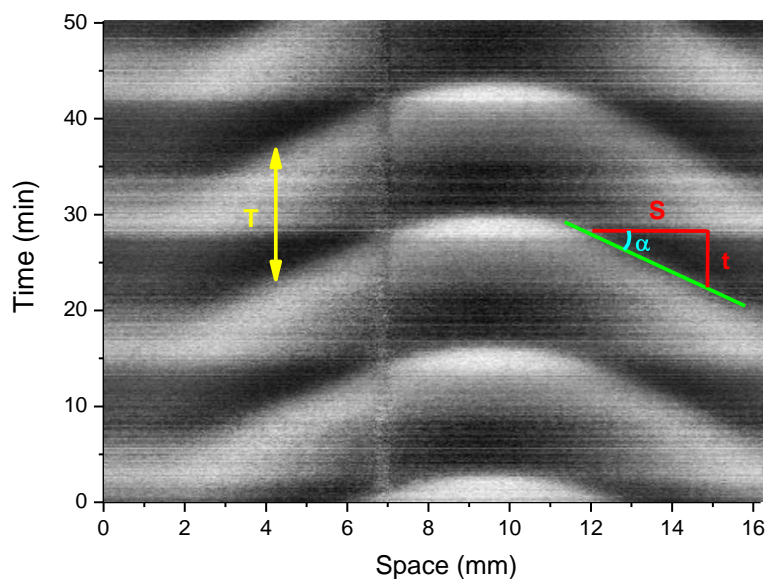


**Figure 3.6:** An example of time-space plot for evaluation of spatio-temporal dynamics of patterns. The white lines represent propagating NADH waves. The slope of the lines is a measure of the wave velocity (green line). The period (T) was measured as the distance between two successive waves in the vertical direction.

(Appendix A.2). The intensity profile of a horizontal line for all images of the movie was plotted as a function of time. An example of such a time-space plot is shown in Figure 3.6. The white lines represent propagating NADH waves. Time-space plots were used to calculate the velocity and the period of waves. The wave velocity was calculated from the slope of the tangent fitted to the displacement of the wave front (green line in Figure 3.6). The period of waves was determined from the time-space plot as the distance between two successive waves in the vertical direction (indicated with T in Figure 3.6).

### 3.4 Optimization of experimental conditions

Open spatial reactors are widely used for the investigation of spatial patterns in chemical systems, such as the Belousov-Zhabotinsky (BZ) reaction [40;41] and the Chlorite-iodide-malonic acid (CIMA) reaction [42-44]. In the present study such a reactor, was designed and implanted for the first time to investigate the spatio-temporal dynamics of glycolysis in yeast extract.

At the beginning of this study, the components of the reactor, which play an important role for the pattern formation in the open spatial reactor, needed to be optimized. One of these components is the gel, which represents the diffusive layer, in where the yeast extract is partially fixed. Moreover, the gel prevents the formation of undesired convection patterns. Another important component of the reactor, which must be optimized, is the membrane which separates the gel from the CSTR. This membrane should support a sufficiently effective diffusion of the substances from the reservoir of the reactor into the gel and back. In addition, the membrane should prevent the loss of proteins from the gel. Consequently, the gel and the membrane have to be carefully chosen to provide adequate conditions for the formation of spatio-temporal patterns.

### 3.4.1 Selection of the gel

To select the proper type of gel, it should be considered, that the gelation temperature of the gel must not be higher than 23 °C, otherwise the yeast extract will be denaturated during mixing with the gel. In addition, the gel ready for use should be hard and easy to handle. In order to select the type of agarose with the above mentioned characteristics, the gel was prepared from different types of agarose and mixed with the yeast extract (for details see section 3.3.2). The results of the experiments indicate that the agarose type IX A is the most suitable to trap the yeast extract in the gel since it is fluid at 23 °C and can be easily mixed with the yeast extract. To obtain the hard gel, which is easy to handle, the concentration of agarose (Type IX A) was varied from 1.5 % to 1.8 % (w/v). The optimal results were found with an agarose concentration of 1.6-1.65 % (w/v) (Table 3.5). For future experiments the gel was prepared from 1.65 % (w/v) agarose (Type IX A).

**Table 3.5:** Properties of the gel at different agarose concentrations.

<b>Concentration of agarose (Type IX A) in gel, % (w/v)</b>				
<b>1.5 %</b>	<b>1.6 %</b>	<b>1.65 %</b>	<b>1.7 %</b>	<b>1.8 %</b>
Soft gel	Hard gel, easy to handle	Hard gel, easy to handle	Very hard gel, difficult to mix	Very hard gel, difficult to mix

### 3.4.2 Selection of the membrane

#### 3.4.2.1 Test of membrane permeability

In order to choose an appropriate membrane, which supports a sufficient diffusion of glycolytic intermediates, the relevant diffusion properties of different membranes were tested. For this purpose, the reactor was fed with a solution of NADH in phosphate buffer. In this case the agarose gel was prepared only with water. NADH is one of the main intermediates of glycolysis and can be easily monitored by its intrinsic fluorescence. Since the molecular weight of NADH is in the range of other glycolytic intermediates, the diffusion behaviour of NADH should provide qualitative information about the exchange of glycolytic intermediates through the membrane.

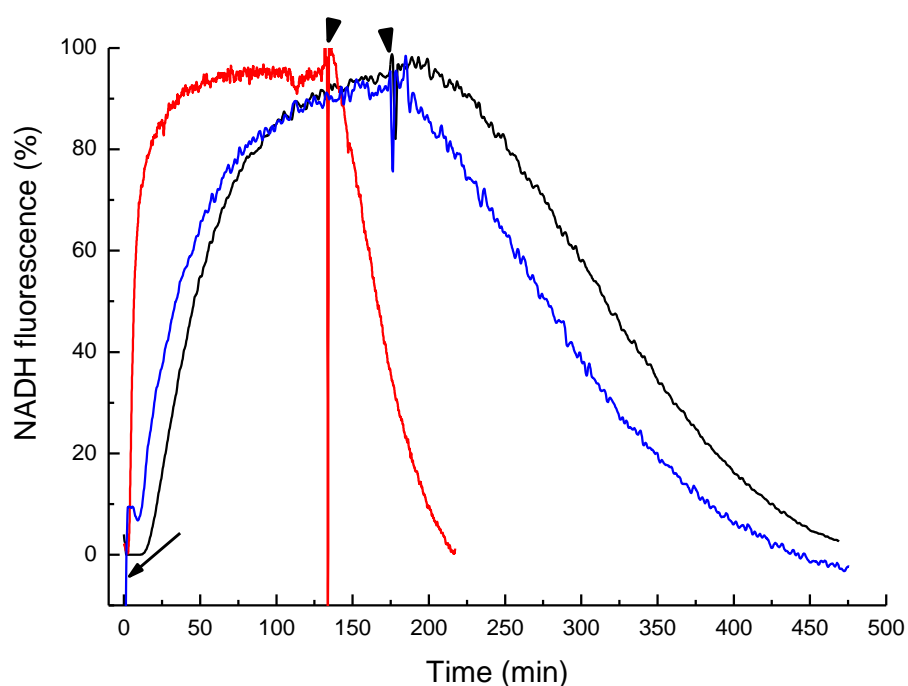


**Figure 3.7:** Transport of NADH into the agarose gel (1.65% (w/v)) through different types of membranes. First, the reactor was fed with 50 mM  $\text{KH}_2\text{PO}_4$  buffer, pH 6.5, which was replaced after 15 min ( $t = 0$  in the figure, indicated by an arrow) by a solution of 1 mM NADH in 50 mM  $\text{KH}_2\text{PO}_4$ , pH 6.5. After 2 h the feeding solution was changed back to the buffer (arrow head). Cellulose triacetate membrane (black line), Anodisc membrane (red line), Nitrocellulose membrane (blue line). For each time trace the highest fluorescence value was taken as 100 %.



Figure 3.7 shows the kinetics of the NADH fluorescence increase in the gel when the reactor was fed with NADH solutions. Removing NADH from the feeding solutions results in a decrease of the fluorescence in the gel, demonstrating an efficient communication between the gel and the CSTR through the membrane. The experiments were performed with three different types of membranes: an Anodisc membrane (type: Anodisc 25, from Whatman) with 20 nm pore size, a nitrocellulose membrane with the molecular weight (MW) cut-off 10 kD (Schleicher & Schuell), and a cellulose triacetate membrane with MW cut-off 10 kD (Sartorius). The Anodisc membrane was used for comparison, because in control experiments this membrane has been proven to support the formation of Turing patterns in the chemical CIMA reaction in this reactor.

The initial rates of the change in NADH fluorescence obtained with these membranes are listed in Table 3.6 for comparison. The results show that the Anodisc membrane has by far the highest permeability. However, the Anodisc membrane is not appropriate for our experiments, because its pore size is too large (larger than the size of enzymes). Membranes made of cellulose triacetate or nitrocellulose have smaller pores (10 kD) and are designed for the retention of proteins. The data show that the transport

**Table 3.6:** Initial rates of NADH transport through different types of membranes. The data were calculated from fluorescence measurements as shown in Figure 3.7. They are expressed in % of change in NADH fluorescence per minute. The maximal change in fluorescence was taken as 100 %. The mean value of three different experiments together with the standard error of the mean (SEM) is shown, except for the Anodisc membrane, where only one representative experiment is given. The middle column of the table shows the initial velocity of NADH transport into the gel ( $V_{in}$ ); the right column shows the initial velocity of NADH disappearance out of the gel ( $V_{out}$ ).

Type of membrane	$V_{in}$ (%/min)	$V_{out}$ (%/min)
Cellulose triacetate membrane (10kD)	$1.6 \pm 0.04$	$0.47 \pm 0.01$
Cellulose triacetate (10 kD) + black nitrocellulose membrane (0.8 $\mu$ m)	$1.16 \pm 0.2$	$0.8 \pm 0.17$
Nitrocellulose membrane (10 kD)	$1.38 \pm 0.05$	$0.46 \pm 0.007$
Anodisc membrane (20 nm)	14.75	1.65

rates through the cellulose triacetate membrane and the nitrocellulose membrane are similar (Figure 3.7, Table 3.6). However, both membranes exhibit undesirable background fluorescence, which is larger in the case of the nitrocellulose membrane compared to the cellulose triacetate membrane. Therefore, the cellulose triacetate membrane was chosen for the experiments.

#### 3.4.2.2 Calibration of NADH fluorescence in the open spatial reactor

Figure 3.8 illustrates the calibration of the fluorescence intensity of NADH in the open spatial reactor. For this purpose, discs of agarose gel containing different NADH concentrations were placed either directly on the cellulose triacetate membrane or on a set consisting of the cellulose triacetate membrane covered by a black nitrocellulose membrane (for details see section 3.3.1). These gel discs were then placed into the empty reactor and the fluorescence of NADH was measured with the optical set up shown in Figure 3.5. As a control, NADH solutions in a quartz cuvette were measured with this set up. When using only the cellulose triacetate membrane as a support for the gel, a saturation of the fluorescence signal for concentrations exceeding 0.5 mM NADH was found. After measuring the autofluorescence of the cellulose triacetate membrane, it was found that the cellulose triacetate membrane exhibits a pronounced fluorescence at 460 nm when excited at 340 nm. This may explain why the NADH calibration curve reaches saturation when the cellulose triacetate membrane is used. When monitoring the NADH solution in a quartz cuvette, a linear relationship between the NADH fluorescence and a concentration up to 1 mM was found. Covering the white cellulose triacetate membrane with a black nitrocellulose membrane (Millipore, pore size 0.8  $\mu\text{m}$ ) eliminates the background fluorescence from the cellulose triacetate membrane and yields similar results as with the cuvette (Figure 3.8).

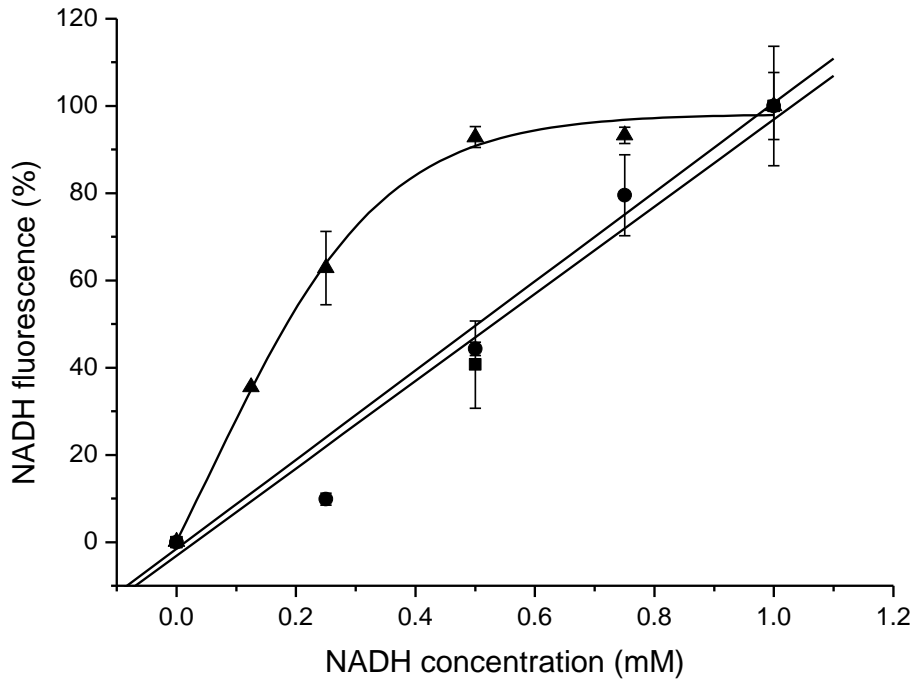


**Figure 3.8:** Fluorescence intensity as a function of NADH concentration. NADH fluorescence was measured in an agarose gel placed on the cellulose triacetate membrane (triangles), or on the set made of black nitrocellulose and cellulose triacetate membranes with the black membrane on top (squares), or in a quartz cuvette (for reference, circles). The solid lines represent fits of the experimental data with either a linear fit (circles and squares) or with the Boltzmann function (triangles). The highest fluorescence value of each calibration curve was taken as 100 %, and corresponds to 177 grey levels for the cellulose triacetate membrane, 19 grey levels for the set made of black nitrocellulose and cellulose triacetate membranes, and 20 grey levels for the quartz cuvette.

The fluorescence intensity of NADH for the set of the cellulose triacetate and black membrane was calibrated for different sensitivity settings of the camera. The results of the calibration are summarized in Table 3.7. The concentration of NADH can be determined from the following relationship:

$$[\text{NADH}] = \frac{G}{m} + a \quad (3.16)$$

where,  $G$  is the fluorescence intensity of NADH,  $m$  is the slope of the calibration line, and  $a$  is an offset.

**Table 3.7:** Summary of the calibration results of the NADH fluorescence intensity for different sensitivities of the camera. The NADH fluorescence at different sensitivity settings of the camera was measured in an agarose gel placed on the set consisting of a cellulose triacetate membrane covered by a black nitrocellulose membrane. The experimental procedure was performed as described for Figure 3.8. For each sensitivity setting of the camera, the results of two different measurements were averaged and their mean value was fitted linearly.

Sensitivity of camera (Units)	Slope of calibration line, (grey level/mM)	Offset, (mM)
620	47.18	0.37
630	73.63	0.32
640	89.9	0.24
650	110.5	0.18
660	156.8	0.185
670	191.1	0.15
680	223.1	0.116
690	261.1	0.076
700	300.6	0.09

The permeability of this set of membranes differs from that of the uncovered cellulose triacetate membrane (Figure 3.9, Table 3.6). When this set of membranes was used, the initial rates of NADH transport into the gel decreases by about 28 %. However, the amount of NADH diffused into the gel is the same (about 0.9 mM) for both cases (Figure 3.9). By feeding the reactor with 1 mM NADH solution, the NADH concentration in the gel increases up to 0.9 mM (Figure 3.9). This indicates that in the absence of reactions 90 % of NADH fed into the reactor was recovered in the gel. When the NADH was removed from the feeding solution (see arrow heads in Figure 3.9), the concentration of NADH in the gel decreases and finally reaches 0 mM. These results demonstrate that the exchange between the feeding chamber and the gel through the cellulose triacetate membrane as well as through the set of the cellulose triacetate and black membrane works properly.

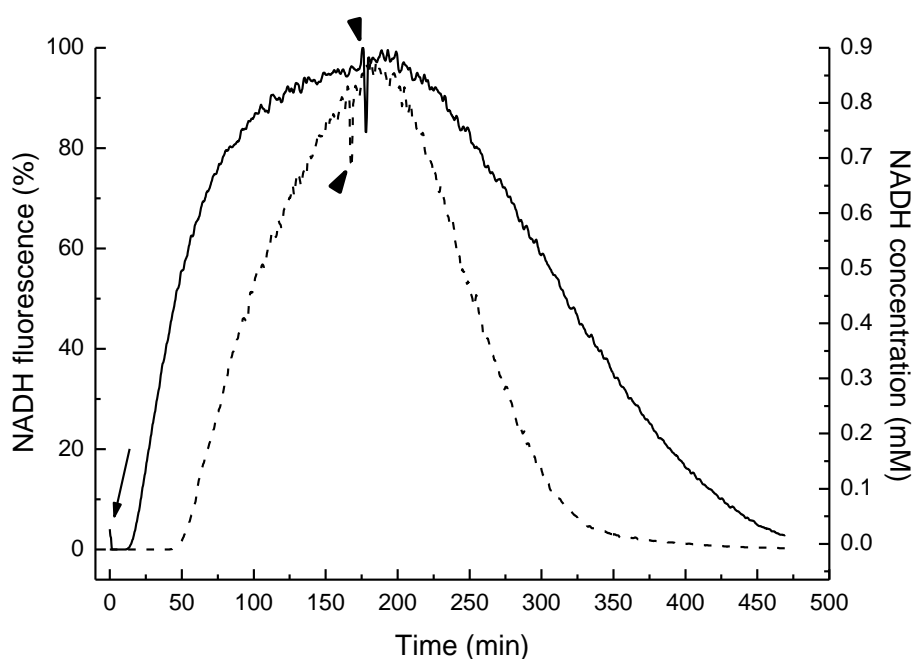


**Figure 3.9:** Decrease of NADH transport rate with the set of two membranes. The time trace for the NADH transport through the set of the cellulose triacetate and black nitrocellulose membrane (dashed line) and through the cellulose triacetate membrane alone (solid line) is shown. The left ordinate shows the normalized NADH fluorescence and the right ordinate shows the corresponding NADH concentration. The arrow indicates the time points of the replacement of the phosphate buffer with a 1 mM NADH solution and the arrow heads indicate the change of solution back to the phosphate buffer. The experimental procedure was the same that described for Figure 3.7.

## 4 Results

### 4.1 Temporal dynamics of glycolysis in an open spatial reactor

#### 4.1.1 Glycolytic oscillations

The permanent supply of fresh reactants through the open spatial reactor allows to maintain the system far away from thermodynamic equilibrium and in a constant and well-defined state. In order to induce oscillatory glycolysis, the yeast extract has to be supplied with the substrate of glycolysis (sugar). Because of a permanent diffusion of substances out of the gel, it is necessary also to feed all low-molecular weight components, e.g. salts and buffer, which are required to maintain oscillatory glycolysis. In particular, adenine and pyridine nucleotides must be fed, because they are tightly connected to the glycolytic pathway, but are not synthesized during glycolysis.

Glycolytic oscillations in the open spatial reactor under continuous feeding and stirring are displayed in Figure 4.1. After an induction time (not shown), oscillations with a period of 5.5 min were observed. Due to the openness of the reactor, oscillations should last as long as the reactor is fed with substrates. However, they already damp out after about 2 h. There are several possible reasons for this damping. For example, 1) the pores of the membrane could be clogged, 2) there might be a leak of an unknown metabolite, 3) the enzymes might be denaturated, and/or 4) the ratio of the adenine nucleotides might be inappropriate to support oscillations. Generally, the problem could originate either in the yeast extract kinetics or in the reactor components.

#### 4.1.2 Effect of adenine nucleotides on glycolytic oscillations

In order to analyse the factors that lead to the damping process, shown in Figure 4.1, the concentrations of various glycolytic intermediates in the outlet of the reactor were analysed (for details see section 3.1.5). The results are shown in Figure 4.2. The concentrations of all species vary from the oscillatory to the damped phase. Most pronounced are changes in the concentrations of adenine nucleotides: adenosine triphosphate (ATP) decreases 33 fold and adenosine monophosphate (AMP) increases 7 fold. These changes point to a strong activation of the enzyme phosphofructokinase (PFK) at the transition from the oscillatory to the damped phase. The decrease of the

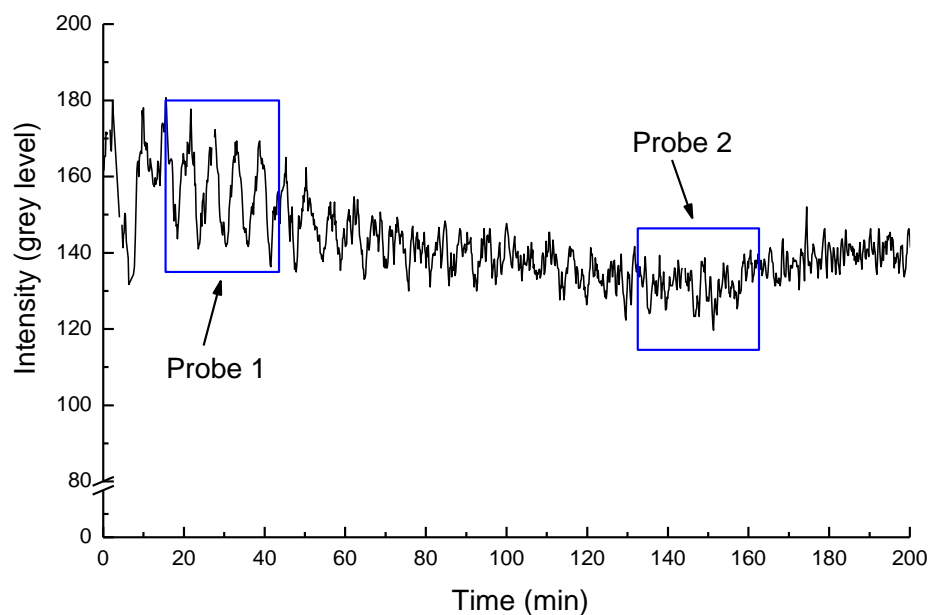


**Figure 4.1:** Glycolytic oscillations of the yeast extract in the open spatial reactor. The reactor was continuously fed with trehalose, non-recycling substrates, salts and buffer. For the experimental procedure and composition of the feeding solution see section 3.3.3. The stirring rate is 500 rpm. The feeding rate is 6.2 ml/h. The protein concentration in the yeast extract is 24 mg/ml. The rectangular boxes mark the time intervals during which probes from the outlet of the reactor were taken for the enzymatic analysis of glycolytic intermediates.

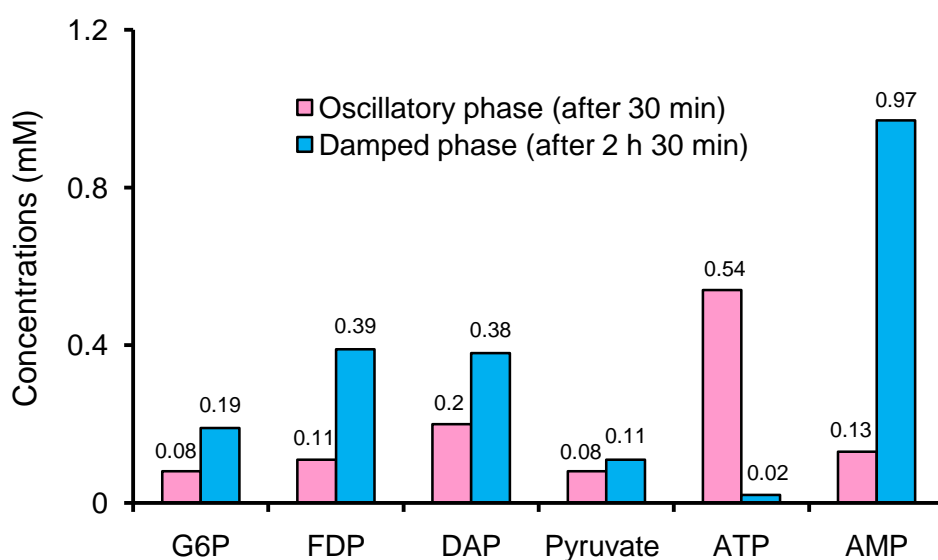


**Figure 4.2:** Determination of glycolytic intermediates during the oscillatory and the damped phases. The probes were taken at the time instants marked in Figure 4.1 as probe 1 (after 30 min) and 2 (after 2 h and 30 min), respectively.

concentration of ATP, the inhibitor (and substrate) for this enzyme, and the concomitant increase of the concentration of the activator (AMP) results in a full activity of the PFK (no negative feedback), which is also supported by the 3.5-fold increase in fructose-1,6-diphosphate (FDP) concentration in this experiment. It is suggested that the supply of ATP (by the pump) was smaller than the demand (activity of kinases), so that the adenylate kinase (AK) converts most adenosine diphosphate (ADP) into ATP and AMP. Since ATP is further consumed, this yields a permanent production of AMP.

To decrease the consumption of ATP by hexokinase (HK) and PFK, the product of these enzymes, glucose-6-phosphate (G-6-P) and fructose-1,6-diphosphate (FDP) were added to the feeding solution. Additionally, for reducing the ATPase activity and increasing the supply of adenine nucleotides, the concentrations of  $\text{KH}_2\text{PO}_4$  and adenine nucleotides in the feeding solution were increased. When running the reactor under these conditions (for composition of the feeding solution see legend to Figure 4.3), the analysis of the glycolytic intermediates in the eluate demonstrates, that the ratio of the adenine nucleotides does not change markedly during the first 4 h of feeding (Figure 4.3). This indicates that the supply-demand problem, observed in Figure 4.2, is now solved. As a result the duration of the oscillatory phase is doubled.

However, the damping process is still observed after 4 h, indicating that additional, yet unknown factors are involved in the maintenance of the sustained oscillations. This damping might be caused by the components of the open spatial reactor, as for example, the membrane may be bent, which leads to a direct communication between the gel and the CSTR.

In these experiments an O-ring made of rubber was used to press the membrane to the holder (Figure 3.3). This was done to ensure that a direct communication between the gel and the CSTR is prevented. However, during the course of the experiments there were indications that the O-ring impaired the formation of the oscillations. Hence, the next experiment was performed without the O-ring.

After removal of the O-ring, the oscillatory phase was prolonged for more than 10 h, when feeding with the components described in Figure 4.3. A similar duration of the oscillatory phase was also found for the experiments performed with a recipe described in Figure 4.1. In this case, the duration of oscillations was increased from 2 h up to 10 h (Figure 4.4). Apparently, the O-ring, which was introduced to squeeze the membrane



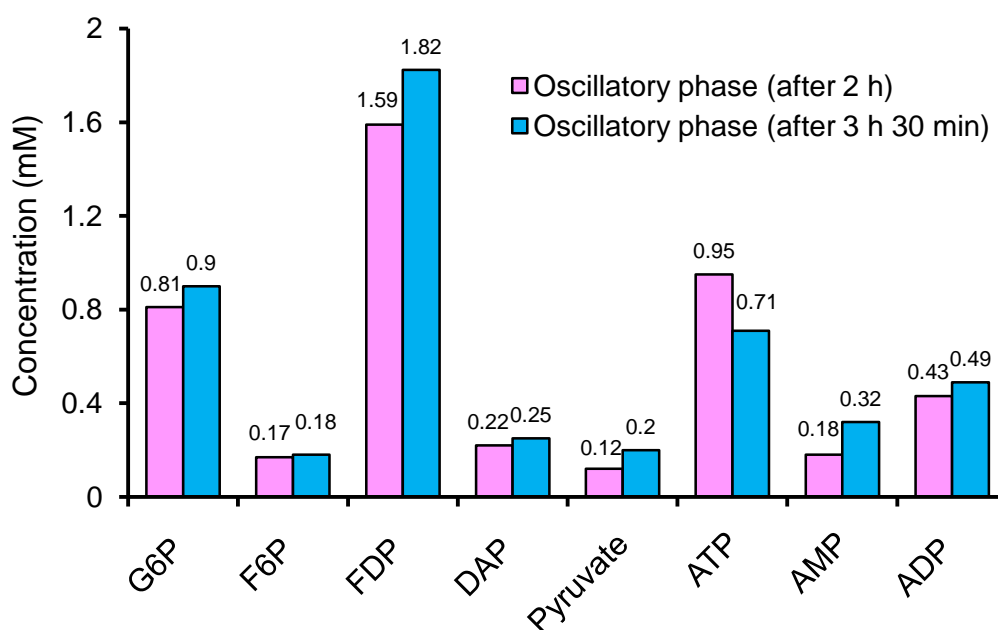


**Figure 4.3:** Effect of increased supply of adenine nucleotides on the glycolytic oscillations. The feeding solution contained (final concentrations): 0.84 mM ATP, 0.66 mM ADP, 1 mM FDP, 1 mM G-6-P, 3.5 mM MgCl<sub>2</sub>, 0.8 mM NAD, 100 mM KH<sub>2</sub>PO<sub>4</sub> pH 6.5, 100 mM KCl, 50 mM Trehalose. The stirring rate is 500 rpm. The feeding rate is 6.6 ml/h. The protein concentration in the yeast extract is 24 mg/ml. The probes were taken 30 min and 210 min after the start of feeding (both during the oscillatory phase).

tightly to the holder and prevent the direct communication between the enzymes trapped in the gel and the CSTR, instead, induced the bending of the membrane. This probably induced the leak of the enzymes from the gel and early damping of oscillations.

The analysis of glycolytic intermediates in the outlet of the reactor demonstrates that the ratio of adenine nucleotides does not change significantly during the transition from the oscillatory to the damped phase after the O-ring was removed from the reactor (Figure 4.5). Moreover, it is important to note that the ratio of adenine nucleotides in the damped state (after 16 h of feeding) is still appropriate to induce the negative feedback on the PFK reaction. This indicates that damping of glycolytic oscillations in this experiment is not induced due to the supply-demand problem, as it was found for Figure 4.1. Obviously, additional factors are required to increase the duration of glycolytic oscillations in the open spatial reactor. These factors will be discussed in the next section.

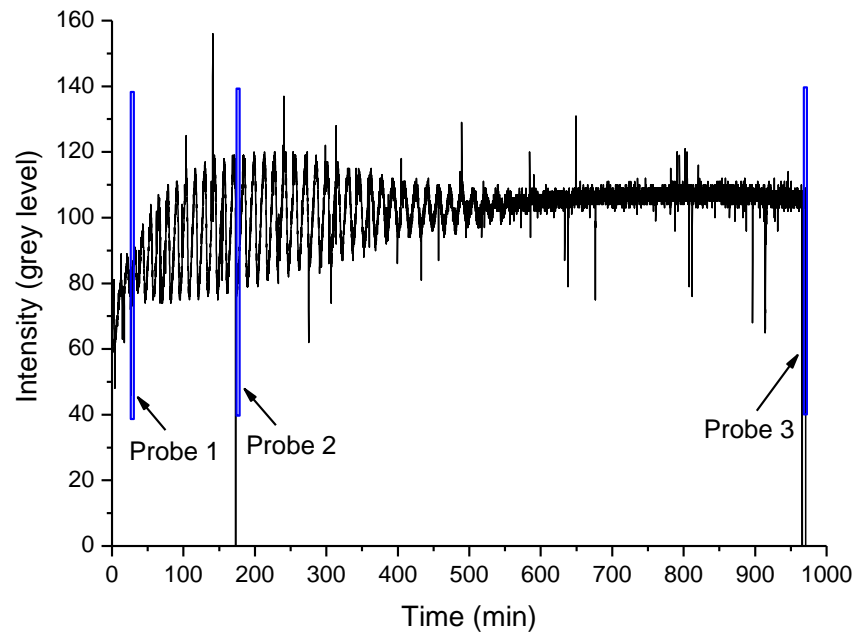


**Figure 4.4:** Glycolytic oscillations in the open spatial reactor after removal of the O-ring from the reactor. The reactor was fed with the same solutions as for Figure 4.1. For the experimental procedure see section 3.3.3. The blue marks indicate the time intervals in which the probes from the outlet of the reactor were taken for the enzymatic analysis of the glycolytic intermediates. The stirring rate is 500 rpm. The feeding rate is 6.6 ml/h. The protein concentration in the yeast extract is 24 mg/ml.

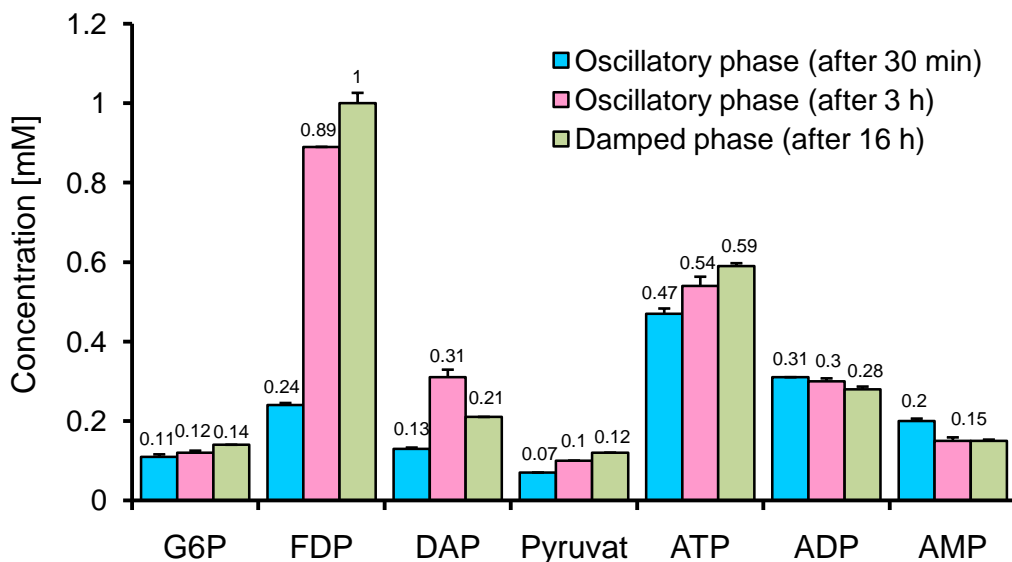


**Figure 4.5:** Determination of glycolytic intermediates after removal of the O-ring from the reactor. The probes were taken at the time instants marked in Figure 4.4 as probe 1 (after 30 min), probe 2 (after 3 h), and probe 3 (after 16 h).

### 4.1.3 Effect of the protein concentration on the duration of oscillations

In section 4.1.2 the experimental conditions were established under which the yeast extract oscillates for about 10 h. This is about five times longer than the oscillations observed under batch conditions. However, the duration of oscillations can be further increased by varying the protein concentration of the yeast extract.

Among the proteins of yeast extract are the enzymes, which are catalysts of the glycolytic reactions, and consequently, a variation of the concentration of these enzymes should lead to changes in the dynamics of the oscillations. Because it is not possible to determine the concentration of each individual enzyme, the concentration of all enzymes and proteins, present in the yeast extract was used as a measure for the enzyme concentration (for the measurement of protein concentration see section 3.1.4).

Figure 4.6 displays the duration of oscillations as a function of the protein concentration. An increase of the protein concentration from 23 to 80 mg/ml results in a prolongation of the glycolytic oscillations from 10 up to 40 h. An example of such long-lasting oscillations is shown in Figure 4.7.

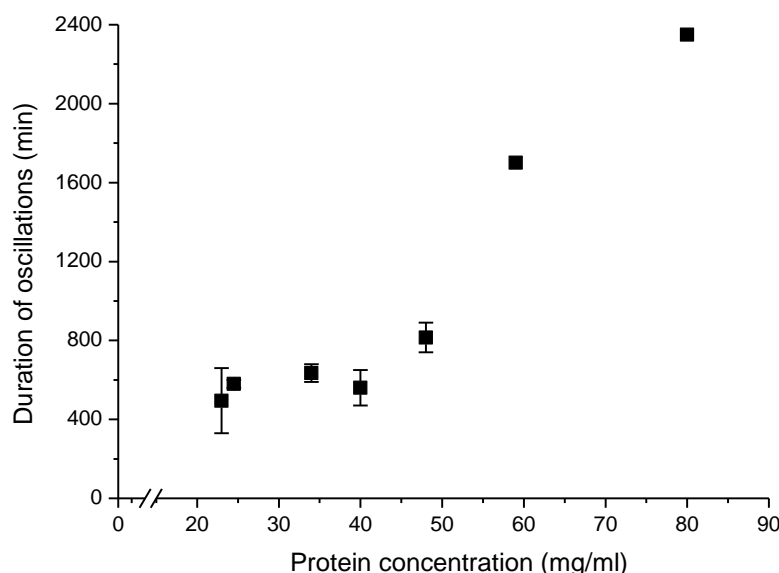


**Figure 4.6:** Effect of protein concentration on the duration of oscillations. The protein concentration was determined by the Lowry method (see section 3.1.4). The results represent the mean of at least three different experiments, except for protein concentrations higher than 60 mg/ml, where only one representative experiment is given. The standard deviation is shown as error bars.

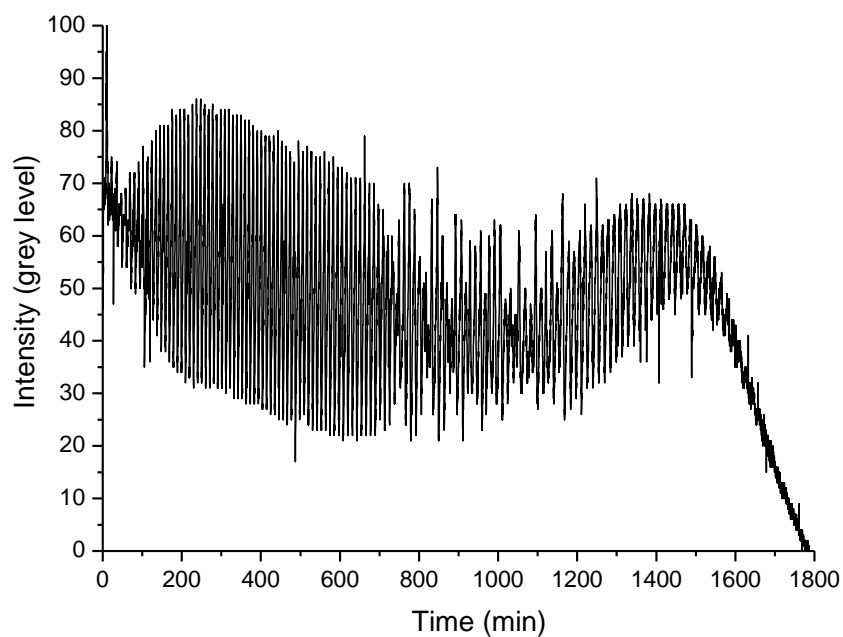


**Figure 4.7:** Sustained glycolytic oscillations in the open spatial reactor. The experiment was performed with a protein concentration of 59 mg/ml. For the experimental procedure and composition of the feeding solution see section 3.3.3.

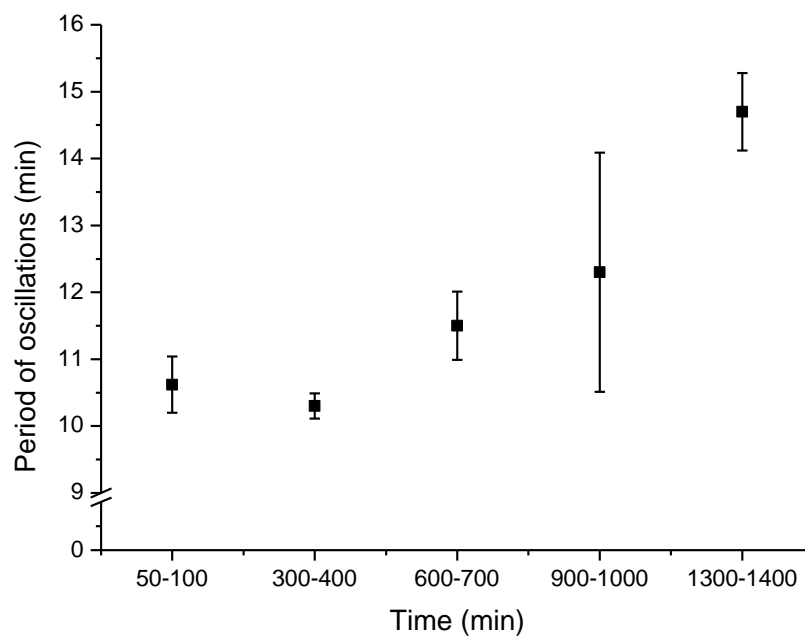


**Figure 4.8:** Increase of period of oscillations in the course of experiment. The period was calculated at different time points of the experiment shown in Figure 4.7. The protein concentration of yeast extract is 59 mg/ml. The standard deviation is shown as error bars.

The period of oscillations is not constant and increases from 10.5 min to 14.5 min in the course of the experiment (Figure 4.8).

## 4.2 Formation of glycolytic patterns in an open spatial reactor

When the autocatalytic reaction is coupled to mass transport processes, such as diffusion, oscillatory glycolysis is associated with the generation of reaction-diffusion waves (see section 2.4). This has been first shown by theoretical analysis [79] and later confirmed experimentally [20;100]. The open spatial reactor has a diffusive layer supporting the coupling of an autocatalytic reaction and diffusion, which is a necessary condition for the formation of spatio-temporal patterns.

### 4.2.1 Temporal development of spatial patterns

Figure 4.9 displays travelling NADH waves in the open spatial reactor. After an induction time of about 20 min, NADH waves were spontaneously generated. The dynamics of these waves is illustrated in the form of a time-space plot in Figure 4.10. At first NADH waves propagate from the centre of the gel to the borders (Figure 4.9-A). These outwardly propagating waves are indicated with the arrow marked A in the time-space plot (Figure 4.10). The waves break up into small wave segments when reaching a certain distance from the borders of the gel. After a transient phase, which lasts approximately for 1 h, the NADH waves become more stable and develop into rotating spirals and/or outwardly propagating large waves. The formation of rotating spirals is indicated with a black oval mark in the time-space plot (Figure 4.10). One of these spirals indicated with an arrow marked B in the time-space plot (Figure 4.10) is shown in Figure 4.9-B. After a while, these waves start to propagate mainly in the middle of the gel, and do not reach the borders, whereas spatial oscillations were observed at the borders of the gel. They are indicated by a red oval mark in Figure 4.10. Finally, towards the end of the experiment, small outwardly propagating, short-distance waves popped up randomly (Figure 4.9-C). These waves are indicated by an arrow marked C in the time-space plot (Figure 4.10).

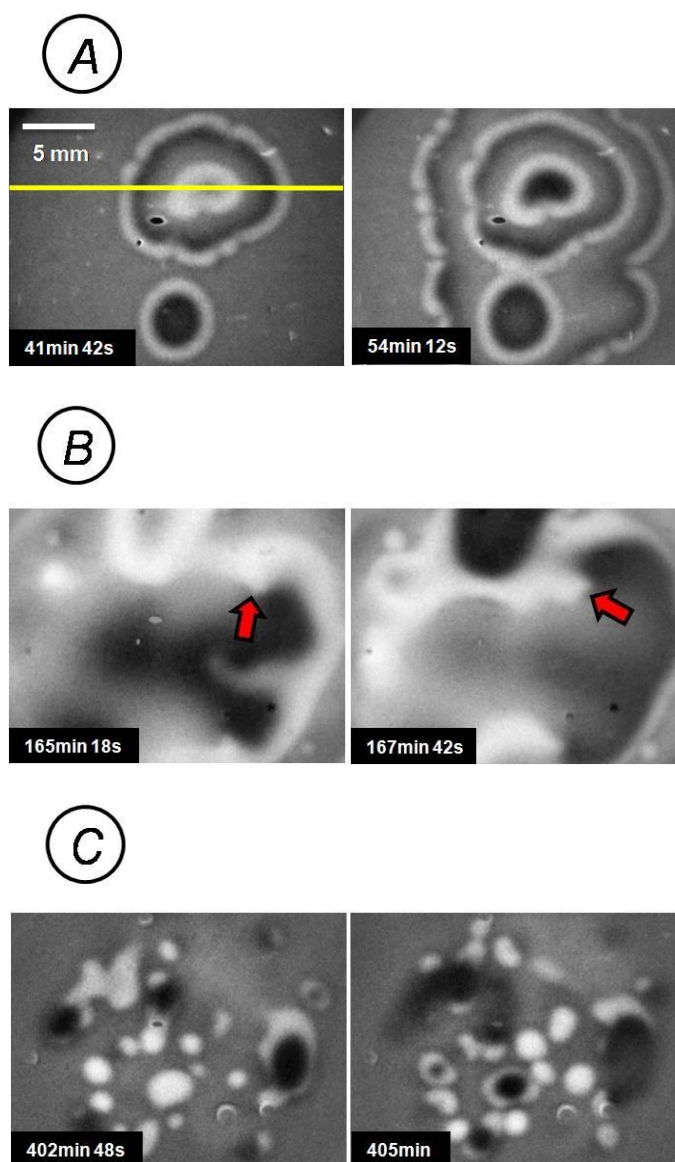


**Figure 4.9:** Spontaneous generation of NADH waves in the open spatial reactor. The spatial distribution of NADH in the gel was monitored with a camera (see section 3.3.4). Note, that the area of observation is the gel at three different time points, which are indicated with the arrows marked A, B and C in Figure 4.10). Grey levels quantify the NADH concentration, with white corresponding to maximum and black to minimum. For the experimental procedure and composition of the feeding solution see section 3.3.3. The protein concentration is 40 mg/ml. (A) Outwardly propagating NADH waves, which break up into small wave segments upon reaching a certain distance from the borders of the gel. (B) Counterclockwise rotating spiral. The tip of the spiral is indicated by a red arrow. (C) Outwardly propagating short distance waves.

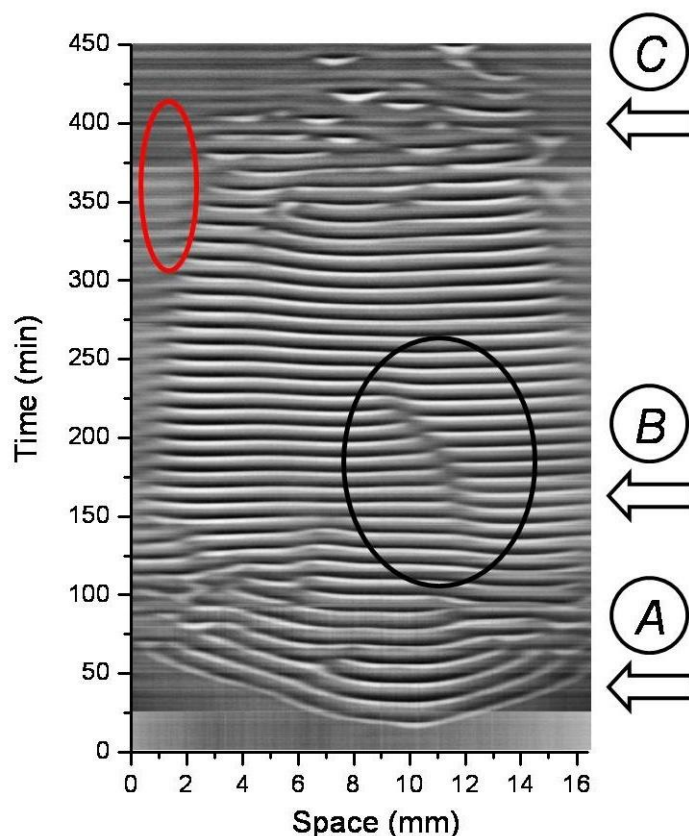


**Figure 4.10:** Time-space plot of propagating NADH waves, shown in Figure 4.9. The horizontal yellow line in the left image of Figure 4.9-A marks the image line that was used for construction of this time-space plot. The intensity profile of this line from each image of the movie was plotted as a function of time. The arrows marked A, B, and C indicate the time instant when the waves shown in Figure 4.9 appear. The black and red ovals mark a rotating spiral (see Figure 4.9-B) and the spatial oscillations, respectively.

#### 4.2.2 Effect of the protein concentration on the spatio-temporal dynamics of glycolysis

In section 4.1.3 the effect of the protein concentration on the temporal dynamics of glycolysis was investigated. It was shown that an increase of the protein concentration results in an increase in the duration of oscillations. Since glycolytic oscillations are associated with the generation of travelling NADH waves, it is also worthwhile to investigate the effect of protein concentration on the spatial pattern formation.

When the protein concentration was varied between 23 and 91 mg/ml, different types of spatial patterns were observed.

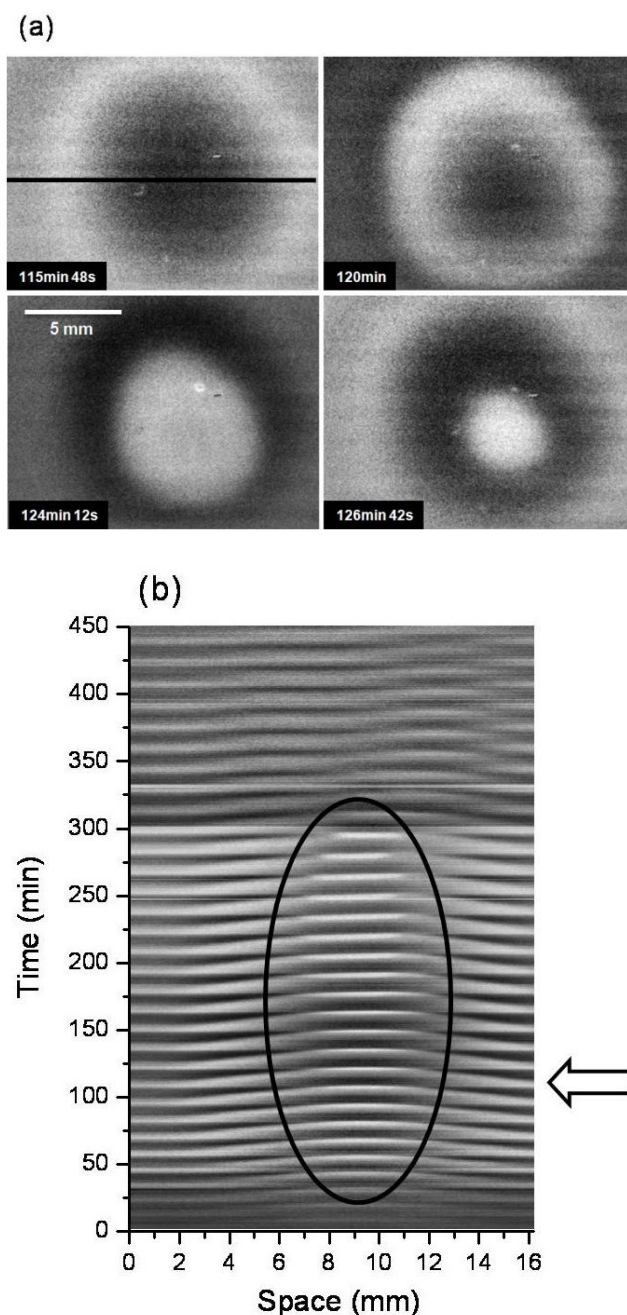


**Figure 4.11:** (a) Inwardly propagating NADH waves in the open spatial reactor. Large circular NADH waves spontaneously emerge after an induction time and propagate from the borders of the gel to the centre. The spatial distribution of NADH in the gel was monitored with a camera. Grey levels quantify the NADH concentration, with white corresponding to maximum and black to minimum. The protein concentration of the yeast extract is 25 mg/ml. (b) Time-space plot of the large inwardly propagating NADH waves. The horizontal line indicated in the first image of (a) marks the image line that was used for construction of a time-space plot. The intensity profile of this line from each image of the movie was plotted as a function of time. An oval mark indicates the annihilation of the inwardly propagating waves in the centre of the gel. An arrow indicates the time point at which the waves in (a) occur. For the experimental procedure and composition of the feeding solution see section 3.3.3.



For protein concentrations from 23-34 mg/ml, large inwardly propagating circular waves were always found. An example of these waves is shown in Figure 4.11a. Circular-shaped waves propagate from the borders of the gel and annihilate in the middle. Annihilation of the waves is indicated by an oval mark in the time-space plot (Figure 4.11b). The time-space plot illustrates ordered propagation of the waves in time. Only towards the end of the experiment, the waves can change their dynamics and start to propagate from the left of the gel to the right (Figure 4.11b). In some experiments they change their dynamics from inwardly propagating to outwardly propagating waves or spiral(s). Transition from the inwardly propagating waves to the outwardly propagating spirals will be shown in section 4.3.2.1. Changes of the wave dynamics in the later stage of the experiment are also observed at a protein concentration of 34 mg/ml. In this case the waves change their direction only from inwardly to outwardly propagating waves.

For protein concentrations of 40-59 mg/ml, outwardly propagating waves are always found in the beginning of the experiment (Figure 4.9-A). After a transient phase, lasting for about 1 h, these waves developed into patterns with large thickness. These patterns can form either rotating spiral(s) or outwardly propagating circular waves (Figure 4.9-B). The thickness of the waves before and after the transient phase increases from 0.67 mm to 2 mm. Finally, in the end of the experiment, small outwardly propagating short distance waves are always observed (Figure 4.9-C). The detailed description of the dynamical changes of these waves is given in section 4.2.

Starting from a protein concentration of 71 mg/ml, dot-shaped NADH waves were always found as shown in Figure 4.12a. The time instant when these waves appear is indicated with an arrow marked A in the time-space plot (Figure 4.12b). In the beginning of the experiment, dot-shaped waves emerge randomly in the gel and later develop into outwardly propagating short-distance waves. Shortly thereafter, spatial oscillations, which randomly propagate through the gel, are observed in addition to the short-distance propagating waves. The spatial oscillations can be seen in the domain of the time space plot indicated with arrows marked B and C (Figure 4.12b). In the time interval indicated with an arrow B (Figure 4.12b), both spatial oscillations (indicated by the red arrows) and outwardly propagating short-distance waves (indicated by the yellow circles) coexist. However, towards the end of the experiment, (arrow marked C

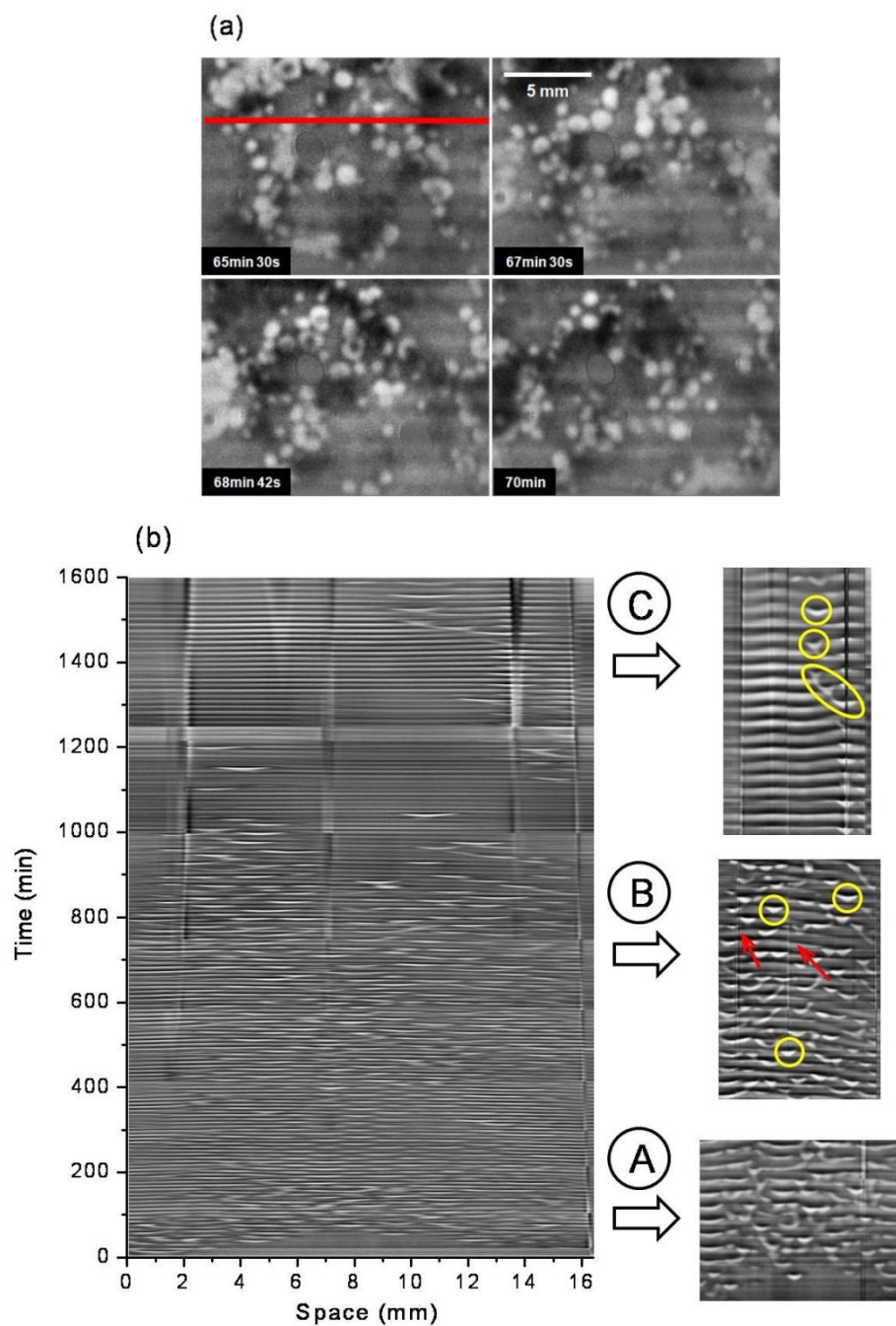


**Figure 4.12:** (a) Dot-shaped NADH waves in the open spatial reactor. Later, these patterns develop into short-distance propagating waves. For the experimental procedure and composition of the feeding solution see section 3.3.3. The protein concentration of the yeast extract is 91 mg/ml. (b) Time-space plot of the dot-shaped NADH waves. The plot was constructed along the horizontal line, indicated in the first image of (a). The intensity profile of this line from each image of the movie was plotted as a function of time. The arrows marked A, B, and C indicate the magnification of the time-space plot at different instants of time. An arrow marked A indicates the time point at which the waves in (a) are shown. The yellow oval and circles in the time-space plot indicated with an arrow B and C mark the outwardly propagating short-distance waves. The red arrows in the time-space plot indicated with B mark spatial oscillations.

**Table 4.1:** Summary of all types of waves observed in the open spatial reactor at different protein concentrations.

Type of waves	Protein concentration (mg/ml)							
	23-28	34	40	47-49	59	71	80	91
Inwardly propagating large circular waves	X	X						
Outwardly propagating large circular waves	X	X	X	X	X			
Large rotating spiral(s)			X	X	X			
Segmented waves			X	X	X			
Outwardly propagating short-distance waves			X	X	X	X	X	X
Dot-shaped waves						X	X	X
Only spatial oscillations					X	X	X	X
Coexistence of trigger waves and spatial oscillations			X	X	X	X	X	X
Coexistence of dot-shaped waves, planar waves and spatial oscillations						X	X	X
Coexistence of short-distance propagating waves and spatial oscillations					X	X	X	X

in Figure 4.12b) mainly spatial oscillations are found together with a few outwardly propagating short-distance waves, which are indicated by the yellow oval and the circles in Figure 4.12b-C.

The different types of waves which are observed at protein concentrations of yeast extract ranging from 23 to 91 mg/ml are summarized in Table 4.1. In general, seven different types of waves and wave combinations are observed during glycolysis in the open spatial reactor. These are inwardly and outwardly propagating large target waves, large rotating spiral(s), segmented waves, dot-shaped waves, outwardly propagating short-distance waves and spatial oscillations.

For low protein concentrations, one or two types of waves are found, while for protein concentrations higher than 40 mg/ml, five or six types of waves and wave combinations are observed. The most common types of waves are the outwardly propagating short distance waves and trigger waves coexisting with spatial oscillations.

### 4.2.3 Analysis of the wave dynamics

In order to characterize the propagation dynamics of the waves, the velocity, period, and thickness of the waves were analysed at different protein concentrations in the yeast extract. The velocity and period of the waves were obtained from the time-space plots (see section 3.3.5).

For some type of waves, as for example the outwardly and inwardly propagating large waves, it was not possible to measure the wavelength, because two subsequent waves could not be observed in a single image (see Figure 4.13b). Therefore, for all types of waves, the thickness of the waves was evaluated instead of the wavelength. The thickness of the waves ( $d$ ) was measured directly from the images as shown in Figure 4.13. The relationship between the wavelength and the thickness of the waves is given by:  $d = (\lambda - r)$ , where,  $d$  is the thickness of the wave,  $\lambda$  is the wavelength of the waves, and  $r$  is the distance between two subsequent waves.

The analysis of the waves was performed for the following most frequently observed types of waves: inwardly and outwardly propagating large waves, segmented waves and outwardly propagating short-distance waves (see Table 4.1).

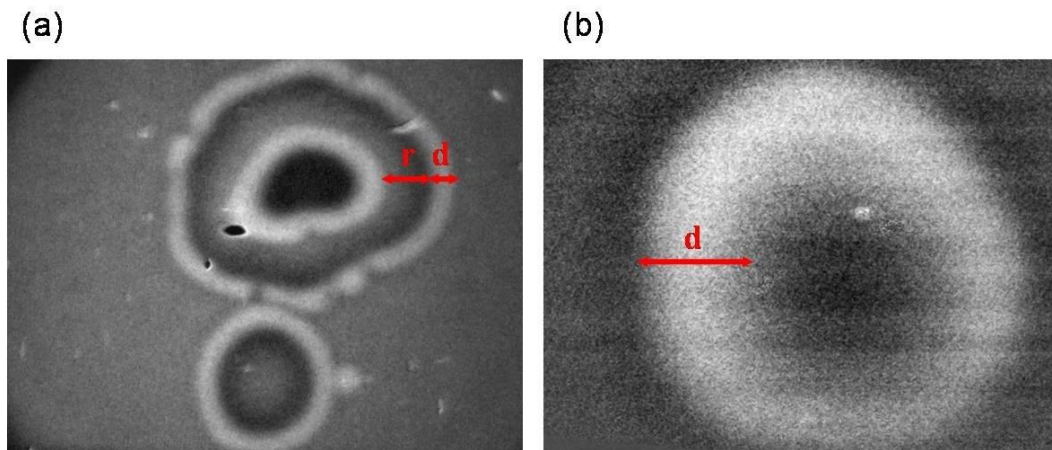


**Figure 4.13:** Determination of wave thickness from the images. “r” corresponds to the distance between two subsequent waves, “d” corresponds to the thickness of the waves. (a) Outwardly propagating waves, (b) inwardly propagating large waves. Please, note that two inwardly propagating waves could not be observed in one experiment. Size of images are  $16.2 \times 12.4$  mm.

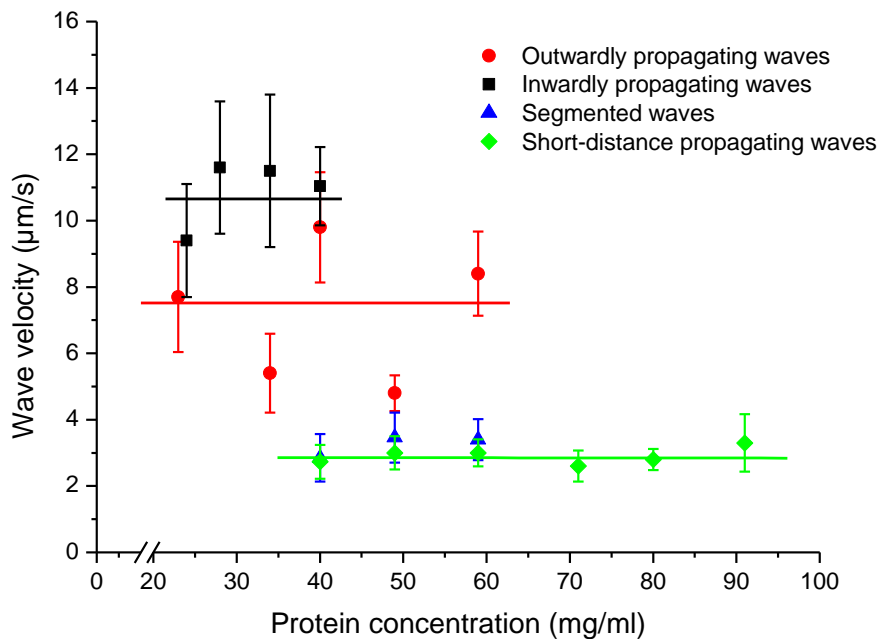


**Figure 4.14:** Velocity of different types of waves as a function of protein concentration. The velocity was calculated from the slope of the lines in the time-space plot (see section 3.3.5). The results represent the mean of two to four different experiments. The standard deviation of these results is shown as error bars. The solid lines are drawn to indicate three different ranges of the velocity in dependence on the type of the waves. The black line corresponds to the inwardly propagating waves, the red line to the outwardly propagating waves and the green line to the short distance propagating waves and segmented waves.

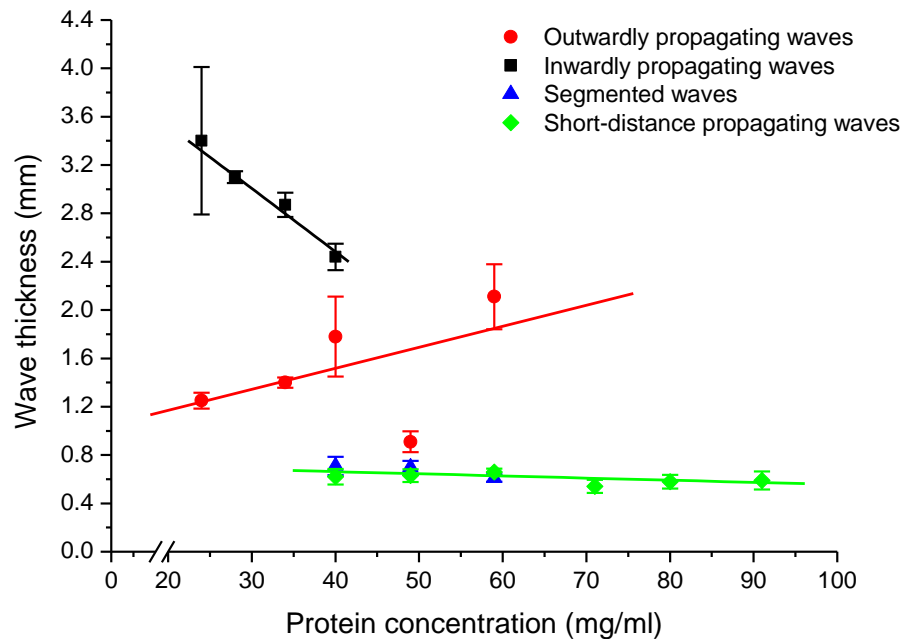


**Figure 4.15:** Thickness of different types of waves as a function of protein concentration. The thickness of the waves was measured from the images as shown in Figure 4.13. The results represent the mean of two to four different experiments. The standard deviation of these results is shown as error bars. The solid lines are drawn to indicate three different ranges of the thicknesses depending on the type of the waves. The black line corresponds to the inwardly propagating waves, the red line to the outwardly propagating waves and the green line to the short distance propagating waves and segmented waves.

The results of the analysis show that the velocity and thickness of the different types of waves can be separated into 3 distinct ranges. These ranges are indicated by the lines in Figure 4.14 and Figure 4.15. Each of this range corresponds to one type of wave, except for the segmented waves and short distance propagating waves. These two types of waves have similar values of the velocity and thickness, and can be considered as belonging to one range (green line in Figure 4.14 and Figure 4.15).

Each type of wave is characterized by a particular value for the velocity and thickness. The velocity of each type of waves is constant and does not change when varying the protein concentration (Figure 4.14). However, the thickness of the waves is constant only for the segmented waves and short distance propagating waves, but varies for the outwardly and inwardly propagating waves with protein concentration (Figure 4.15). By increasing the protein concentration of the yeast extract from 23 to 91 mg/ml

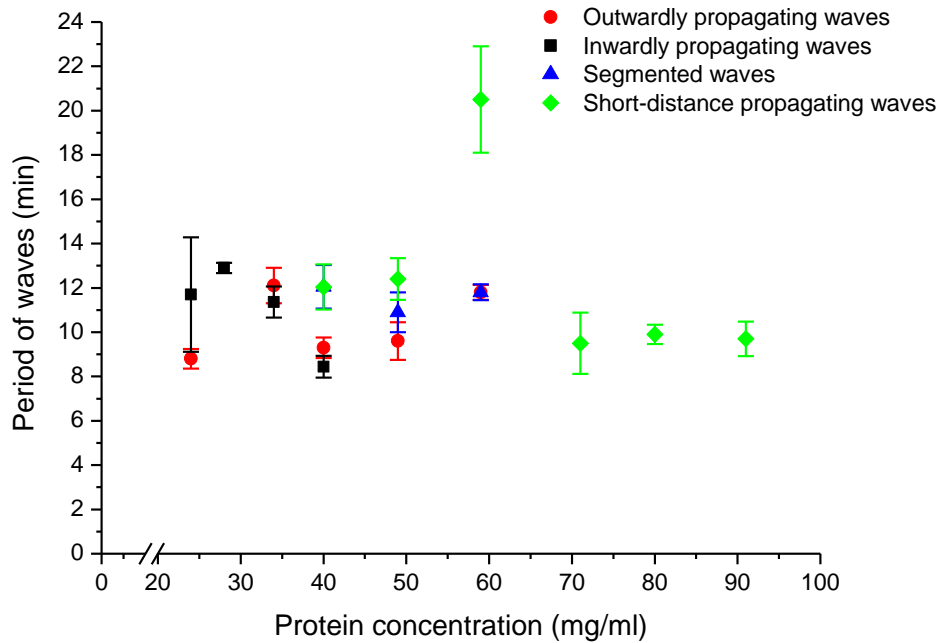


**Figure 4.16:** Period of different types of waves as a function of the protein concentration. The period was calculated from the time-space plot as a distance between two wave maxima in a vertical direction (see section 3.3.5). The results represent the mean of two to four different experiments. The standard deviation of these results is shown as error bars.

the thickness of the inwardly propagating waves decreases from 3.6 to 2.4 mm, while that of the outwardly propagating waves increases from 1.2 to 2.0 mm.

The period is similar for all type of waves and varies between 8 and 14 min for different protein concentrations (Figure 4.16).

When comparing the dynamics of the different wave types, one can see that the inwardly propagating waves have the highest values for the thicknesses and propagation velocities, which are given by 3 mm and 11  $\mu\text{m/s}$ , respectively. Outwardly propagating waves propagate at a somewhat slower velocity (7.5  $\mu\text{m/s}$ ) and they have half of the thicknesses of the inwardly propagating waves (1.6 mm). Finally, the slowest waves with the narrowest profiles are found for the segmented and short-distance propagating waves, which have thicknesses of 0.6 mm and propagate with velocities of 2  $\mu\text{m/s}$ .

#### 4.2.4 Phase waves and reaction diffusion waves

The differences in wave velocity and thickness described in the section 4.2.3 show clearly that the various types of waves differ not only in their structural properties, but also in their dynamical characteristics. The most pronounced differences are found for the inwardly propagating waves. The velocity and thickness of these waves are significantly higher than the velocity and thickness of the outwardly propagating, short-distance propagating and segmented waves. This suggests that the mechanism of wave formation for the inwardly propagating waves is different from that of the other types of waves.

From theoretical studies of wave dynamics using the complex Ginzburg-Landau equation, it was suggested that the inwardly propagating waves correspond to phase waves with an inwardly pointing phase velocity [61;63;101] (see section 2.1.2).

In order to check whether the inwardly propagating waves correspond to phase waves, experiments were performed with a gel, which was separated into two pieces by means of an impenetrable barrier (see section 3.3.2). These experiments were conducted with yeast extract at low protein concentrations (24.5 mg/ml), where inwardly propagating large waves were observed, and with yeast extract at high protein concentrations (59 mg/ml, where outwardly propagating waves were found. In the case of phase waves, it is expected that the waves will cross the barrier and propagate into the other half of the gel, while reaction-diffusion waves cannot cross the barrier.

The temporal sequence of the spatial structures for protein concentrations of 24.5 mg/ml and 59 mg/ml is shown in Figure 4.17 and Figure 4.18, respectively. For inwardly propagating large waves (protein concentration 24.5 mg/ml), it was found that the waves propagate from the borders of the gel to the centre without stopping at the barrier. The yellow arrows in Figure 4.17 indicate how the waves, formed below the barrier, cross the barrier and propagate to the upper part of the gel. This suggests that inwardly propagating waves are phase waves, and propagate due to the phase shifted oscillations.



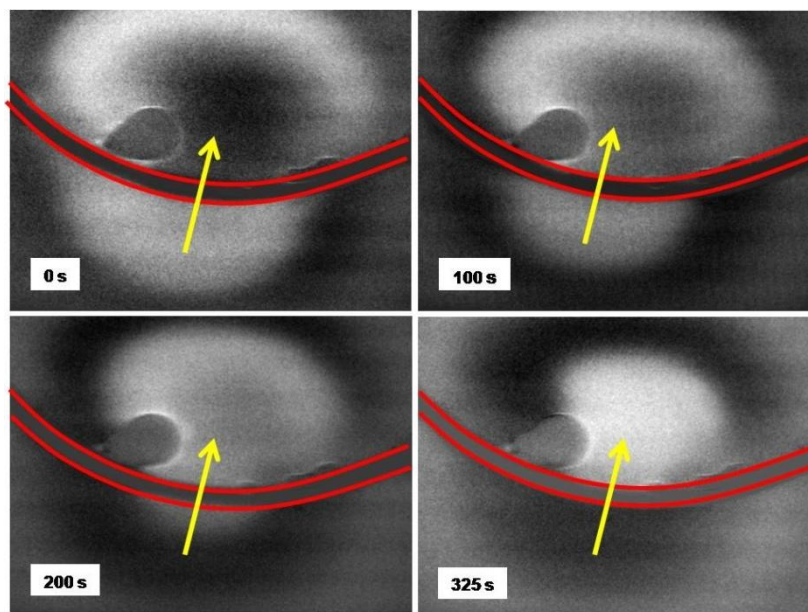


**Figure 4.17:** Inwardly propagating NADH waves in the gel with a barrier. An O-ring from rubber was used as a barrier to separate the gel into two pieces (for details see section 3.3.2). The O-ring in the gel is indicated by red curves. The yellow arrows indicate how the waves cross the barrier and propagate from the lower part to the upper part of the gel. The protein concentration of the yeast extract is 24.5 mg/ml. For the experimental procedure and composition of the feeding solution see section 3.3.3. The image size is 15.1 mm  $\times$  12 mm.

A different behaviour is observed for the outwardly propagating waves (protein concentration 59 mg/ml). In this case, the outwardly propagating waves are observed in both halves of the gel. However, the waves propagating in one half of the gel can neither cross the barrier nor propagate to the other half of the gel (Figure 4.18). This kind of behaviour is expected when the dynamics of the waves is described by means of a coupling between reaction and diffusion. Thus, it is suggested that outwardly propagating waves correspond to reaction-diffusion waves.

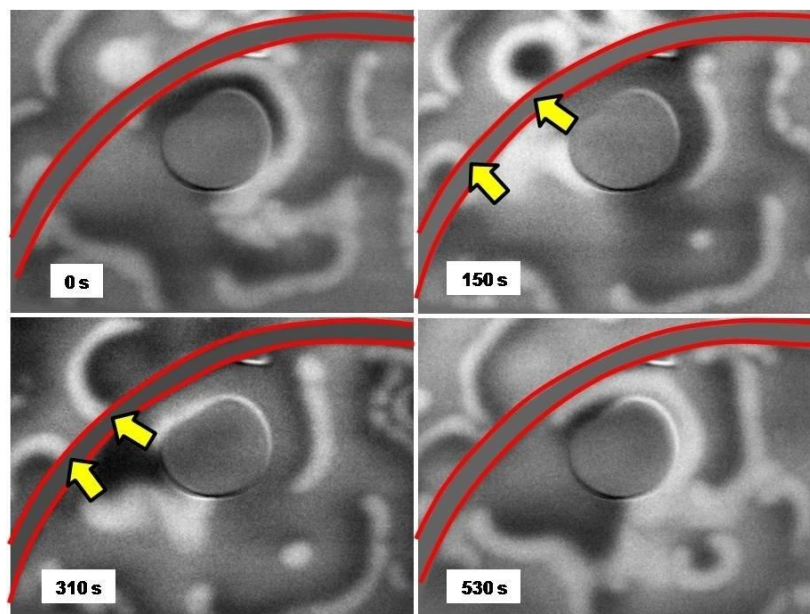


**Figure 4.18:** Outwardly propagating NADH waves in the gel with a barrier. An O-ring from rubber was used as a barrier to separate the gel into two pieces (for details see section 3.3.2). The red curve marks indicate the O-ring in the gel. The yellow arrows indicate how the outwardly propagating waves hit the barrier and cannot cross it. The protein concentration of the yeast extract is 59 mg/ml. For the experimental procedure and composition of the feeding solution see section 3.3.3. The image size is 15.1 mm  $\times$  11.2 mm.

#### 4.2.5 Dispersion relation at different protein concentrations

As additional parameter for characterization of the wave dynamics, namely, the dependence of the wave velocity on the wavelength was measured. This relationship is called dispersion relation. In general, dispersion relations characterize the dependence of the wave frequency on the wavelength and play an important role for understanding the dynamics of wave propagation (see section 2.1.1.1). Since the velocity is proportional to the wave frequency, the dispersion relation can be equally constructed by plotting the velocity of the waves as a function of the wavelength. Both, wave velocity and wavelength, were determined from the time-space plots. An example of such a time-space plot is shown in Figure 4.19. The wavelength ( $\lambda$ ) is determined as the distance between two subsequent wave fronts, and the wave velocity is given as the derivative of tangent of the second consecutive wave front (green line in Figure 4.19).

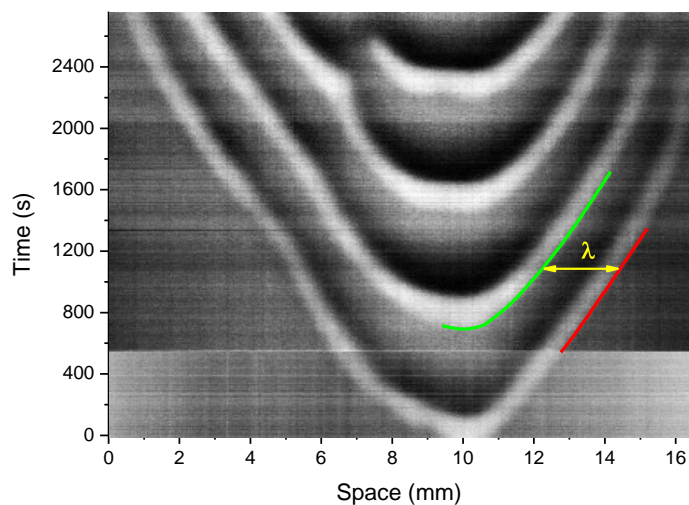


**Figure 4.19:** An example of a time-space plot, used for construction of dispersion curves. The first and second wave fronts are marked with red and green lines, respectively. The wavelength is indicated by  $\lambda$ . The velocity is calculated from the derivative of the tangent of the second wave front (green line). The protein concentration of the yeast extract is 40 mg/ml.

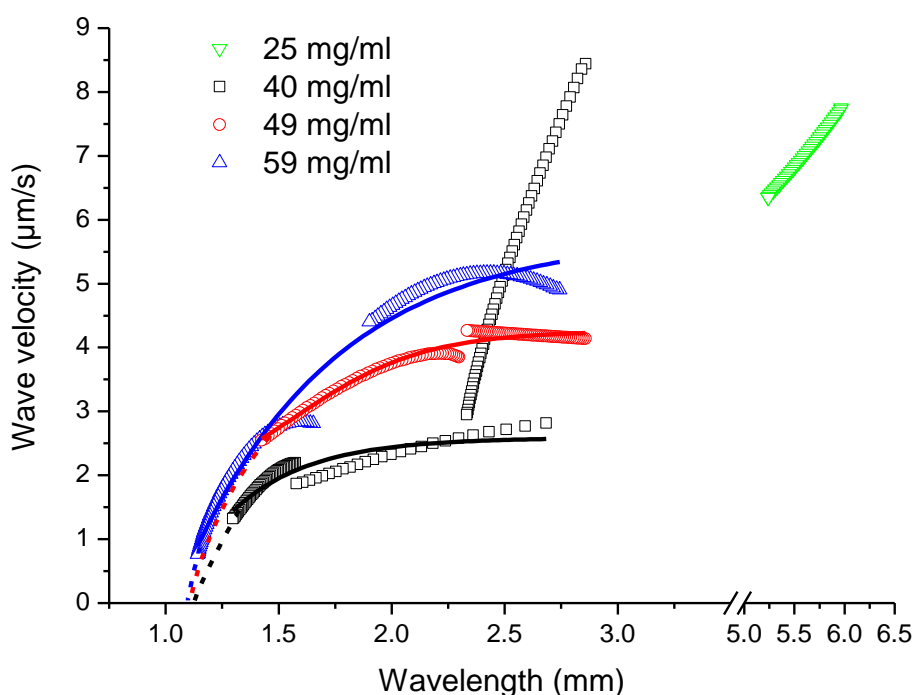


**Figure 4.20:** Dispersion curves for outwardly propagating waves at protein concentrations of 40 mg/ml (black squares), 49 mg/ml (red circles) and 59 mg/ml (blue triangles), and inwardly propagating waves at protein concentration of 25 mg/ml (green triangles). The solid and dashed lines represent fits and extrapolation of experimental data, respectively.

The dispersion relation was measured for outwardly propagating waves at protein concentrations of 40 mg/ml, 49 mg/ml and 59 mg/ml, and inwardly propagating large waves at a protein concentration of 25 mg/ml. The resulting dispersion curves are displayed in Figure 4.20. The velocity of outwardly propagating waves increases monotonously with increasing wavelength, approaching a constant velocity at 2.3  $\mu\text{m/s}$ , 4.2  $\mu\text{m/s}$ , and 5.2  $\mu\text{m/s}$  for protein concentrations of 40 mg/ml, 49 mg/ml, and 59 mg/ml, respectively (black, red, and blue lines in Figure 4.20). This type of dispersion curve corresponds to classical reaction-diffusion waves (see section 2.1.1.1) [58;59].

The extrapolation of the experimental data shows that the extraction of the absolute refractory zone of outwardly propagating waves approaches the same value (1.1 mm) for different protein concentrations (Figure 4.20). This suggests that the concentration profile of the inhibitor (ATP) in the outwardly propagating waves is not significantly affected by the protein concentration.

Interestingly, the dispersion relation of the outwardly propagating waves at a concentration of 40 mg/ml protein contains an additional branch, which grows infinitely for increasing wavelengths (Figure 4.20). This type of dispersion curve corresponds to the dispersion relation of phase waves (see section 2.1.2) [58;59]. A similar relationship is also observed for the inwardly propagating large waves (green triangles in Figure 4.20). Unfortunately, it was not possible to obtain this relationship for low values of velocity and wavelength of the inwardly propagating waves, because two subsequent wave maxima could not be observed in a single image (see section 4.2.3). The minimal wavelength which could be measured was 5.2 mm.

### 4.3 Analysis of spatio-temporal dynamics of glycolytic patterns

#### 4.3.1 Analysis of spatio-temporal turbulence at high protein concentrations

In this section the spatio-temporal dynamics of waves at high protein concentrations will be analysed. As it was already shown in section 4.2.2 at protein concentrations higher than 71 mg/ml, dot-shaped NADH waves were always observed (see Figure 4.12a). These waves appear randomly in the gel displaying irregular behaviour from the beginning of the experiment. In order to characterize the irregular dynamics of these patterns, the time-space plot of these waves (Figure 4.21a) was analysed by calculating the temporal and spatial correlation functions. For comparison, both correlation functions were also calculated for synchronously propagating inward waves (Figure 4.21b).

In order to calculate the spatial and temporal correlation function, an IDL programme was written by Frank Rietz (Group of Non-linear Phenomena, Otto-von-Guericke University of Magdeburg) according to reference [102;103]. The formula of these authors is given by:

$$C(t) = \frac{\langle \Delta G_t(r', t_0) \Delta G_t(r', t_0 + t) \rangle_{r'}}{\langle (\Delta G_t)^2 \rangle_{r'}} \quad (4.17)$$

$$C(r) = \frac{\langle G(r_0, t') G(r_0 + r, t') \rangle_{t'}}{\langle G^2 \rangle_{t'}}$$

where,  $\Delta G_t(r, t) = G(r, t) - \langle G(r) \rangle_t$ ,  $C(t)$  is the temporal correlation coefficient,  $C(r)$  is the spatial correlation coefficient,  $G$  is the grey level,  $t'$  and  $r'$  are the time and space, respectively, index zero indicates the starting point, and angular brackets represent an average over time or space.

Application of this programme to the time-space plots yields the following results. Figure 4.22 shows the temporal correlation functions for synchronously propagating inward waves (red line) and dot-shaped NADH waves (blue line). The temporal correlation coefficient for inwardly propagating waves oscillates periodically between 0.9 and -0.8, reflecting coherent behaviour of these waves in time. In contrast, the temporal correlation coefficient of NADH dot-shaped waves oscillates with rapidly damping amplitude and approaches zero at large values of  $t$  (Figure 4.22). This indicates

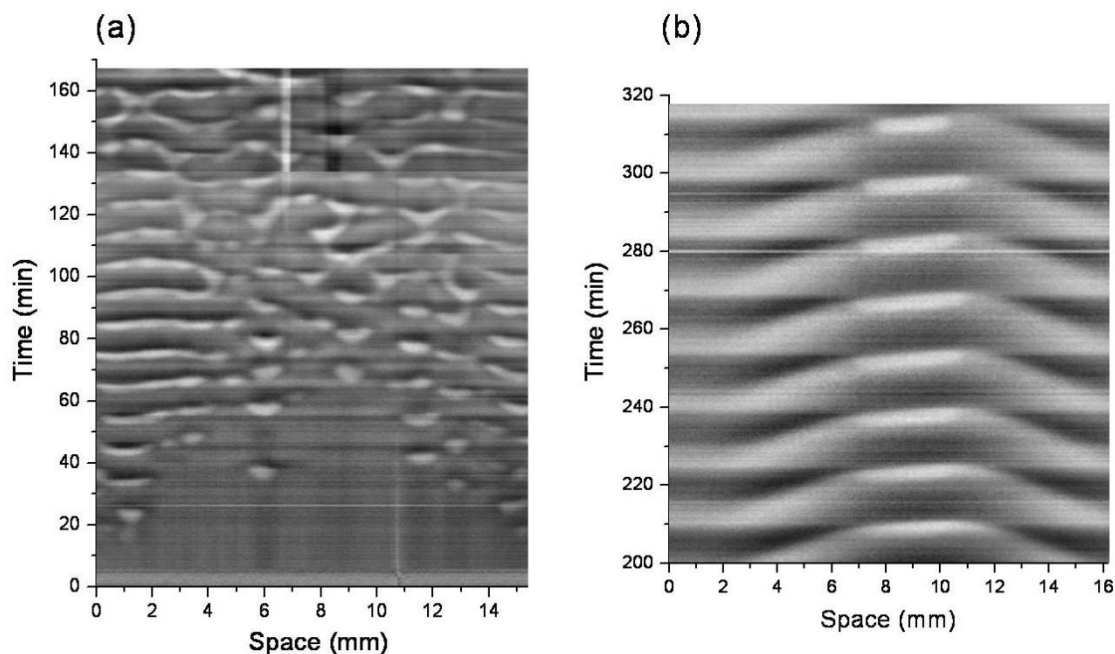


**Figure 4.21:** (a) Time-space plot of dot-shaped NADH waves. The temporal behaviour of dot-shaped NADH waves and the entire dynamics of these waves are shown in Figure 4.12. The protein concentration of the yeast extract is 71 mg/ml. (b) Time-space plot of synchronously propagating inward waves. The temporal behaviour of these waves and the time-space plot of the entire experiment are shown in Figure 4.11. The protein concentration of the yeast extract is 25 mg/ml. Please note, that in (b) the waves in the middle and in the borders have the same intensity, which is seemingly brighter in the middle.

that the temporal behaviour of dot-shaped NADH waves is incoherent.

Figure 4.23 shows the spatial correlation function for both types of waves. The spatial correlation function of synchronously propagating inward waves remains constant until the next maximum appears, where the correlation function shows a sharp transition to the anti-correlated phase (Figure 4.23). For the dot-shaped NADH wave the correlation function remains constant for small distances ( $r \leq 0.1$  mm), indicating a strong local coupling and approaching zero at larger values of  $r$  (Figure 4.23). In the range from 0.2 mm to 1.6 mm the correlation function exhibits power-law decay (black line in Figure 4.23). According to references [102-104], this implies the presence of chaotic motions in the dot-shaped NADH waves.

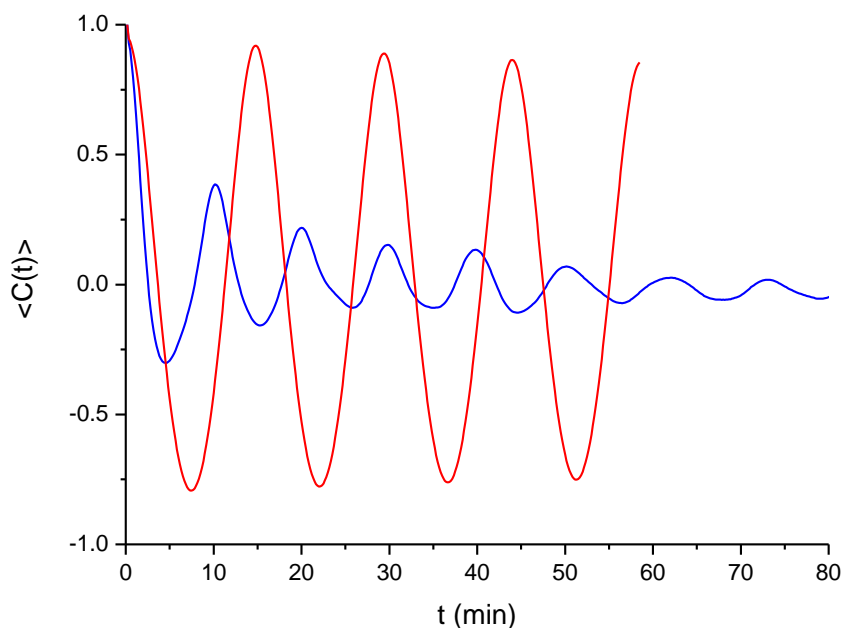


**Figure 4.22:** The temporal correlation function for synchronously propagating inward waves (red line) and dot-shaped NADH waves (blue line). The temporal correlation function was calculated from the time-space plots shown in Figure 4.21.

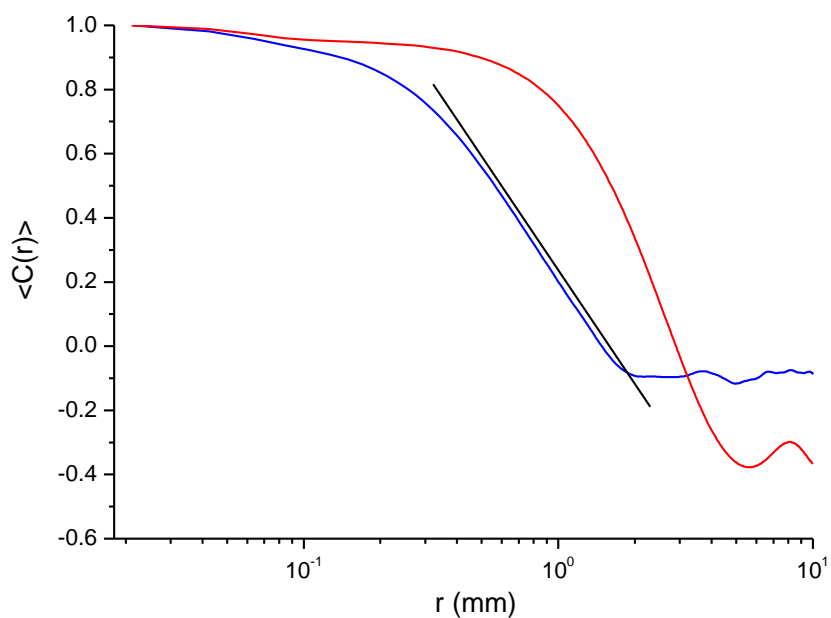


**Figure 4.23:** Spatial correlation function for synchronously propagating inward waves (red line) and dot-shaped NADH waves (blue line). The radius ( $r$ ) is plotted in logarithmic scale. The spatial correlation function was calculated from the time-space plots shown in Figure 4.21. The black line indicates the slope of power-law decay (-1.18) for dot-shaped NADH waves.

### 4.3.2 Desynchronisation of spatial patterns at low protein concentrations

The structure of glycolytic waves in the open spatial reactor changes from one type to another in the course of an experiment (see section 4.2). During this change, the waves pass through a transient phase, which is characterized by complex spatio-temporal patterns. One possible reason for this behaviour could be desynchronization of the wave dynamics over time.

To analyse the coherence of the patterns in general and to check whether desynchronization is involved during the transient phases, the dynamics of the spatio-temporal patterns was analysed by the Karhunen-Loève (KL) decomposition. This was done for a protein concentration of 24 mg/ml, where the waves change their propagation dynamics from inwardly propagating waves to outwardly propagating target waves or spiral waves.

#### 4.3.2.1 Transition from inwardly propagating patterns to outwardly propagating spirals

Figure 4.24 shows temporal oscillations of the NADH fluorescence averaged over a small area ( $40 \times 40 \text{ pix}^2$ ) indicating a local oscillatory dynamics. The analysis of this time series in conjunction with the observed spatio-temporal patterns suggests a division of the experiment into three distinct time intervals. The first interval (0-120 min) is clearly non-stationary. It is characterized by a rapid decrease of the NADH fluorescence. Here an equilibration between the gel and the feeding solutions takes place, since the metabolic/ionic compositions in the gel and in the reactor are different at the beginning of the experiment. Interestingly, large inwardly propagating circular waves are observed during this stage of the experiment (Figure 4.25) with a thickness and wave velocity of 4 mm and 14  $\mu\text{m/s}$ , respectively.

In the course of the second interval (120-240 min), a transition from inwardly propagating waves to outwardly propagating spirals is found (Figure 4.26), while the local dynamics acquires a second, modulating frequency (Figure 4.24, interval 2). This modulation could be caused by the interaction between two competing patterns in the transition region.



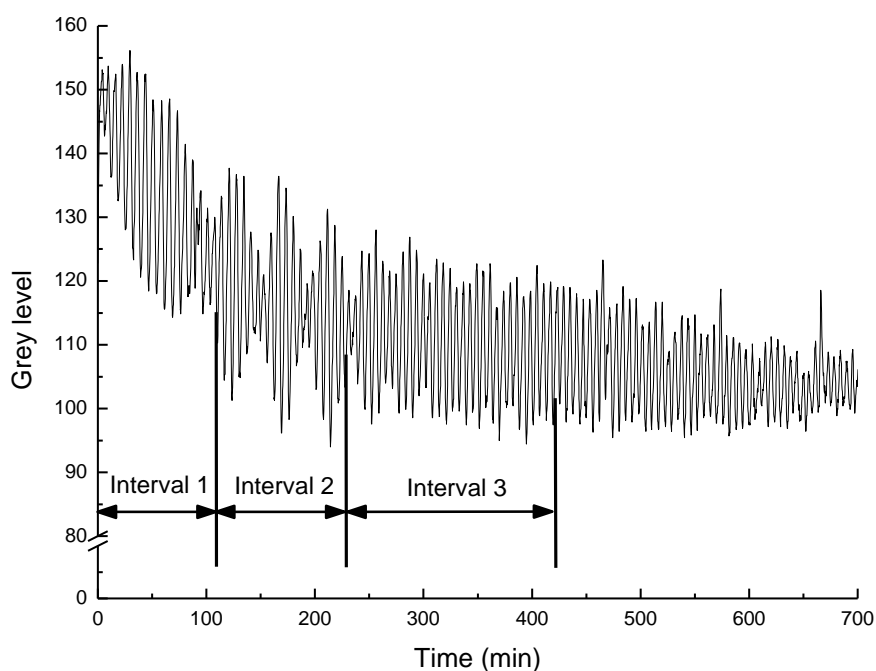


**Figure 4.24:** Temporal dynamics of yeast extract in the open spatial reactor. Intensity of NADH fluorescence was averaged over a small area ( $40 \times 40 \text{ pix}^2$ ) taken from the total observation area ( $540 \times 740 \text{ pix}^2$ ). The protein concentration of the yeast extract is 24 mg/ml. For the experimental procedure and composition of feeding solution see section 3.3.3. The experiment was divided into three distinct time intervals. Each interval was analysed separately by KL decomposition.

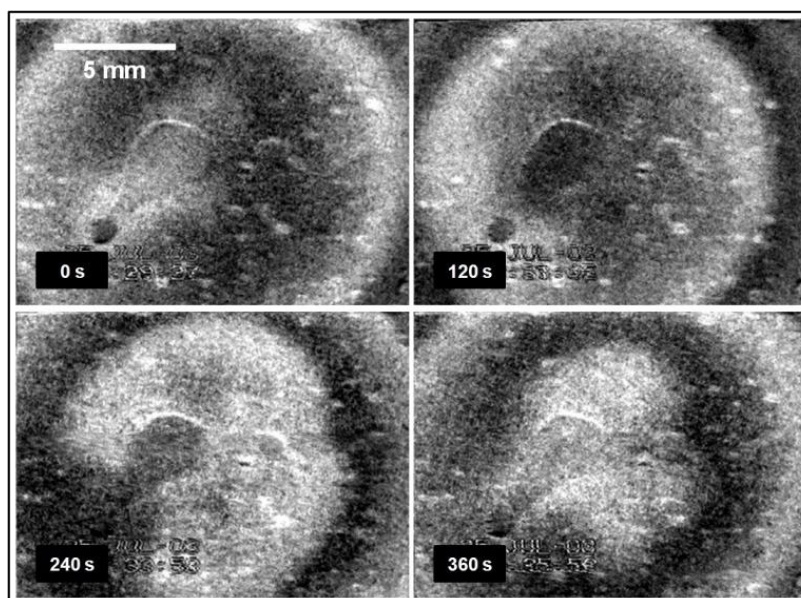


**Figure 4.25:** Spatial dynamics of yeast extract in the time interval 1, indicated in Figure 4.24. The spatial distribution of NADH in the gel was monitored with a camera (see section 3.3.4). Grey levels quantify the NADH concentration, with white corresponding to maximum and black to minimum. Large circular NADH waves propagate from the borders of the gel to the centre.

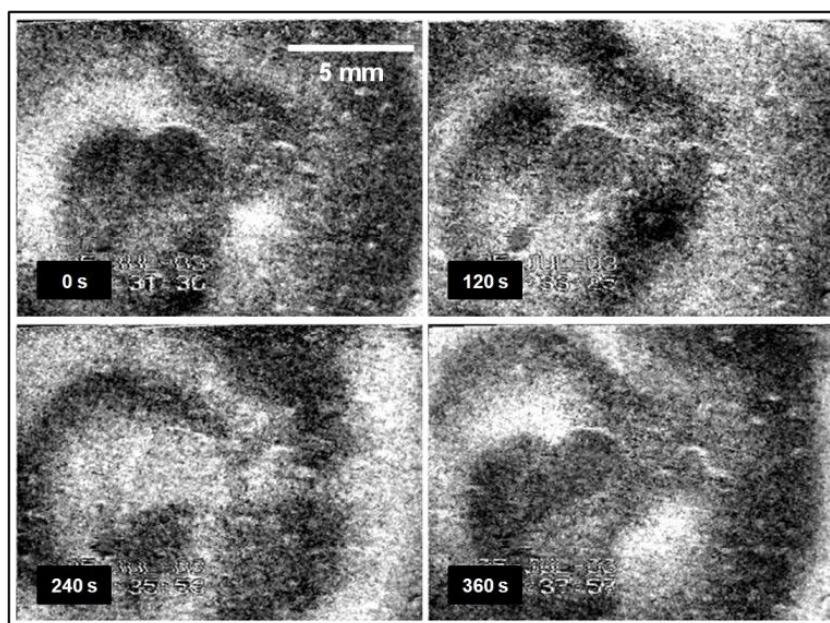


**Figure 4.26:** Spatial dynamics of yeast extract in the time interval 2, indicated in the Figure 4.24. Grey levels quantify the NADH concentration, with white corresponding to maximum and black to minimum. Transient phase, where transition from inwardly propagating NADH waves to outwardly propagating spirals takes place.

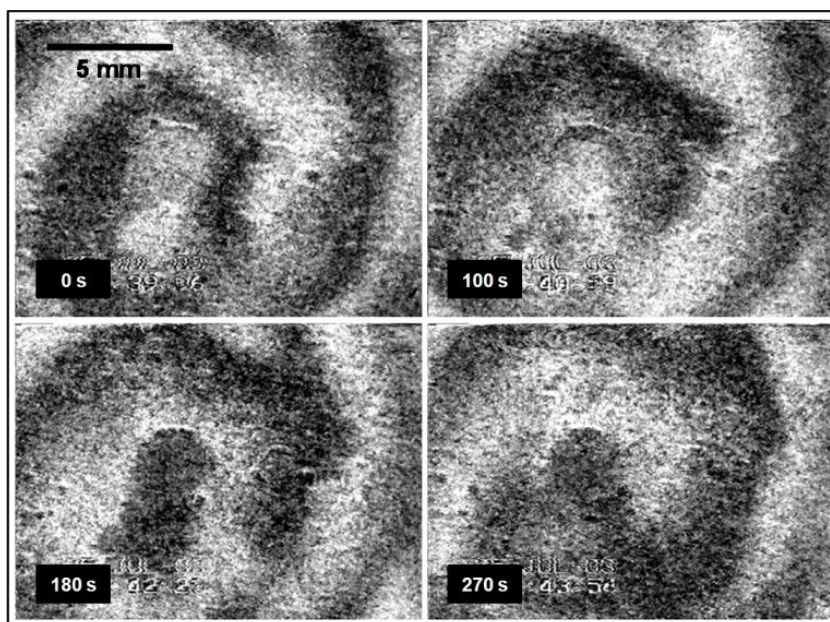


**Figure 4.27:** Spatial dynamics of yeast extract in the time interval 3, indicated in the Figure 4.24. Grey levels quantify the NADH concentration, with white corresponding to maximum and black to minimum. In the interval 3 large outwardly propagating spiral waves are observed. The spiral is enclosed in the centre of the figure.

The last stage of the experiment, from 240 to 430 min, is characterized by outwardly propagating spirals with a wavelength of 5 mm and velocity of 10  $\mu\text{m/s}$  (Figure 4.27).

#### 4.3.2.2 Analysis of the coherence of the patterns by the KL decomposition

The spatio-temporal dynamics of each time interval were analyzed separately by the KL decomposition (see section 3.1.6). The KL eigenvalue spectrum for time interval 1 (Figure 4.28a) shows that 80 % of the total variance is captured by the first two modes ( $V_2 = 0.80$ , cf. section 3.1.6, Eq. (3.13)). Consequently, the inwardly propagating waves observed during the initial stage of the experiment are sufficiently described by the first two modes. The presence of two dominant modes reflects a high degree of spatial correlation of the spatio-temporal structures. This coherence is also observed in the phase portrait of the temporal amplitudes  $a_1(t)$  and  $a_2(t)$  associated with the first two KL modes (Figure 4.28b). The trajectory approaches a limit cycle in the course of time indicating an essentially two dimensional structure of the phase space.

Finally, to confirm that the glycolytic oscillations are synchronized in different regions of the reactor, the phase differences between local oscillations in three different regions (see Figure 4.29) of the total area of observation were compared (Figure 4.30). For this purpose, a KL analysis was performed only within small regions, which are indicated in Figure 4.29. After about 20 min the phase differences ( $\Delta\varphi_{12}$ ) between the

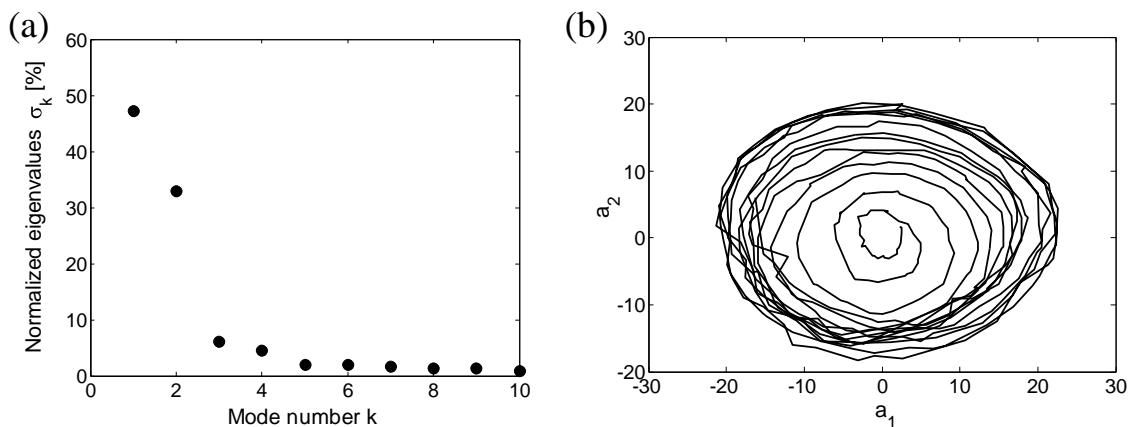


**Figure 4.28:** (a) Normalized eigenvalue spectrum  $\sigma_k$  for the whole area of observation ( $540 \times 740 \text{ pix}^2$ ) in the time interval 1, (b) the phase portrait of the temporal amplitudes  $a_1(t)$  and  $a_2(t)$  associated with the first two KL modes for the same interval.

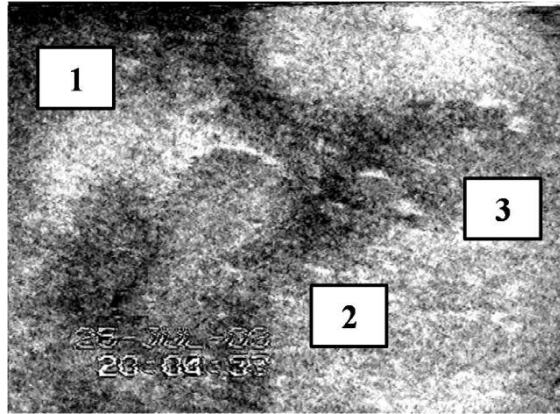


**Figure 4.29:** Three different regions of the total area of observation. The numbers in each region indicate the index of the region. The indicated regions were analysed by the KL decomposition. In each region the phase relations between the first and second KL modes ( $\varphi_{12}$ ), and third and fourth KL modes ( $\varphi_{34}$ ) were measured.

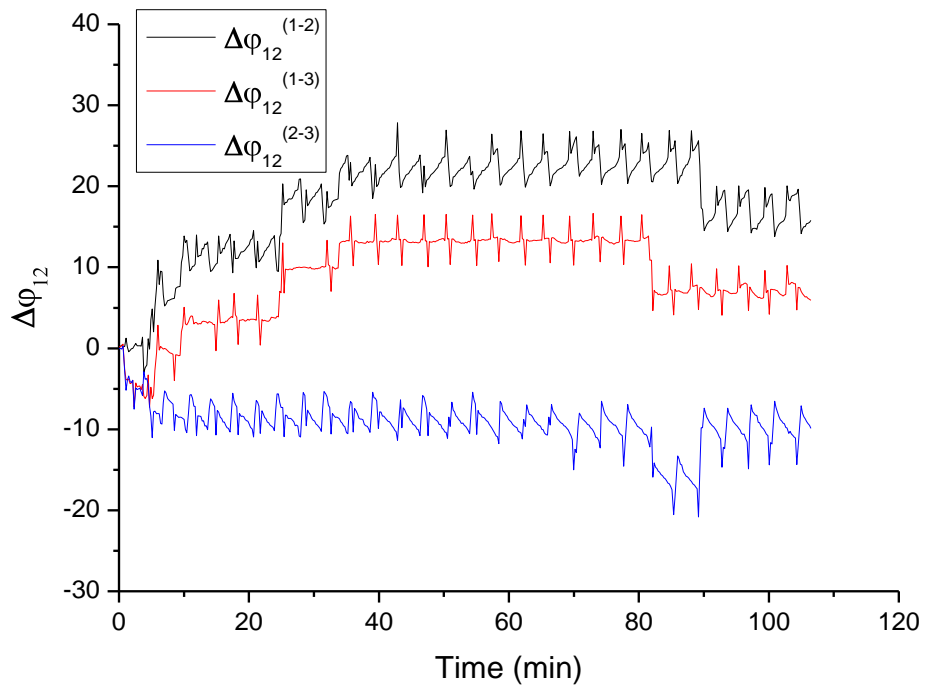


**Figure 4.30:** Temporal behaviour of the phase differences  $\Delta\varphi_{12}^{(i-j)} = \varphi_{12}^{(i)} - \varphi_{12}^{(j)}$  between the first and second KL modes in three different regions (indicated in Figure 4.29) of the total area of observation during interval 1.  $\varphi_{12}^{(i)}$  and  $\varphi_{12}^{(j)}$  are the phase relations between the first and second KL modes in the region  $i$  and  $j$ , respectively.  $i$  and  $j$  are the indices of the three regions indicated in Figure 4.29.

first two KL modes assume a nearly constant behaviour indicating that the waves are synchronized and propagate uniformly with a constant phase shift during the time interval 1 (Figure 4.30).

In the time interval 2, where the transition from inwardly propagating target patterns to outwardly propagating spirals takes place, the number of leading KL modes increases (Figure 4.31a). To account for the same statistical variance as during interval 1, at least 6 KL modes ( $V_6 = 0.86$ ) are needed to describe the dynamical behaviour of the waves. The first two KL modes are still dominant capturing 46 % of the total variance. The phase plane plot of the first two KL amplitudes reveals a more complex structure than the simple limit cycle behaviour during interval 1. In accordance with the presence of two frequencies during interval 2 (cf. Figure 4.24), the trajectory in Figure 4.31b could be interpreted as a 2d projection of a higher dimensional torus.

The last stage of the experiment (interval 3) is characterized by outwardly propagating spirals. Similarly to the previous interval, at least 6 modes ( $V_6 = 0.81$ ) are needed to reconstruct the dynamics of the spirals (Figure 4.32a). Interestingly, while the eigenvalue spectrum is comparable to that of interval 2, the phase plane projection of the first two KL amplitudes has a significantly different shape (Figure 4.32b). Thus, the temporal behaviour of the large scale spatial structures during interval 3 is irregular as compared to interval 1 and 2. However, the coherently rotating spirals are visible during interval 3. This suggests that the transition to the irregular behaviour during the later stages of the experiment is associated with some kind of spatial desynchronization. In order to study this hypothesis, the phase differences between local oscillations in three different regions, which are indicated in Figure 4.29, were measured. The phase differences between the first two KL modes ( $\Delta\phi_{12}$ ) show a nearly constant behaviour in the interval from 260 to 400 minutes (Figure 4.33a). This indicates that the irregular structures appearing in the later stage of the experiment still retain some coherent behaviour, which is described by the first two KL modes. In contrast, the phase differences between the third and fourth KL modes ( $\Delta\phi_{34}$ ) show irregular behaviour in time (Figure 4.33b), pointing to some spatial desynchronization.

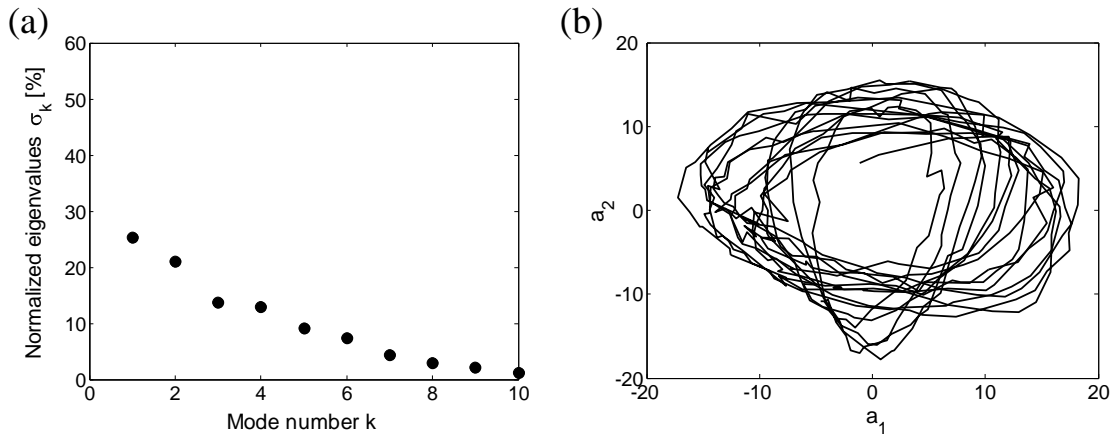


**Figure 4.31:** (a) Normalized eigenvalue spectrum  $\sigma_k$  for the whole area of observation ( $540 \times 740 \text{ pix}^2$ ) in the time interval 2, (b) the phase portrait of the temporal amplitudes  $a_1(t)$  and  $a_2(t)$  associated with the first two KL modes for the same interval.

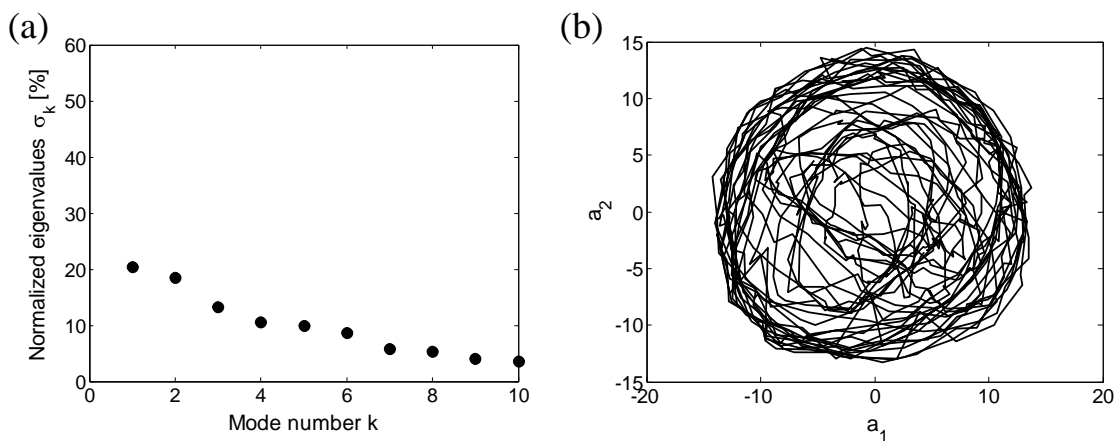


**Figure 4.32:** (a) Normalized eigenvalue spectrum  $\sigma_k$  for the whole area of observation ( $540 \times 740 \text{ pix}^2$ ) in the time interval 3, (b) the phase portrait of the temporal amplitudes  $a_1(t)$  and  $a_2(t)$  associated with the first two KL modes for the same interval.

#### 4.3.2.3 Separation of spatial scales during interval 3

The observation that the dynamics of the spatio-temporal patterns becomes irregular on the large scale during interval 3 prompted to investigate whether these structures retain some coherence on smaller spatial scales. It was found that in the last stage of the experiment a separation of spatial scales takes place. On the large scales (e.g. the entire area of observation) the patterns are spatially desynchronized as measured by the number of KL modes needed for reconstruction as well as by the phase differences

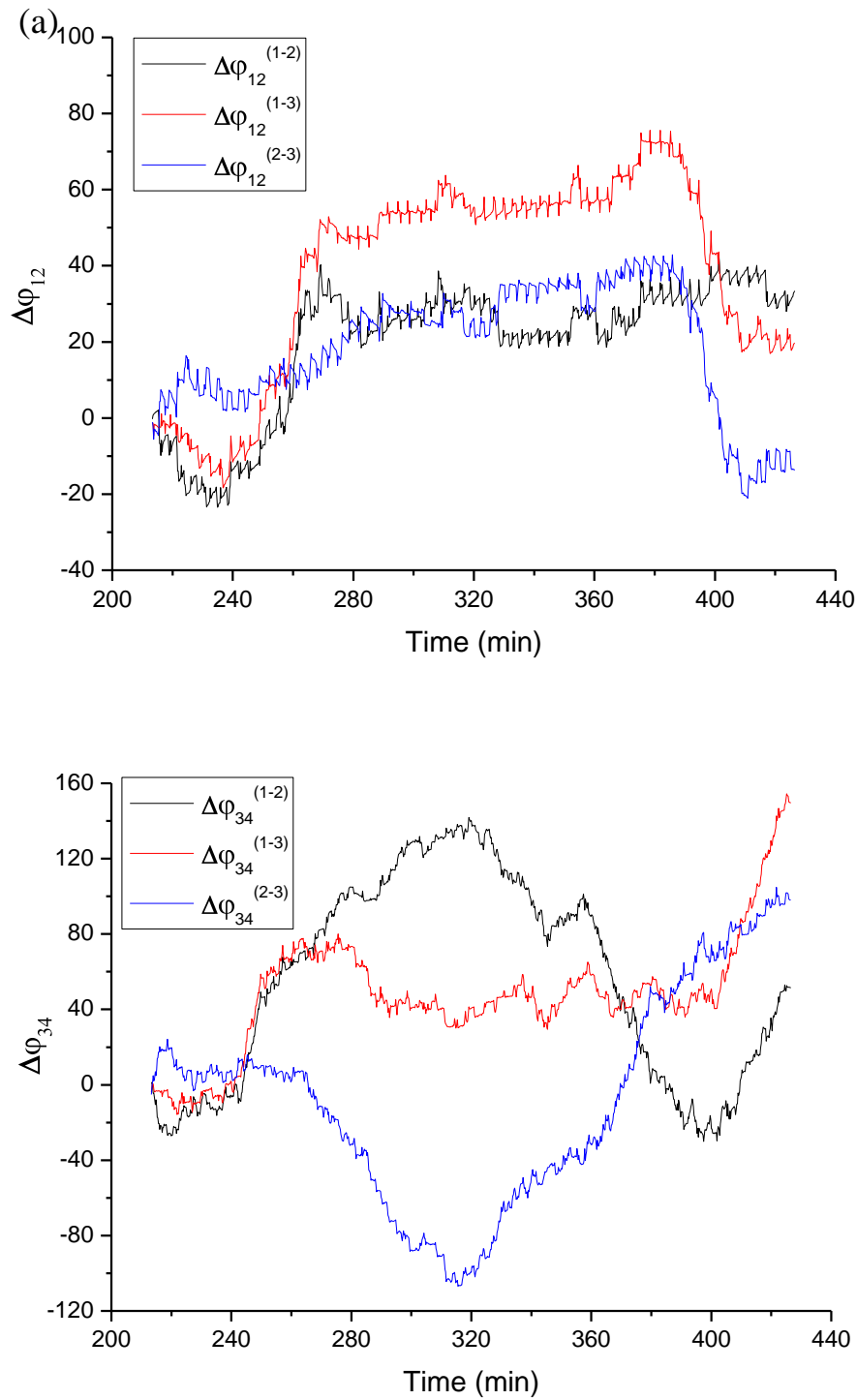


**Figure 4.33:** Temporal behaviour of the phase differences in three different regions (see Figure 4.29) of the total area of observation during interval 3, (a) between the first and second KL modes  $\Delta\varphi_{12}$ , and (b) between the third and fourth KL modes  $\Delta\varphi_{34}$ . The numbers in branches (1-2, 1-3, 2-3) indicate the indices of regions (see in Figure 4.29), between which the phase differences were measured.

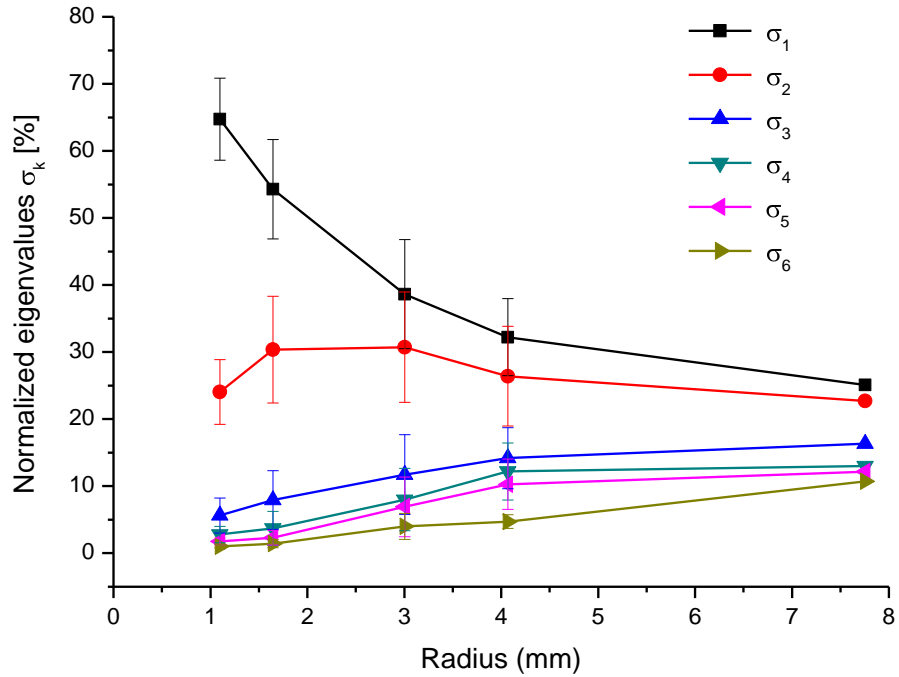


**Figure 4.34:** Effect of increasing of the area of observation ( $AO$ ), expressed by effective radius,  $r = \sqrt{AO/\pi}$ , on the contribution of the first 6 KL modes ( $\sigma_k$ ) during the interval 3. KL analysis was performed for at least three different non-overlapping regions of equal size, which were randomly chosen from the total area of observation. The results represent the average contribution of the first six KL modes to the spatio-temporal pattern. The standard deviation of these results is shown as error bars.

between local oscillations in different regions of the gel. However, on smaller scales the patterns during interval 3 are still synchronized as will be shown now.

First, the dependence of the number of KL modes needed for reconstruction on the size of the area was analyzed (Figure 4.34). For this purpose, an effective radius was assigned to the local area of observation ( $AO$ ) as  $r = \sqrt{AO/\pi}$ . Then, a local KL analysis was performed for at least three different non-overlapping regions of equal size that were arbitrarily chosen from the total area of observation. By making the area smaller and smaller, the average contribution of the first 6 KL modes to the spatio-temporal pattern during interval 3 was obtained as a function of the local observation area or, equivalently, as a function of effective radius. Most importantly, the contribution of the first mode increases rapidly with decreasing radius of the domain of interest (Figure 4.34). It captures 65 % of the total variance for the smallest analyzed radius ( $r = 1$  mm).



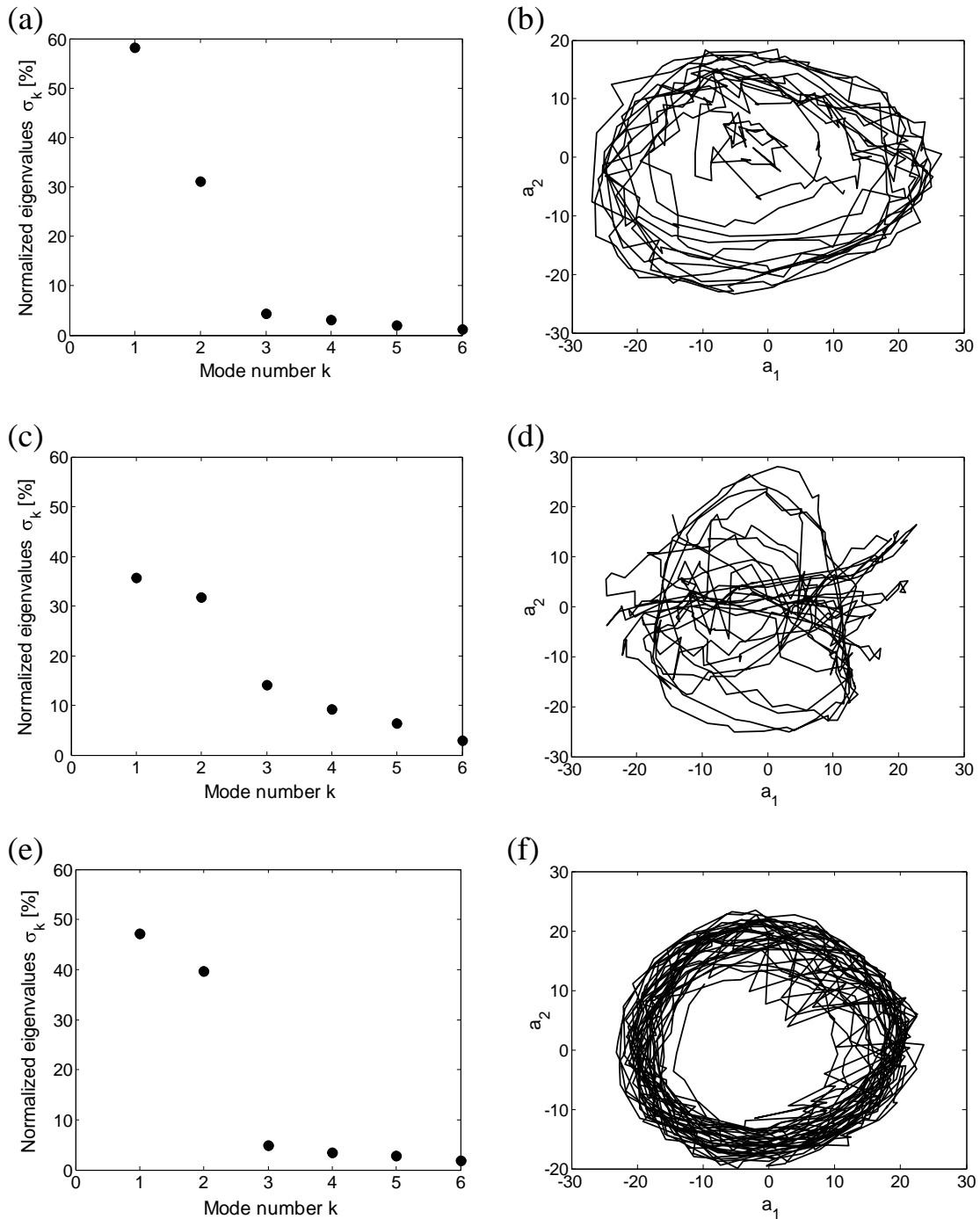


**Figure 4.35:** KL analysis of the area with radius  $r = 3\text{mm}$  ( $200 \times 300 \text{ pix}^2$ ): (a) distribution of KL modes in the time interval 1, (b) the phase portrait of the temporal amplitudes  $a_1(t)$  and  $a_2(t)$  associated with the first two KL modes for the time interval 1, (c) distribution of KL modes in the time interval 2, (d) the phase portrait of the temporal amplitudes  $a_1(t)$  and  $a_2(t)$  associated with the first two KL modes for the time interval 2, (e) distribution of KL modes in the time interval 3, (f) the phase portrait of the temporal amplitudes  $a_1(t)$  and  $a_2(t)$  associated with the first two KL modes for the time interval 3.

This is more than twice as large as the contribution of the first mode, obtained when the entire image ( $r = 7.7$  mm) was analyzed by KL decomposition (Figure 4.34). The contribution of the higher modes is marginal for small radii and increases for larger ones. Thus, the spatio-temporal patterns during interval 3 are sufficiently described by the first two KL modes on spatial scales  $r \leq 3$  mm, where the mode spectrum exhibits a sharp transition (Figure 4.35e). More importantly, the phase plane projection of the first two KL amplitudes  $a_1$  and  $a_2$  exhibits simple limit cycle behaviour similar to that observed during interval 1 on the large scale (cf. Figure 4.28b), which demonstrates that they are evolving coherent in time.

Figure 4.35 summarizes the coherence properties of the spatio-temporal patterns during all three intervals at the transition point  $r = 3$  mm. For interval 1 and 3, the first two KL modes are sufficient to account for the locally observed patterns since there are clear cut-offs in the eigenvalue spectra between the second and the higher modes (Figure 4.35a,e). Also, the corresponding phase space projections show a limit cycle behaviour for the trajectories of the corresponding KL amplitudes  $a_1$  and  $a_2$  (Figure 4.35b,f). This clearly demonstrates the local coherence of the spatio-temporal patterns. By contrast, the cut-off in the eigenvalue spectrum during interval 2 (Figure 4.35c) is less obvious, indicating that two KL modes are probably not sufficient to account for the local spatio-temporal dynamics during this transient interval. Moreover, the trajectory in the phase plane projection of the first two KL modes is highly irregular (Figure 4.35d). This means that the dominant modes do not evolve coherently in time during interval 2.

## 5 Discussion

An open spatial reactor was designed and optimized for investigations of glycolytic reaction-diffusion waves in a layer of yeast extract under well defined and stationary conditions. In this reactor reaction-diffusion coupling is achieved by fixation of the yeast extract in an agarose gel. The openness of the system is maintained by constant feeding of the gel-fixed yeast extract with substrates and sugar. Under these conditions glycolytic oscillations lasting for about 40 h were observed (Figure 4.6). This is about 10 times longer than the lifetime of the glycolytic oscillations observed at batch conditions [21]. There is an induction time, during which an equilibration between the gel and the feeding solution takes place, because the metabolic/ionic compositions in the gel and in the reactor are different at the start of experiment. This adaptation process is reflected by a decrease of the NADH fluorescence amplitude, which reaches a constant value after approximately 2 h (see Figure 4.7, Figure 4.24).

The disaccharide trehalose was used as the sugar source of glycolysis for feeding of the yeast extract. This sugar is split into 2 units of glucose by the enzyme trehalase, which is present in the yeast extract. Since this enzyme works at low activity in the yeast extract (30 nmol/(mg prot.×min), [30]), there is a slow and constant input of glucose into glycolysis. This means, that the trehalose concentration can reach quite high concentrations throughout the gel and then can act as a “substrate buffer” for glycolysis. It is assumed that only small fractions of trehalose (the input species into the gel) are converted, since the conversion rate is low, as compared with feeding rate. This may explain, why oscillations with a period of about 10 min can be observed, although the typical diffusion time ( $d^2/D$ ) perpendicular through the gel is estimated to be 28 min for the 1.3 mm thick gel. Here,  $d$  is the thickness of the gel, and  $D$  is the diffusion coefficient, which is taken to be  $10^{-5}$  cm<sup>2</sup>/s for the small molecules.

### 5.1 Impact of the feedback regulation of PFK

An important prerequisite for the maintenance of constant glycolytic oscillations is a proper balance between the ATP-consuming and ATP-providing processes as has been already reported for oscillatory glycolysis under batch conditions [75]. If this balance is perturbed, the glycolytic oscillations damp out (see Figure 4.1). This damping process

can be explained based on the feedback regulation of PFK by ATP (inhibitor) and ADP, AMP (activators) [105] as shown in Figure 5.1.

When the ATP concentration in the feeding solution is too low, all ATP is consumed in the upper part of glycolysis by HK and PFK for phosphorylation of glucose. This occurs during the transition from the oscillatory to the damped state (see Figure 4.2). As a result, the feedback inhibition of PFK by ATP is no longer possible. On the other hand, the increasing concentration of ADP results in activation of the PFK. This increased kinase activity even enlarges the consumption of ATP, so that the demand for ATP for phosphorylation of glucose overcomes the supply of ATP. The increase in ADP concentration leads to a shift of the equilibrium of the AK-catalysed reaction to the formation of AMP and ATP. Due to the imbalance between supply and demand, the ATP produced from the AK-catalysed reaction is immediately consumed by the kinases, which results in the accumulation of AMP (see Figure 4.2, Figure 5.1). Under these ATP-limiting conditions, the PFK is fully activated (high concentration of AMP), whereas a negative feedback is no longer possible, since the ATP concentration is too low. Accordingly, the nonlinearity of the PFK reaction does not contribute any more, resulting in abolishment of the oscillations. This leads to an increased PFK mediated flux as demonstrated by the rise of the FDP concentration in the non-oscillatory state (Figure 4.2).

A substantial effect of the ATP/ADP ratio on the glycolytic flux has also been observed in living cells. Koebmann and co-authors [106] reported that an increased expression of ATPase in *E. coli* cells markedly decreases the ATP/ADP ratio, which leads to a marked increase of the glycolytic flux. Such a condition is similar with the situation in our system in the damped phase, where the ATP/ADP ratio is getting low (Figure 4.2). Similarly, Kroukamp and co-authors [107] found an increase of the flux through glycolysis when the ATP demand in the yeast cells was modulated by addition of uncouplers, i.e. substances, which uncouple electron transport from oxidative phosphorylation in the mitochondria, resulting in a decrease of the ATP/ADP ratio.

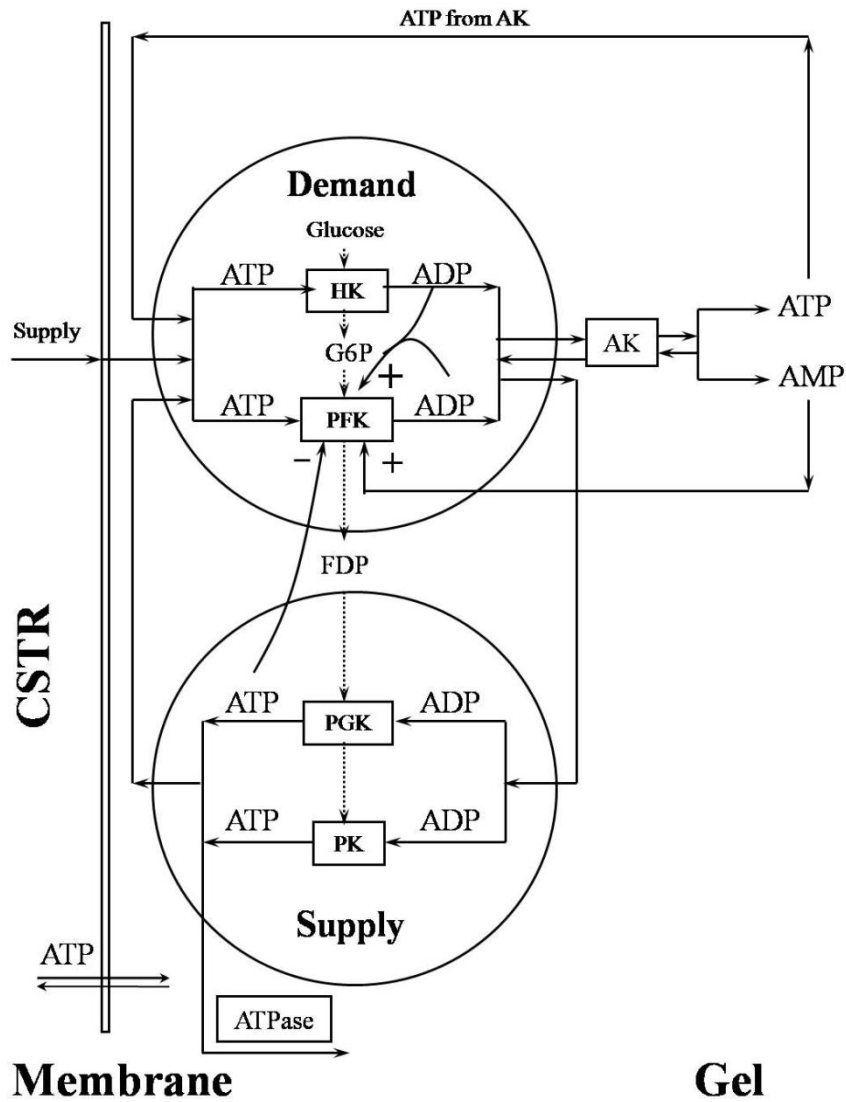


**Figure 5.1:** Simplified scheme for the control of glycolytic oscillations in the open spatial reactor, based on feedback regulation of the PFK. The left side represents the CSTR, which is separated from the gel-fixed yeast extract by a membrane. The right side represents the gel-fixed yeast extract, where glycolysis takes place. This scheme demonstrates the steps involving ATP during glycolysis in the open spatial reaction. The system conceptually can be divided into a “supply” and “demand” blocks in term of the production (supply) and usage (demand) of ATP. The upper part of glycolysis represents a demand block, consuming the ATP, whereas the lower part of glycolysis represents a supply block, producing ATP. In addition ATP is also supplied by diffusion from the CSTR and by AK reaction. For the detailed scheme of glycolysis including single reaction steps see Figure 2.5.

The results of theoretical metabolic control analysis, performed by Thomas and Fell [108] to study the role of the ATP demand for the control of the glycolytic flux showed that the control of glycolytic flux depends primarily on the activation of PFK by AMP and on ADP inhibition of ATPase. These results support our view that control of PFK diminishes rapidly as the AMP concentration increases.

Larsson and co-authors [109] used permeabilized yeast cells to study the control of the glycolytic flux. By this method they were able to adjust the concentrations of the adenine nucleotides as well as other glycolytic intermediates within the cells. They found that the ATP/AMP ratio strongly depends on the initial concentration of ATP and glucose. Similar to our findings, low initial ATP concentrations were completely converted to AMP, whereas at higher ATP levels the ATP consumption was reduced and the AMP production was negligible. This was accompanied by a complete suppression of FDP formation and accumulation of G-6-P and F-6-P at high ATP concentrations. Larsson and co-authors explained this behaviour by a control of the glycolytic pathway through feedback inhibition of PFK by ATP.

Schellenberger and co-authors [110] used an open reconstituted enzyme system consisting of PFK (ATP-consuming) and pyruvate kinase (ATP-producing) as well as glucose-6-phosphate isomerase and AK. They found different stationary states for this system with respect to the concentrations of intermediates, depending on the activity of PFK and PK. A transition between ATP-producing and ATP-consuming stationary states could be explained by the allosteric properties of PFK. A self-stabilisation of the energy charge could be achieved by increasing the activity of the PK [39].

All these data demonstrate that the flow through glycolysis strongly depends on the ATP and AMP concentrations. In our opinion, this control is due to the allosteric feedback regulation of PFK. A negative feedback is required in order to reduce the flux through this enzyme reaction. This ensures that the activity of the kinase is small enough in order to maintain a “reasonable” energy charge. If the ATP concentration falls below a critical value, the insignificant negative feedback as well as the strong positive feedback by AK-generated AMP lead to a full activation of the PFK. This in turn leads to a nearly complete consumption of ATP, such that ATP becomes limiting for phosphorylation of glucose, i.e. the ATP-demand overcomes the ATP-supply. Our results also demonstrate that the oscillations of the glycolytic pathway can only occur,

when the ATP concentration is sufficiently large to permit the negative feedback of PFK to be effective (Figure 4.3 and Figure 4.5).

The group of Westerhoff has obtained similar experimental results but, based on theoretical analysis, came to different interpretations [111-114]. Calculation of the control coefficients yielded a strong control of glucose transport and ATPase activity over the glycolytic pathway, whereas PFK was nearly ineffective. To our opinion, this interpretation is not complete. Since both, glucose transport and ATPase activity, lead to a marked decrease of ATP, the allosteric properties of PFK cannot be neglected for control of glycolysis.

## **5.2 Effect of the protein concentration on the spatio-temporal patterns**

Among the proteins of yeast extract are the enzymes which are the catalysts of the glycolytic reaction and play an important role in regulation of glycolysis. Changes in the protein concentration can drastically influence the dynamical properties of the system. The influence of the protein concentration on glycolytic oscillations has been studied by Das and Busse [76]. They observed an increase of the period of oscillations from 20 min to 6 h, when the protein concentration of the yeast extract was diluted from 40 mg/ml to 2 mg/ml. Moreover, they showed that a decrease in the protein concentration results in a change of the shape of the oscillations from the spike to the relaxation type. These results indicate that the protein concentration can influence the dynamical properties of the system, and hence can serve as a powerful tool for changing the system properties of glycolysis in the open spatial reactor.

When the protein concentration of the yeast extract in the open spatial reactor was increased from 23 to 81 mg/ml, the duration of the glycolytic oscillations was prolonged from 10 h to 40 h (Figure 4.6). This fourfold increase of the oscillatory phase that was induced by the increase of the protein concentration could be explained as follows. Since the experiments last one to two days, the enzymes of yeast extract become denaturated during this long period of time. With increasing protein concentration, the amount of enzymes that retain their activity by the end of the experiment increases. Hence, at high protein concentrations, the ratio of functioning enzymes to the denaturated enzymes is high enough to provide long lasting oscillatory glycolysis.

A characteristic property of oscillatory systems is the formation of spatio-temporal patterns due to the coupling of a non-linear reaction with diffusion. The gel-fixed yeast extract represents a diffusive layer that enables reaction-diffusion coupling. Accordingly, the generation of travelling NADH-waves in this gel, associated with the appearance of glycolytic oscillations, was found (Figure 4.9).

The dynamics of glycolytic waves in an open spatial reactor were investigated at different protein concentrations in the yeast extract. By varying the protein concentration from 23 to 91 mg/ml, seven different types of glycolytic travelling NADH waves were observed in the open spatial reactor (Figure 5.2, Table 4.1). These are inwardly and outwardly propagating large target waves, large rotating spiral(s), segmented waves, dot-shaped waves, outwardly propagating short-distance waves and spatial oscillations. In addition, for high protein concentrations the coexistence of different types of waves with the spatial oscillations was also found. The dynamical properties of some of these waves will be discussed in the next section.

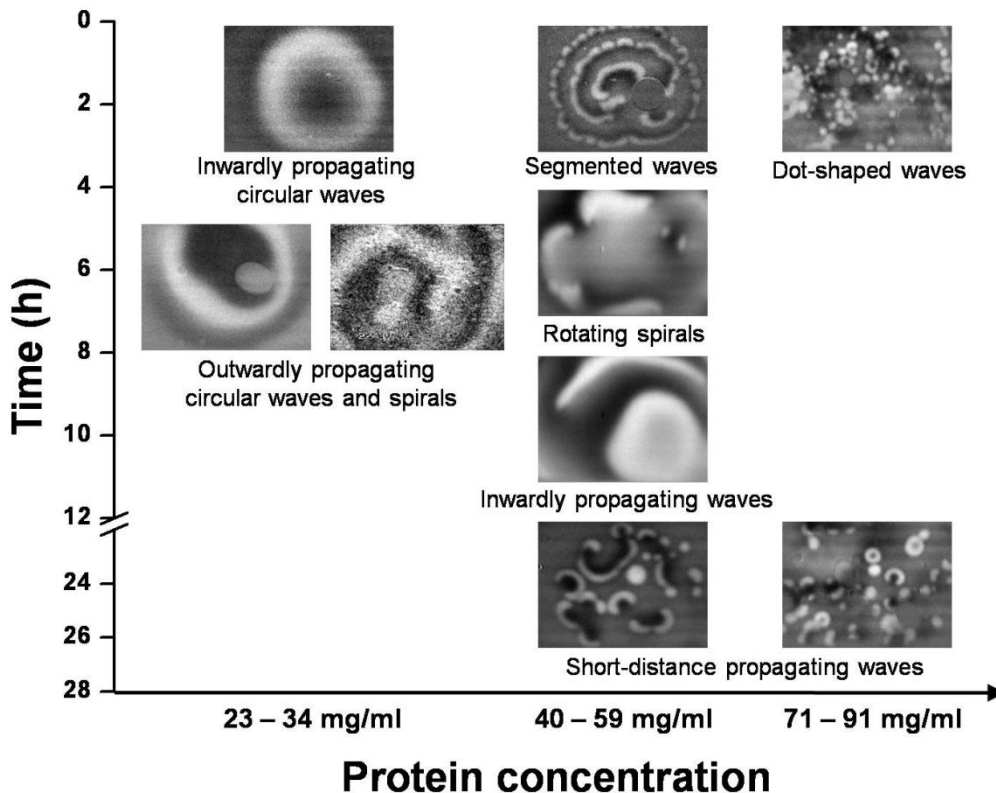


**Figure 5.2:** Schematic overview of patterns found during glycolysis in the yeast extract.



The formation of different types of patterns in dependence of the protein concentration in the yeast extract might be induced due to the change of the two important parameters of the system. One of these parameters is the spatial coupling, i.e. the mean distance between the proteins in the gel. When the protein concentration is low, the spatial coupling between the proteins is also low. This leads to the formation of simple inwardly and outwardly propagating target patterns. By increasing the protein concentration, the spatial coupling between the proteins also increases and leads to the formation of more complex dynamical structures, such as spirals, segmented waves, outwardly propagating large circular waves. Finally, at very high protein concentrations the turbulent patterns, in the form of dot-shaped waves, are formed. Another parameter that might be affected by change of the protein concentration in the yeast extract is the flux through glycolysis.

The presence of a multitude of different patterns when the protein concentration is varied may have important impacts for biological systems with spatial gradients of the protein, e.g. in developing *Drosophila oocytes* [115-119].

### 5.2.1 Inwardly propagating target waves

The inwardly propagating target waves have been observed at protein concentrations of 23 to 34 mg/ml. These waves initially start to propagate from the border of the gel to the middle where they exhibit mutual annihilation. Later these waves develop into the outwardly propagating target or spiral waves (Figure 4.11). This type of spatio-temporal structures has so far only rarely been reported in experiments [60], while many theoretical investigations have been performed to elucidate the propagation mechanism of these waves.

Theoretical studies of wave dynamics using the complex Ginzburg-Landau equation (CGLE) suggest that inwardly propagating target and spiral waves should generically occur in oscillatory media close to the onset of oscillations, where the frequency of the bulk oscillations is larger than the frequency of the inwardly propagating waves [61-63;65;101]. According to these investigations inwardly propagating target and spiral waves are generic solutions of the complex Ginzburg-Landau equation with a negative phase velocity such that the phase velocity and the group velocity point to opposite directions (see section 2.1.2). In that sense, the

inwardly propagating waves observed at low protein concentrations of yeast extract could correspond to phase waves with an inwardly pointing phase velocity.

On the other hand, it is possible that spatial gradients in certain system parameters may also lead to inwardly propagating patterns [56;120]. Since there are no-flux-boundary conditions in the local edges of the gel, (i.e. x-y plane) and formation of local gradients at the edges in the gel cannot be excluded, this scenario should be also considered as an alternative explanation for the occurrence of inwardly propagating target waves.

#### 5.2.1.1 Desynchronization of the inwardly propagation waves

The inwardly propagating target waves observed in the yeast extract (see interval 1, Figure 4.25) often spontaneously develop into outwardly propagating target or spiral waves after about 100 min. This occurs via a transition phase, where the inwardly propagating target waves become unstable and give rise to outwardly propagating spirals that randomly emerge in the gel (see interval 2, Figure 4.26). This transition region lasts for approximately 120 min until the outward propagation of the spirals become stabilized and the target patterns disappear (see interval 3, Figure 4.27).

KL analysis of the spatio-temporal patterns shows that the transition from inwardly propagating target waves to spirals is accompanied by desynchronization and spatial decoherence. The spatio-temporal structures observed during the last stage of the experiment (interval 3, Figure 4.24) are characterized by two different spatial scales. The spatial dynamics is desynchronized on scales larger than  $r \geq 3\text{mm}$  (where  $r$  corresponds to the effective radius of the observation area), while it still retains some correlation on smaller scales ( $r \leq 3\text{ mm}$ , Figure 4.34). The dynamics of the patterns on the smaller scales can be sufficiently described by only the first two KL modes (Figure 4.35e, Figure 4.35f). The question arises whether these two dominant KL modes have any biological interpretation of glycolytic pathway.

For this purpose, the local spatio-temporal dynamics of the leading KL modes at the spatial scale  $r = 3\text{ mm}$  were compared with the results of a simulation of travelling glycolytic waves. The simulation was performed by Anastasia Lavrova (Group of Theoretical Biophysics, Humboldt University Berlin) using the Selkov model for glycolysis (see section 2.5.2). The one dimensional Selkov model [86], which describes

the temporal dynamics of glycolysis, was extended by including the diffusion term to describe the spatial patterns [120].

The two dominant KL modes and the time evolution of these modes ( $a_1$  and  $a_2$ ) are shown in Figure 5.3. The spatial structures of the first and the second KL modes look similar, but slightly shifted with respect to each other (Figure 5.3c).

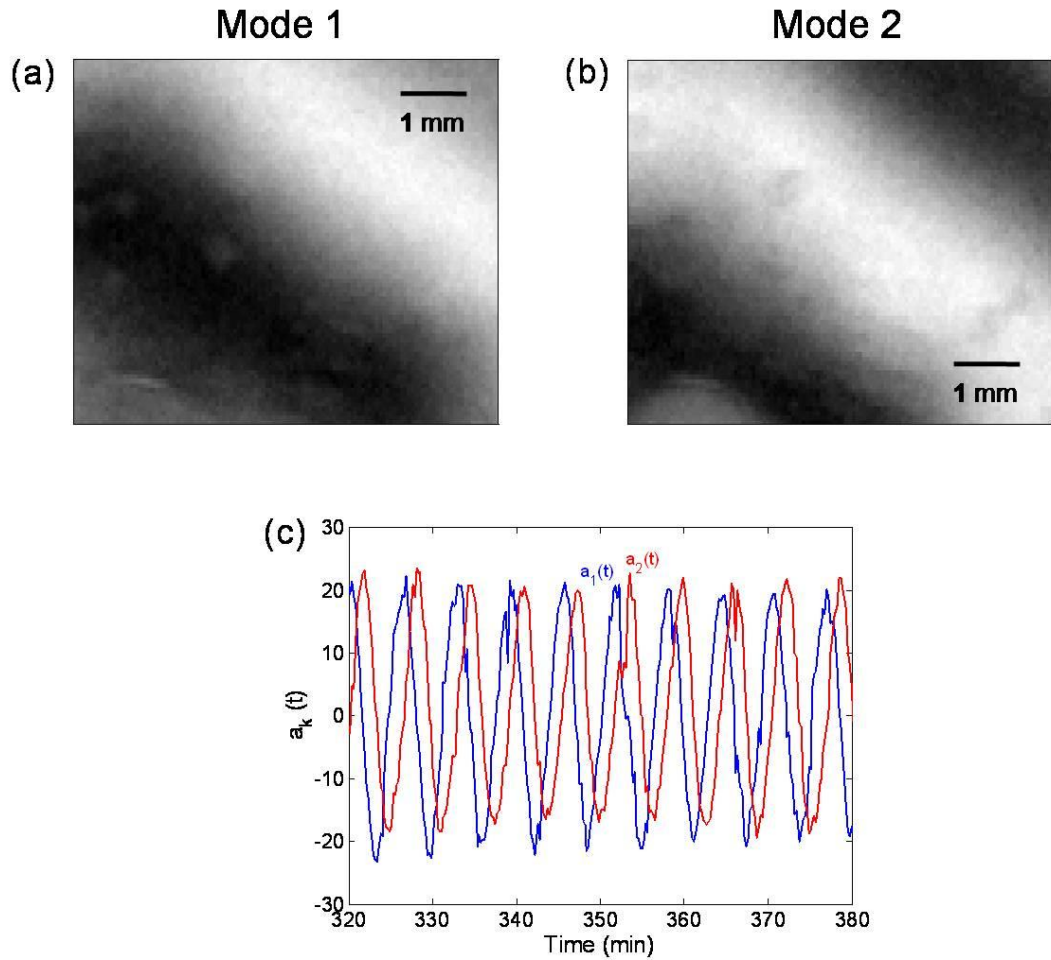


**Figure 5.3:** Results of the KL analysis of the area with effective radius of  $r = 3$  mm ( $200 \times 300$  pix<sup>2</sup>) for the time interval 3 of the experiment shown in Figure 4.24. (a), (b) first two dominant KL modes, and (c) the temporal amplitudes  $a_1(t)$  and  $a_2(t)$  associated with these two KL modes. For the experimental procedure and composition of the feeding solution see section 3.3.3. Grey levels quantify the NADH concentration, with white corresponding to maximum and black to minimum.

The results of the simulation are shown as time-space plots for the  $x$  and  $y$  variables of the modified Selkov model in Figure 5.4 [120]. The phase shifts between the  $x$  and  $y$  variables in the simulation (Figure 5.4c) and between the first ( $a_1$ ) and the second ( $a_2$ ) KL modes (Figure 5.3c) are comparable, and amount to  $60^\circ$  and  $100^\circ$ , respectively. Thus, the spatio-temporal behaviour as well as the phase differences between the first two KL modes ( $a_1$  and  $a_2$ ) and the two variables ( $x$  and  $y$ ) exhibit similar dynamics. This suggests that the spatio-temporal dynamics of the leading KL modes in the interval 3 on small scales ( $r \leq 3\text{mm}$ ) can be sufficiently described by the  $x$  and  $y$  variables of the extended Selkov model [120].

In order to interpret the role of the  $x$  and  $y$  variables in the sense of glycolytic dynamics, the phase shift between these variables was compared with the phase shift between glycolytic intermediates during oscillatory glycolysis. The phase relation between different glycolytic intermediates has been experimentally measured by Hess and co-authors [75]. They showed that all glycolytic metabolites can be summarized in two groups (Figure 5.5), based on their phase relation. In each group the glycolytic metabolites oscillate  $180^\circ$  out of phase, whereas these two groups differ by a variable phase angle  $\Delta\alpha$ , which is approximately  $45^\circ$  (see Figure 5.5). The phase angle  $\Delta\alpha$  between the two groups of glycolytic metabolites is comparable to the phase shift of  $60^\circ$ , which was obtained between the  $x$  and  $y$  variables of the modified Selkov model. Therefore, it can be roughly assumed that these two variables ( $x$  and  $y$ ), which represent the leading KL modes, describe the two groups of glycolytic metabolites shown in Figure 5.5.

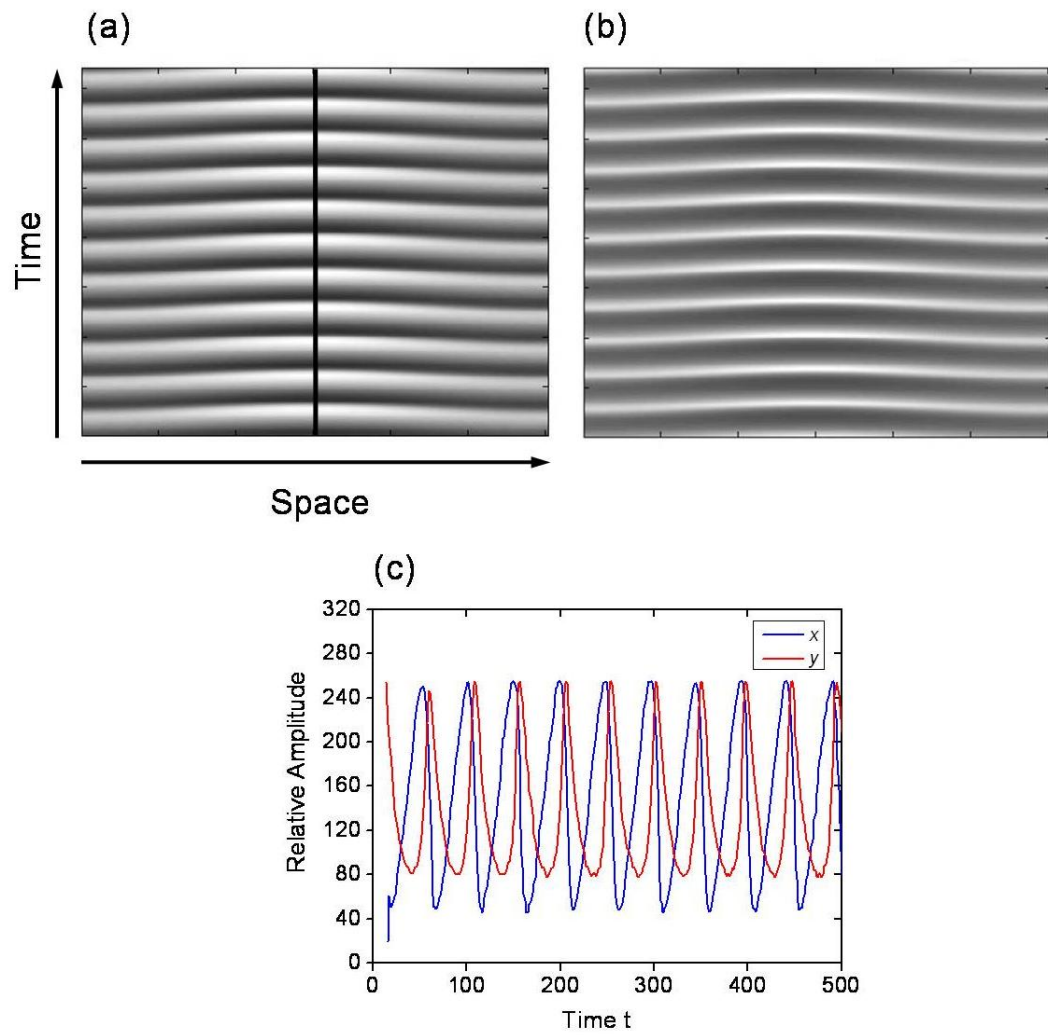


**Figure 5.4:** Time space plots of the variables  $x$  (a) and  $y$  (b) obtained from the extended Selkov model (from Lavrova [120]). (c) Temporal dynamics of these variables, measured from the time-space plots along a vertical line indicated in (a).

For a more accurate description of the dominant KL modes precise experimental data sets are required, which account for the kinetics of single glycolytic intermediates. There are first measurements of temporal dynamics of the glycolytic pathway by Mair and co-authors [121]. They showed that the kinetic properties of all glycolytic metabolites can be simultaneously measured by Fourier transform infrared (FT-IR) spectroscopy. In spite of the high complexity of the glycolytic pathway, they could quantitatively reproduce the temporal behaviour of some glycolytic metabolites and the known phase relations between most of them [75]. This provides the basis for future investigations of the kinetic properties of single glycolytic intermediates during oscillatory glycolysis.

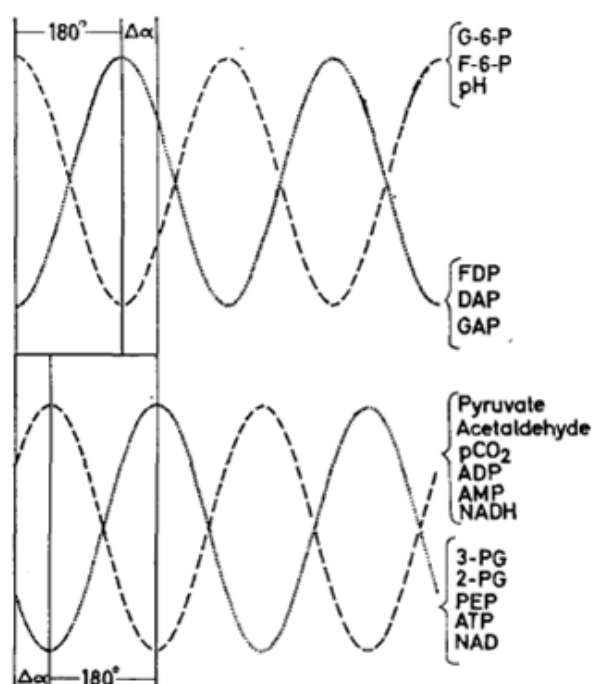


**Figure 5.5:** The phase relation of glycolytic intermediates during oscillatory glycolysis. The amplitude of the concentrations is normalized (from [75]).

### 5.2.2 Segmented waves and “bubbles”

Recently, Vanag and Epstein reported on the types of patterns, which were formed in the BZ system, when the reagents of the BZ reaction were dispersed in water in oil microemulsion (the BZ-AOT system) [122-124]. These patterns were called dashed or segmented waves and could be found only in a narrow range of parameter values, such as droplet radius, the volume fraction of the dispersed phase, and chemical composition. Segmented waves were formed when target or spiral waves broke up into wave segments and gaps. It is suggested that this type of waves should be also observed in living systems, which often display travelling waves, multiple steady states, and species with extremely different diffusion coefficients [123].

When the protein concentration in the yeast extract was varied from 40 to 59 mg/ml segmented waves could be observed during glycolysis of yeast extract in the open spatial reactor (Figure 4.9 (A)). These waves emerge by segmentation of the outwardly propagating target waves as the latter reach a certain distance from the centre (Figure 4.9 (A)). Similar to the segmented waves observed in the BZ-AOT system, these waves also require ordinary target waves as precursor and cannot be formed spontaneously [123].

Vanag and Epstein showed that low wave velocities are necessary for the formation of segmented waves [123]. This observation is in agreement with the velocity of wave segments in the yeast extract, which amount to 2  $\mu\text{m/s}$  (Figure 4.14). Moreover, it is also in good agreement with the velocity of segmented BZ-AOT waves (2  $\mu\text{m/s}$ ).

From experimental and theoretical investigations Vanag and Epstein concluded that the length of the segmented waves in the BZ-AOT system depends only on the chemical parameters of the system [123] and not on the geometry of the system [125]. It is not clear whether this hypothesis holds also for the segmented waves in the yeast extract and it should be clarified in the future experimental studies.

Vanag and Epstein proposed a mechanism for the emergence of segmented waves, which suggests that segmented waves are propagating 1D Turing structures in a system exhibiting several steady states, one of which is stable and spatially homogenous but excitable, in which local superthreshold perturbations generate trigger waves [123]. The other one is a spatially inhomogeneous pseudo-Turing (PT) unstable steady state with a characteristic Turing wavelength, which is driven to a different stable state, steady or

oscillatory, by an infinitesimal perturbation. However, PT instability and excitability are necessary but not necessarily sufficient conditions for the description of segmented waves [123]. It might be necessary also to consider the curvature of segmented waves and its influence on the velocity [126].

Waves similar to the segmented waves were also observed in other systems. Showalter and co-authors have shown that global negative feedback can lead to formation of wave segments propagating along a straight line in the excitable photosensitive BZ reaction [127]. The propagation of wave segments is strongly dependent on the excitability of the reaction. At higher light intensities, the excitability of the system is low, whereas a decrease in the intensity of illumination leads to an increase of the excitability of the system. Using this feature, they have been able to control and stabilize the size of the segments by applying feedback control algorithm.

Another system where similar wave segments have been observed is the catalytic oxidation of carbon monoxide (CO) on a Pt (110) single-crystal surface, where CO molecules and oxygen atoms were adsorbed from the gas phase [128;129]. Within a very narrow range of conditions, the wave segments, which were characterized as dissipative solitons, were formed. The wave segments always propagate in the same direction (either forward or backward) along straight lines parallel to the crystallographic (001) direction of the surface. Interestingly, these wave segments propagate at a constant velocity of about 3  $\mu\text{m/s}$ , which is similar to the velocity of the segmented waves found in the yeast extract and BZ-AOT system.

When the concentration of BZ-AOT reactants and the volume fraction of the dispersed phase was varied by 10 %, small concentric waves were observed, which emerge randomly, grow slightly and disappear without collision with other waves [124]. Vanag and Epstein called these waves “bubbles”. Interestingly, when the protein concentration of yeast extract was increased up to 71 mg/ml and higher, a similar type of pattern, named dot-shaped waves, (Figure 4.12a) was also observed in the yeast extract.



### 5.2.3 Different types of waves: Phase waves or Reaction-Diffusion waves?

It is known that, if the kinetics of the underlying reaction-diffusion system is oscillatory, then both trigger waves and phase waves can be formed (see section 2.1.2) [55;59]. Since theoretical studies of the CGLE suggest that the inwardly propagating waves can only occur in an oscillatory medium [61;63], it can be concluded that the kinetic part of the reaction-diffusion equation of glycolysis in the open spatial reactor is oscillatory. Thus, depending on the system parameter, phase waves or trigger waves can be observed. From the experimental point of view the propagation mechanism of inwardly propagating waves observed in the yeast extract still remains unclear.

In order to clarify whether inwardly propagating waves represent phase waves or trigger waves, experiments were performed, in which the gel was separated by an impermeable barrier (Figure 3.4). It is known that phase waves are induced due to phase shifted oscillations in the oscillatory medium and are not stopped by a barrier [55;57]. The experiments were performed for two different conditions: for inwardly propagating target waves and outwardly propagating waves. In the case of the inwardly propagating target waves the waves could cross the barrier (Figure 4.17), demonstrating the properties of phase waves; whereas the outwardly propagating waves were impeded by the barriers (Figure 4.18), demonstrating the properties of reaction-diffusion waves.

An additional confirmation that inwardly propagating target waves represent phase waves can be obtained from the analysis of the velocity of the waves, since it is known that the velocity of phase waves is generally much higher as the velocity of trigger waves [55;58]. Bodet and co-authors showed that the velocity of the phase waves in the BZ system is about fourfold higher than the velocity of the trigger waves [56]. Similar results were found also for the inwardly propagating waves in the yeast extract, which are 2 to 4 fold larger than the velocity of the other types of glycolytic waves.

A more precise distinction between phase and target waves was proposed by Aliev and Biktashev based on the analysis of the shape of the dispersion curve [58] (see section 2.1.2, Figure 2.3). According to this quantification, it could be assumed that the inwardly propagating target waves show the dispersion relation typical of phase waves, and the outwardly propagating waves show “normal dispersion”, which corresponds to the reaction-diffusion waves (Figure 4.20).

An exception is the dispersion relation for protein concentrations of 40 mg/ml (Figure 4.20). At this protein concentration, a dispersion curve with two overlapping branches is observed. One branch is found at wavelengths of 1.29 to 2.68 mm and corresponds to the dispersion of reaction-diffusion waves. The second branch with infinitely increasing wave velocity is found at wavelengths of 2.33 to 2.86 mm and corresponds to the dispersion of phase waves [58;59]. The existence of two branches at 40 mg/ml protein concentration might be explained according to the theory of transition of the phase waves to the trigger waves [55;56]. When the solution in contact with the catalyst oscillates, it first generates a phase wave. If the phase gradient between the initiated phase wave and the adjacent areas is large, then this phase wave will start to propagate slower. If the velocity of this phase wave is sufficiently slow it can initiate a trigger wave that will propagate through the oscillatory medium [55;130].

Interestingly, analysis of velocity and thickness of glycolytic waves at different protein concentrations show that at protein concentration of 40 mg/ml both phase waves (inwardly propagating target waves) and trigger waves (outwardly propagating waves, segmented waves, and short-distance propagating waves) are observed (Figure 4.14 and Figure 4.15). This protein concentration acts as transition point, below which, in the beginning of experiment, phase waves in the form of inwardly propagating target patterns and above which reaction-diffusion waves in the form of segmented and short-distance propagating waves are formed.

## Outlook

The results of this study demonstrate that the spatio-temporal dynamics of glycolysis can be efficiently investigated by means of the open spatial reactor introduced in this work. For future research the following scientific tasks are of increased interest:

- Recently, theoretical investigations of the Selkov model showed that the concentration changes of immobilized PFK changes the effective diffusion of ADP and ATP in such a way that the diffusion coefficient of ATP (inhibitor) becomes much larger than that of ADP (activator) [131]. This occurs due to the different binding constants of the PFK for ADP and ATP. Under appropriate conditions, the theoretical studies predict the appearance of Turing patterns in glycolysis on spatial scales of single cells (10  $\mu\text{m}$ ). For this, the concentration of PFK has to be increased in such manner that the ratio of the  $D_{\text{ATP}}/D_{\text{ADP}}$  markedly increases. Such experiments could be optimally performed with the open spatial reactor presented in this work.
- In order to have increased external control on the system, glucose should be used as a feeding substrate. This requires thorough analysis of the balance between ATP-consuming and ATP-producing reactions at different glucose concentrations.
- The metabolic complexity of the yeast extract can be gradually increased by adding cellular organelles, e.g. mitochondria, thus supporting a detailed investigation of the influence of particular metabolic pathways on the spatio-temporal pattern formation. By systematically increasing the complexity, the conditions present in real cells could be approached.

## Appendix A

The programs for image enhancement and construction of time-space plot are presented below for documentation reasons. These programs were written by Ulrich Storb and Chaiya Luengviriya from Biophysics Group, Otto-von-Guericke University of Magdeburg, in IDL (Interactive Data Language).

### A.1 IDL program for construction of time-space plots

#### (*timespaceplot\_freedirection\_v6*)

```

Pro timespaceplot_freedirection_v6 ,NOSHOW = noshow , $
    FIRSTIMAGE = firstimage , $
    LASTIMAGE = lastimage , $
    SUBIMAGE = subimage , $
    no_area = no_area , $
    setvalue = setvalue , $
    avg_width = avg_width

COMMON COORD,xa,xe,ya,ye,win_draw,win_plot, $
    WID_BUTTON_extrema,WID_BUTTON_print, $
    WID_BASE_MIDDLE,win_neighbor,win_neighbor2, $
    slider_neighbor,WID_LABEL_x,WID_LABEL_y, $
    WID_LABEL_GRAYVAL,mousex,mousey
COMMON VELO, WID_BUTTON_delete,WID_BUTTON_plot_velocity, $
    row,WID_BUTTON_print_table,SYS,frame_list, $
    testbild,testbild2,line_index,anzahl,ortho
COMMON MOVIE,width,height,number,film,times, $
    rot_index,index,loaded,range, $
    ep_gestartet,ap_gestartet,file,delayfile, $
    extrema_pressed
COMMON PLOT, line,maxi,mini,smline,WID_DRAW_plot, $
    magnif,magnif2,level,smooth_level,z, $
    WID_BUTTON_Compute,bw_wb, $
    hat_width,sigma,mex_hat,lap_level, $
    front_width,spatial_width,temporal_width, $
    neighbor_width,gray_width,neighbor_width2, $
    old_spatial_width,old_temporal_width, $
    extrema_lupe,bottom_left,upper_right,avlines

.....
;; Geometry of the screen. Any idea how to get
;; it from IDL? Send an e-mail to
;; storb@physik.uni-magdeburg.de
.....
bildschirmweite = 960
bildschirmhoehe = 720

.....
;; Some system depending stuff
.....
IF ( !VERSION.OS EQ "Win32" ) THEN BEGIN
    dir = "e:\temp"
    os_list = "dir /B /L "
    os_del = "del "
    fdln = "\"
    recursive = "*.*"
    nonrecursive = "*"
ENDIF
IF ( !VERSION.OS EQ "linux" ) THEN BEGIN
    dir = "/work/storb"

```

```

os_list  = "ls -ld "
os_del   = "rm "
fdlm     = "/"
recursive = "*"
nonrecursive = "*.*"
ENDIF
IF ( !VERSION.OS EQ "sunos" ) THEN BEGIN
dir      = "/work/storb"
os_list  = "/usr/bin/ls -ld "
os_del   = "rm "
fdlm     = "/"
recursive = "*"
nonrecursive = "*.*"
ENDIF

.....
;; Some other useful settings
.....
dreistellig = "(I3.3)"
vierstellig = "(I4.4)"

.....
;; Prepare loading names of images
.....
file = DIALOG_PICKFILE(/READ,FILTER="*.*",PATH=".",TITLE="Select Folder of imgs",/MULTIPLE_FILES)
IF ( file(0) EQ "" ) THEN RETURN
.....
;; Change to desired folder
.....
pfad = drivename(file(0))+dirname(file(0))
print,"Imagefolder in ",pfad
CD,pfad,CURRENT=old_dir
:temppfad = filepath("","/TMP)
temppfad = "E:"
s=size(file)
scenes=""
FOR i=0,s(1)-1 DO BEGIN
.....q.....
;; Create list of all Movies
.....
;IF ( !VERSION.OS EQ "Win32" ) THEN SPAWN,"dir /B /L /ON *.tif > " +temppfad+"filelist"
; IF ( !VERSION.OS EQ "linux" ) THEN SPAWN,"ls -l imgs* > " +temppfad+"filelist"
;IF ( !VERSION.OS EQ "sunos" ) THEN SPAWN,"/usr/bin/ls -l imgs* > " +temppfad+"filelist"
.....
;; Read list of all Movies
.....
:OPENR,unit,temppfad+"filelist",/GET_LUN
:scenes = [scenes,read_all_lines(unit)]
:CLOSE,unit
:FREE_LUN,unit
SPAWN,"dir /B /ON *.tif ", scenes
ENDFOR
;IF ( !VERSION.OS EQ "Win32" ) THEN SPAWN,"del " +temppfad+"filelist"
;IF ( !VERSION.OS EQ "linux" ) THEN SPAWN,"rm " +temppfad+"filelist"
;IF ( !VERSION.OS EQ "sunos" ) THEN SPAWN,"rm " +temppfad+"filelist"
nroflines = size(scenes)
nroflines = nroflines(1)-1
images = scenes(1:nroflines)
s=size(images)

:outdir = DIALOG_PICKFILE(/READ,FILTER="*.*",PATH=".",TITLE="Select Folder to save subimages")
;IF ( outdir EQ "" ) THEN RETURN

IF ( NOT(KEYWORD_SET(noshow)) ) THEN wind = 1 ELSE wind = 0
IF ( NOT(KEYWORD_SET(firstimage)) ) THEN firstimage = 0
IF ( NOT(KEYWORD_SET(lastimage)) ) THEN lastimage = s(1)-1
number = lastimage - firstimage + 1

```

```

.....
;; Prepare loading images.
;; That means:
;;   - detect size of images
;;   - Allocate memory needed
.....

outdir = pfad + 'timespace_plot\'
spawn,'md ' + outdir

file = DIALOG_PICKFILE(/READ,FILTER='*.tif',PATH=".",TITLE="Select an image to show sub-area")
originalfile = file

filewithoutext = basename(originalfile,/NO_EXTENSION)
extension = basename(originalfile,/EXTENSION)
CASE extension OF
  ".tif": BEGIN
    testbild = REVERSE(READ_TIFF(originalfile),2)
    ;testbild = READ_TIFF(originalfile)
  END
  ".gif": BEGIN
    READ_GIF,originalfile,testbild
  END
  ".hed": BEGIN
    testbild = read_hed(originalfile,0)
  END
ELSE:
ENDCASE

;testbild = reform(testbild(0,*,*))

filmsize = SIZE(testbild)
sizex = filmsize(1)
sizey = filmsize(2)
xsize = sizex
ysize = sizey
xleft = 0
xright = sizex-1
ybottom = 0
ytop = sizey-1

;;modified
xleftj = intarr(no_area)
xrightj = intarr(no_area)
ybottomj = intarr(no_area)
ytopj = intarr(no_area)
plot_direction = strarr(6,no_area)

IF KEYWORD_SET(setvalue) THEN BEGIN

  file = DIALOG_PICKFILE(TITLE='select the file of coordinates of sub areas')
  OPENR, Unit, File, /GET_LUN
ENDIF

testbild0 = testbild

FOR j = 0, no_area -1 DO BEGIN

;IF (KEYWORD_SET(subimage) ) THEN BEGIN

  WINDOW,7,xsize = sizex , sizey = sizey , $
  xpos = bildschirmweite/2 - sizex/2 , $
  ypos = bildschirmhoehe/2 - sizey/2 , $
  title='Select a point on the image'
  WSET, 7
;-----
testbild2 = testbild
x1 = 0
x2 = 0
ok_con = 'Yes'

```

```

while ok_con eq 'Yes' do begin
    testbild3 = testbild2

    TV,testbild2

    ok = dialog_message(/Information,"Select the first point on the image.")
    rdpix,testbild
    x = !mouse.x
    y = !mouse.y
    print,x,y

    testbild2(x,y-2:y+2) = 255
    testbild2(x-2:x+2,y) = 255
    TV,testbild2

    key = "a"
    ok = dialog_message(/Information,"Move the selected point by l:left,r:right")
    WHILE NOT (key EQ 'c') DO BEGIN

        testbild2 = testbild3
        minx = max([0,x])
        maxx = min([xsize-1,x])
        testbild2(x,y-2:y+2) = 255
        testbild2(x-2:x+2,y) = 255

        TV,testbild2

        print, 'get key'
        key = GET_KBRD(1)

        IF key EQ 'l' THEN x = x - 1
        IF key EQ 'r' THEN x = x + 1
        IF key EQ 'd' THEN y = y - 1
        IF key EQ 'u' THEN y = y + 1

    endwhile

    x1 = x:[x1,x]
    y1 = y
    testbild3 = testbild2
    ok = dialog_message(/Information,"Select the second point on the image.")
    rdpix,testbild
    x = !mouse.x
    y = !mouse.y
    print,x,y

    TV,testbild2

    key = "a"
    ok = dialog_message(/Information,"Move the selected point by l:left,r:right")
    WHILE NOT (key EQ 'c') DO BEGIN

        testbild2 = testbild3
        minx = max([0,x])
        maxx = min([xsize-1,x])

        xa = x1
        xe = x;x2
        ya = y1
        ye = y;y2
        avlines = avg_width
        width = sizex

    calc_bresenham_line

    testbild2(line_index) = 255
    markbegin = line_index(*,0:10)
    testbild2(markbegin) = 0

    TV,testbild2

    print, 'get key'

```

```

key = GET_KBRD(1)

IF key EQ 'l' THEN x = x - 1
IF key EQ 'r' THEN x = x + 1
IF key EQ 'd' THEN y = y - 1
IF key EQ 'u' THEN y = y + 1

endwhile

x2 = x;[x2,x]
y2 = y
;-----
;connect two selected points with a straight line.
xa = x1
xe = x2
ya = y1
ye = y2
avlines = avg_width
width = sizex

calc_bresenham_line
;-----
ok_con = 'No';dialog_message(/question,"Calculate another slope?.")

endwhile
;-----

;line_index ;1D position of 1+2*avlines

testbild(line_index) = 255
markbegin = line_index(*,0:10)
testbild(markbegin) = 0

name_pos = '_x' + string(format='(I3.3)',x1) + '_' + string(format='(I3.3)',x2) $
          + '_y' + string(format='(I3.3)',y1) + '_' + string(format='(I3.3)',y2)

selectpointfile = outdir + 'selectpos' + name_pos + '.jpg'
WRITE_JPEG, selectpointfile, testbild

ENDFOR ;j=0, no_area -1

s = size(line_index)
s = s(2)

;;modified
;file = DIALOG_PICKFILE(TITLE = 'Save average intersity to')
;OPENW, Unit, File, /GET_LUN
;intensity = bytarr(2,lastimage - firstimage + 1)

plottime = lastimage - firstimage + 1
;select_plot_y = intarr(no_area)
;maxsize = max([sizex,sizey])
timespaceimage = bytarr(s,plottime)

FOR i=firstimage, lastimage-1 DO BEGIN

originalfile = images(i)
filewithoutext = basename(originalfile,/NO_EXTENSION)
extension = basename(originalfile,/EXTENSION)
;outfile = drivename(outdir)+dirname(outdir)+fdlm+filewithoutext+extension

;IF ( !VERSION.OS EQ "Win32" ) THEN SPAWN,"md "+ drivename(outdir)+dirname(outdir)+basename(images(i))+fdlm
;IF ( !VERSION.OS EQ "linux" ) THEN SPAWN,"ls -l imgs*" + basename(file(i)) + " > " +temppfad+"filelist"
;IF ( !VERSION.OS EQ "sunos" ) THEN SPAWN,"/usr/bin/ls -l imgs*" + basename(file(i)) + " > " +temppfad+"filelist"
PRINT,' image : ',i-firstimage+1,' of ',number,' file = ', originalfile

;-----
;; Stop processing on demand.
;-----
key_in=GET_KBRD(0)
IF ( key_in EQ "q" ) THEN BEGIN
WDELETE,0

```



```

RETURN
ENDIF

.....
;; Read image.
.....
CASE extension OF
  ".tif": BEGIN
    aaxx = REVERSE(READ_TIFF(originalfile),2)

IF avg_width gt 0 then begin ;plot_xline

  for x = 0,s-1 do begin
    timespaceimage(x,i-firstimage) = mean(aaxx(line_index(*,x)))

  endfor;x
endif else begin
  timespaceimage(*,i-firstimage) = aaxx(line_index(*,x))
endelse

  END
  ".gif": BEGIN
    READ_GIF,originalfile,aaxx
    pict = aaxx(xleft:xright,ybottom:ytop)
    END
  ".hed": BEGIN
    aaxx = read_hed(originalfile,0)
    pict = aaxx(xleft:xright,ybottom:ytop)
    END
  ELSE:
ENDCASE

ENDFOR;i
timespaceimage = bytscl(timespaceimage)
timespaceimage(0:10,0:2) = 0

  outfile = outdir +'timespace'+ name_pos + '.tif'
  write_tiff,outfile,timespaceimage,compression=1,0

PRINT,"done"

END

```

## A.2 IDL program for image enhancement (*contrast\_imgs*)

```

Pro contrast_imgs , BACK_SUB = back_sub , $
  BACK_DIV = back_div , $
  KEEP_MEAN = keep_mean , $
  FIX_MEAN = fix_mean , $
  UNIQUE_AMP = unique_amp , $
  NOSHOW = noshow , $
  NONVERBOSE = NONVERBOSE , $
  LOWERLEVEL = lowerlevel , $
  UPPERLEVEL = upperlevel , $
  FIRSTIMAGE = firstimage , $
  LASTIMAGE = lastimage

IF ( NOT(KEYWORD_SET(lowerlevel))) THEN lowerlevel = 0.0;2
IF ( NOT(KEYWORD_SET(upperlevel))) THEN upperlevel = 1.0; - 0.02
MEDIANWIDTH = 3
ausfall_bilder = 0.00
scratch = 1

.....
;; Geometry of the screen. Any idea how to get
;; it from IDL? Send an e-mail to
;; storb@physik.uni-magdeburg.de
.....

```

```

bildschirmweite = 1024
bildschirmhoehe = 768

.....
;; Prepare loading names of images
.....
file = DIALOG_PICKFILE(/READ,FILTER="*.txt",PATH=".", $
    TITLE="Select list file of movies to enhance contrast")
IF ( file(0) EQ "" ) THEN RETURN
.....
;; Change to desired folder
.....
pfad = drivename(file(0))+dirname(file(0))
print,"Imagefolder is ",pfad
old_dir = ""
CD,pfad,CURRENT=old_dir
OPENR,unit,file(0),/GET_LUN
scenes = read_all_lines(unit)
CLOSE,unit
FREE_LUN,unit
nroflines = size(scenes)
nroflines = nroflines(1)-1
;movies = scenes(1:nroflines)
movies = scenes
s = size(movies)

outdir = DIALOG_PICKFILE(/READ,FILTER="*.*",PATH=".",TITLE="Select Folder to save movies with enhanced contrast")
IF ( outdir EQ "" ) THEN RETURN
print,"destinationfolder is ",drivename(outdir) + dirname(outdir)

IF ( NOT(KEYWORD_SET(noshow)) ) THEN wind = 1 ELSE wind = 0
IF ( NOT(KEYWORD_SET(firstimage)) ) THEN firstimage = 0
IF ( NOT(KEYWORD_SET(lastimage)) ) THEN lastimage = s(1)-1
number = lastimage - firstimage + 1

.....
;; Prepare loading images.
;; That means:
;; - detect number of images
;; - detect size of images
;; - Allocate memory needed, if not available use scratchfile
.....
originalfile = movies(0)
filewithoutext = basename(originalfile,/NO_EXTENSION)
extension = basename(originalfile,/EXTENSION)
CASE extension OF
    ".tif": BEGIN
        testbild = READ_TIFF(movies(0))
        END
    ".gif": BEGIN
        READ_GIF,movies(0),testbild
        END
    ".hed": BEGIN
        testbild = read_hed(movies(0),0)
        END
ELSE:
ENDCASE

filmsize = SIZE(testbild)
sizex = filmsize(1)
sizey = filmsize(2)
nsq = sizex*sizey
back = FLTARR(sizex,sizey)
meanlights = FLTARR(number)
meanlights2 = FLTARR(number)
maxlights = FLTARR(number)
minlights = FLTARR(number)
IF (wind EQ 1) THEN BEGIN
    mean_1 = FLTARR(number)
    ma_1 = FLTARR(number)
    mi_1 = FLTARR(number)
ENDIF
ENDIF

```

```

alpha   = FLTARR(number,511)
beta    = FLTARR(number,511)
maxalpha = FLTARR(number)
maxbeta = FLTARR(number)
zett    = FINDGEN(511) - 255.0
IF ( KEYWORD_SET(back_div) ) THEN BEGIN
    zett = (zett / 255.0) * ALOG(255)
ENDIF
gamma   = FLTARR(number,511)
gammamin = FLTARR(511)
gammamin2 = FLTARR(511)
gammamax = FLTARR(number)
gammashift = FLTARR(number)
IF ( scratch NE 0 ) THEN      $
    pict = FLTARR(sizeX,sizeY,1)  $
ELSE                          $
    pict = FLTARR(sizeX,sizeY,number)

```

.....  
;; If requested, show some illustration of what  
;; we are doing. In the first step we need only  
;; windows to show  
;; - original images  
;; - the calculated background  
.....

```

IF (wind EQ 1) THEN BEGIN
    xinc2 = bildschirmweite / 3
    xinc  = MIN([xinc2,sizeX+5])
    ycorrection = 28
    xcorrection = 56
    y_plot_size = (bildschirmhoehe-sizeY-20-3*ycorrection)/2
    WINDOW,0,xsize = sizeX , ysize = sizeY+20 , $
        xpos = 0*xinc , ypos = bildschirmhoehe-sizeY-20-ycorrection , $
        title='original picture'
    IF ( KEYWORD_SET(back_sub) OR KEYWORD_SET(back_div) ) THEN BEGIN
        WINDOW,2,xsize = sizeX , ysize = sizeY+20 , $
            xpos = 1*xinc , ypos = bildschirmhoehe-sizeY-20-ycorrection , $
            title='background'
    ENDIF
    erase_img = BYTARR(sizeX,20)
ENDIF

```

IF ( KEYWORD\_SET(back\_sub) OR KEYWORD\_SET(back\_div) ) THEN BEGIN  
;==== 1. determine background =====  
IF (wind EQ 1) THEN PRINT,FORMAT = '(\$," start determine background : ") \$  
ELSE PRINT,FORMAT = '(' " start determine background : ")'

FOR i=firstimage, lastimage DO BEGIN

```

    originalfile = movies(i)
    j            = i-firstimage
    IF ( scratch NE 0 ) THEN jj = 0 ELSE jj = j
    ;PRINT,'    image : 'j+1,' of ',number,' file = ', originalfile

```

.....  
;; Stop processing on demand.  
.....

```

key_in=GET_KBRD(0)
IF ( key_in EQ "q" ) THEN BEGIN
    IF (wind EQ 1) THEN BEGIN
        IF ( NOT(KEYWORD_SET(nonverbose)) ) THEN BEGIN
            blabla = DIALOG_MESSAGE("If you want to keep the windows then press yes, otherwise they will be closed", $
                TITLE = "Keep windows?" , /QUESTION )
            blabla = STRUPCASE(blabla)
            IF ( blabla EQ "NO" ) THEN BEGIN
                WDELETE,0 & WDELETE,2
            ENDIF
        ENDIF ELSE BEGIN
            WDELETE,0 & WDELETE,2
        ENDELSE
    ENDIF

```

```

        ENDIF
        STOP
    ENDIF

    .....
    ;; Read image.
    .....
    pict(*,*,jj) = TIF_GIF_HED_READ(originalfile,sizeX,sizeY)

    .....
    ;; Median-filtering the image to get rid of that
    ;; salt&pepper-noise.
    .....
    IF ( MEDIANWIDTH GT 1 ) THEN pict(*,*,jj) = MEDIAN(pict(*,*,jj),MEDIANWIDTH)
    IF ( KEYWORD_SET(back_sub) ) THEN BEGIN
        back = back + pict(*,*,jj)
    ENDIF
    IF ( KEYWORD_SET(back_div) ) THEN BEGIN
        pict2 = pict(*,*,jj)
        unsinn = WHERE(pict2 LT 0.5)
        IF (unsinn(0) GE 0) THEN pict2(unsinn) = 1.0
        pict(*,*,jj) = pict2
        back = back + ALOG(pict(*,*,jj))
    ENDIF
    IF (wind EQ 1) THEN BEGIN
        WSET,0
        TV,BYTE(pict(*,*,jj),0,20)
        TV,erase_img
        XYOUTS,3,5,basename(originalfile)+STRING(FORMAT="( 'img ",I4.4," of ",I4.4)',j+1,number),/DEVICE
        WSET,2
        IF ( KEYWORD_SET(back_div) ) THEN BEGIN
            TV,BYTE(EXP(back/(j+1))),0,20
        ENDIF ELSE BEGIN
            TV,BYTE(back/(j+1)),0,20
        ENDELSE
    ENDIF

ENDFOR

back = back/number
PRINT," MEAN of background image = ",MEAN(back)
PRINT,FORMAT="( "done" )"
IF ( KEYWORD_SET(back_sub) ) THEN BEGIN
    IF (wind EQ 1) THEN PRINT,FORMAT = '( $," start backgroundsubtraction and determination of stretch parameters : " ) $
    ELSE PRINT,FORMAT = '( " start backgroundsubtraction and determination of stretch parameters : " )'
ENDIF
IF ( KEYWORD_SET(back_div) ) THEN BEGIN
    IF (wind EQ 1) THEN PRINT,FORMAT = '( $," start backgrounddivision and determination of stretch parameters : " ) $
    ELSE PRINT,FORMAT = '( " start backgrounddivision and determination of stretch parameters : " )'
ENDIF

ENDIF ELSE BEGIN ; Background handling
    IF (wind EQ 1) THEN PRINT,FORMAT = '( $," start determination of stretch parameters : " ) $
    ELSE PRINT,FORMAT = '( " start determination of stretch parameters : " )'
ENDELSE

    .....
    ;; If requested, show some illustration of what
    ;; we are doing. In the first step we need only
    ;; windows to show
    ;; - original images
    ;; - the calculated background
    ;; - calculated difference / ratio image
    ;; - mean, min and max after applying the cut-off
    ;; Remember, the last three things depend on
    ;; the parameters lowerlevel & upperlevel
    .....
    IF (wind EQ 1) THEN BEGIN
        IF ( KEYWORD_SET(back_sub) ) THEN BEGIN
            WINDOW,3,xsize = sizeX , ysize = sizeY+20 , $
            xpos = 2*xinc , ypos = bildschirmhoehe-sizeY-20-y correction , $
            title='original - back picture'
        ENDIF
    ENDIF

```

```

IF ( KEYWORD_SET(back_div) ) THEN BEGIN
  WINDOW,3,xsize = sizex , ysize = sizey+20 , $
  xpos = 2*xinc , ypos = bildschirmhoehe-sizey-20-y correction , $
  title='original / back picture'
ENDIF
WINDOW,5,xsize = xinc2 , ysize = y_plot_size , $
  xpos = 0*xinc2 , ypos = 0 , $
  title='mean (original), min, max (after cut-off)'
WINDOW,6,xsize = xinc2 , ysize = y_plot_size , $
  xpos = 1*xinc2 , ypos = 0 , $
  title='Distribution (original)'
WINDOW,4,xsize = xinc2 , ysize = y_plot_size , $
  xpos = 2*xinc2 , ypos = 0 , $
  title='Density (original)'
ENDIF

FOR i=firstimage, lastimage DO BEGIN

  j = i-firstimage
  IF ( scratch NE 0 ) THEN jj = 0 ELSE jj = j

  ::::::::::::::::::::::::::::::::::::::
  ;; Stop processing on demand.
  ::::::::::::::::::::::::::::::::::::::
  key_in=GET_KBRD(0)
  IF ( key_in EQ "q" ) THEN BEGIN
    IF (wind EQ 1) THEN BEGIN
      IF ( NOT(KEYWORD_SET(nonverbose)) ) THEN BEGIN
        blabla = DIALOG_MESSAGE("If you want to keep the windows then press yes, otherwise they will be closed", $
          TITLE = "Keep windows?" , /QUESTION )
        blabla = STRUPCASE(blabla)
        IF ( blabla EQ "NO" ) THEN BEGIN
          WDELETE,0 & WDELETE,6
          WDELETE,4 & WDELETE,5
          IF ( KEYWORD_SET(back_sub) OR KEYWORD_SET(back_div) ) THEN BEGIN
            WDELETE,2 & WDELETE,3
          ENDIF
        ENDIF
      ENDIF ELSE BEGIN
        WDELETE,0 & WDELETE,6
        WDELETE,4 & WDELETE,5
        IF ( KEYWORD_SET(back_sub) OR KEYWORD_SET(back_div) ) THEN BEGIN
          WDELETE,2 & WDELETE,3
        ENDIF
      ENDELSE
    ENDIF
    STOP
  ENDIF

  ::::::::::::::::::::::::::::::::::::::
  ;; Read image.
  ::::::::::::::::::::::::::::::::::::::
  IF ( ( scratch NE 0 ) OR ( NOT(KEYWORD_SET(back_sub)) AND NOT(KEYWORD_SET(back_div)) ) ) THEN BEGIN
    originalfile = movies(i)
    ;PRINT,' image : 'j+1,' of ',number,' file = ', originalfile
    pict(*,jj) = TIF_GIF_HED_READ(originalfile,sizex,sizey)
    ::::::::::::::::::::::::::::::::::::::
    ;; Median-filtering the image to get rid of that
    ;; salt&pepper-noise.
    ::::::::::::::::::::::::::::::::::::::
    IF ( MEDIANWIDTH GT 1 ) THEN pict(*,jj) = MEDIAN(pict(*,jj),MEDIANWIDTH)
  ENDIF ; IF ( scratch NE 0 ) THEN BEGIN

  IF (wind EQ 1) THEN BEGIN
    WSET,0
    TV,BYTE(pict(*,jj)),0,20
    TV,erase_img
    XYOUTS,3,5,basename(originalfile)+STRING(FORMAT="( " img ",I4.4," of ",I4.4)'j+1,number),/DEVICE
  ENDIF
  IF ( KEYWORD_SET(back_sub) ) THEN BEGIN
    ;==== background subtraction =====
    pict(*,jj) = (pict(*,jj) - back)
  ENDIF

```



```

PLOT,FLOAT(hist) / FLOAT(max_hist),XRANGE=[0,511.0]
OPLOT,[minlights(j),minlights(j)+0.001],[0,1.0],COLOR=255
OPLOT,[maxlights(j)-0.001,maxlights(j)],[0,1.0],COLOR=65535

;; Show the graylevel distribution
WSET,6
PLOT,FLOAT(r(0:s(1)))/FLOAT(nsq),XRANGE=[0,511.0]
OPLOT,[minlights(j),minlights(j)+0.001], $
  [0,FLOAT(r(minlights(j)))/FLOAT(nsq)+0.1],COLOR=255
OPLOT,[maxlights(j)-0.001,maxlights(j)], $
  [0,FLOAT(r(maxlights(j))) /FLOAT(nsq)+0.1],COLOR=65535

;; Show the course in time of the mean-, max- and min-graylevel
WSET,5
PLOT,meanlights,YRANGE=[-255.0,255.0]
OPLOT,minlights-255,COLOR=255
OPLOT,maxlights-255,COLOR=65535

ENDIF

;IF ( KEYWORD_SET(keep_mean) OR KEYWORD_SET(unique_amp)) THEN BEGIN
  IF ( KEYWORD_SET(back_div) ) THEN BEGIN
    alpha(j,*) = ( ALOG(255.0) - (meanlights(j) + zett) ) $
      / ( maxlights(j) - meanlights(j) )
    beta (j,*) = ( ALOG(255.0) + (meanlights(j) + zett) ) $
      / ( meanlights(j) - minlights(j) )
  ENDIF ELSE BEGIN
    alpha(j,*) = ( 255.0 - (meanlights(j) + zett) ) $
      / ( maxlights(j)-255.0 - meanlights(j) )
    beta (j,*) = ( 255.0 + (meanlights(j) + zett) ) $
      / ( meanlights(j)+ 255.0 - minlights(j) )
  ENDELSE
  FOR k=0,510 DO BEGIN
    gamma(j,k) = min([alpha(j,k),beta(j,k)])
  ENDFOR
  FOR k=0,510 DO BEGIN
    gamma(j,k) = max([gamma(j,k),0.0])
  ENDFOR
;ENDIF
ENDFOR

PRINT,FORMAT=("done")

FOR j=0,510 DO BEGIN
  a1 = MIN(gamma(*,j))
  a2 = MAX(gamma(*,j))
  binsize = (FLOAT(a2)-FLOAT(a1))/255.0
  binsize = MAX([binsize,0.01])
  hist = HISTOGRAM(gamma(*,j)-a1,REVERSE_INDICES=r,BINSIZE=binsize)
  s = size(hist)
  result = WHERE((r(0:s(1))-r(0)) ge number*ausfall_bilder)
  gamma2 = gamma(*,j)-a1
  wegschmeiss = WHERE(gamma2 LT MIN(result))
  IF (wegschmeiss(0) NE -1) THEN gamma2(wegschmeiss) = MIN(result)
  gamma(*,j) = gamma2 + a1
ENDFOR

IF ( KEYWORD_SET(keep_mean) AND KEYWORD_SET(unique_amp)) THEN BEGIN
  FOR j=0,510 DO BEGIN
    gammamin(j) = MIN(gamma(*,j))
  ENDFOR
  gammamax2 = MAX(gammamin,gammaindex2)
  gammamax(*) = gammamax2
  gammashift(*) = gammaindex2-256
ENDIF ELSE BEGIN
  IF ( KEYWORD_SET(keep_mean) ) THEN BEGIN
    FOR j=0,510 DO BEGIN
      gamma2 = gamma(*,j)
      gammamin(j) = TRANSPOSE(gamma2)#gamma2
    ENDFOR
    gammamax2 = MAX(gammamin,gammaindex2)
    gammamax(*) = gamma(*,gammaindex2)
    gammashift(*) = gammaindex2-256
  ENDIF

```

```

ENDIF
IF ( KEYWORD_SET(unique_amp)) THEN BEGIN
  FOR k=0,number-1 DO BEGIN
    gammamax(k) = MAX(gamma(k,*))
  ENDFOR
  gamma3 = MIN(gammamax)
  gammamax(*) = gamma3
  FOR k=0,number-1 DO BEGIN
    gamma2 = gamma(k,*)
    shifts = WHERE(gamma2 GE gamma3)
    gammashift(k) = MIN(ABS(shifts-(511+1)/2));-256
  ENDFOR
ENDIF
ENDELSE
IF ( NOT(KEYWORD_SET(keep_mean)) AND NOT(KEYWORD_SET(unique_amp))) THEN BEGIN
  FOR k=0,number-1 DO BEGIN
    gamma2 = gamma(k,*)
    gammamax(k) = MAX(gamma(k,*),gammaindex2)
    gammashift(k) = gammaindex2-256
  ENDFOR
ENDIF

IF (wind EQ 1) THEN PRINT,FORMAT = '($," start normalization : ")' $
  ELSE PRINT,FORMAT = '('" start normalization : "'

IF (wind EQ 1) THEN BEGIN
  WINDOW,1,xsize = sizex , ysize = sizey+20 , $
  xpos = 3*xinc , ypos = bildschirmhoehe-sizey-20-ycorrection , $
  title='normalized picture'
  WINDOW,7,xsize = xinc2 , ysize = y_plot_size , $
  xpos = 0*xinc2 , ypos = y_plot_size + ycorrection , $
  title='mean, min, max (after stretching)'
  WINDOW,8,xsize = xinc2 , ysize = y_plot_size , $
  xpos = 1*xinc2 , $
  ypos = y_plot_size + ycorrection , $
  title='Distribution (after stretching)'
  WINDOW,9,xsize = xinc2 , ysize = y_plot_size , $
  xpos = 2*xinc2 , $
  ypos = y_plot_size + ycorrection , $
  title='Density (after stretching)'
ENDIF

FOR i=firstimage, lastimage DO BEGIN

  originalfile = movies(i)
  filewithoutext = basename(originalfile,/NO_EXTENSION)
  extension = basename(originalfile,/EXTENSION)
  outfile = drivename(outdir)+dirname(outdir)+filewithoutext+extension
  j = i-firstimage
  IF ( scratch NE 0 ) THEN jj = 0 ELSE jj = j
  ;PRINT,' image : ',j+1, ' of ',number, ' file = ', originalfile

  .....
  ;; Stop processing on demand.
  .....
  key_in=GET_KBRD(0)
  IF ( key_in EQ "q" ) THEN BEGIN
    IF (wind EQ 1) THEN BEGIN
      IF ( NOT(KEYWORD_SET(nonverbose)) ) THEN BEGIN
        blabla = DIALOG_MESSAGE("If you want to keep the windows then press yes, otherwise they will be closed", $
          TITLE = "Keep windows?" , /QUESTION )
        blabla = STRUPCASE(blabla)
        IF ( blabla EQ "NO" ) THEN BEGIN
          WDELETE,0 & WDELETE,1 & WDELETE,9 & WDELETE,4
          WDELETE,5 & WDELETE,6 & WDELETE,7 & WDELETE,8
          IF ( KEYWORD_SET(back_sub) OR KEYWORD_SET(back_div) ) THEN BEGIN
            WDELETE,2 & WDELETE,3
          ENDFOR
        ENDFOR
      ENDFOR ELSE BEGIN
        WDELETE,0 & WDELETE,1 & WDELETE,9 & WDELETE,4
        WDELETE,5 & WDELETE,6 & WDELETE,7 & WDELETE,8
      ENDFOR
    ENDFOR
  ENDFOR

```



```

        IF ( KEYWORD_SET(back_sub) OR KEYWORD_SET(back_div) ) THEN BEGIN
            WDELETE,2 & WDELETE,3
        ENDIF
    ENDELSE
ENDIF
STOP
ENDIF

.....
;; Read image.
.....
IF ( scratch NE 0 ) THEN BEGIN
    pict(*,*,jj) = TIF_GIF_HED_READ(originalfile,sizex,sizey)
    .....
    ;; Median-filtering the image to get rid of that
    ;; salt&pepper-noise.
    .....
    IF ( MEDIANWIDTH GT 1 ) THEN pict(*,*,jj) = MEDIAN(pict(*,*,jj),MEDIANWIDTH)
    IF ( KEYWORD_SET(back_sub) ) THEN BEGIN
        ;==== background subtraction =====
        pict(*,*,jj) = (pict(*,*,jj) - back)
        IF KEYWORD_SET(fix_mean) THEN BEGIN
            pict(*,*,jj) = pict(*,*,jj) - MEAN(pict(*,*,jj))
        ENDIF
    ENDIF
    IF ( KEYWORD_SET(back_div) ) THEN BEGIN
        ;==== background division =====
        pict2 = pict(*,*,jj)
        unsinn = WHERE(pict2 LT 0.5)
        IF (unsinn(0) GE 0) THEN pict2(unsinn) = 1.0
        pict(*,*,jj) = (ALOG(pict2) - back)
        IF KEYWORD_SET(fix_mean) THEN BEGIN
            pict(*,*,jj) = pict(*,*,jj) - MEAN(pict(*,*,jj))
        ENDIF
    ENDIF
    IF ( NOT(KEYWORD_SET(back_sub)) AND NOT(KEYWORD_SET(back_div)) ) THEN BEGIN
        pict(*,*,jj) = (pict(*,*,jj) - meanlights2(j))
    ENDIF
ENDIF ; IF ( scratch NE 0 ) THEN BEGIN

    pict2 = ( ( pict(*,*,jj) - meanlights(j) ) $
        * gammamax(j) + (meanlights(j) + gammashift(j)
    zugross = WHERE(pict2 GT 255.0)
    IF (zugross(0) GE 0) THEN pict2(zugross) = 255.0
    zuklein=WHERE(pict2 LT -255.0)
    IF (zuklein(0) GE 0) THEN pict2(zuklein) = -255.0

IF (wind EQ 1) THEN BEGIN
    WSET,1
    TV,BYTE(pict2 / 2.0 + 128),0,20
    TV,erase_img
    XYOUTS,3,5,basename(originalfile)+STRING(FORMAT=("' img ",I4.4," of ",I4.4)',j+1,number),/DEVICE
    IF ( KEYWORD_SET(back_sub) OR KEYWORD_SET(back_div) ) THEN BEGIN
        WSET,3
        TV,BYTE(pict(*,*,jj) + MEAN(back)),0,20
        TV,erase_img
        XYOUTS,3,5,basename(originalfile)+STRING(FORMAT=("' img ",I4.4," of ",I4.4)',j+1,number),/DEVICE
        WSET,0
        TV,BYTE(pict(*,*,jj) + back),0,20
        TV,erase_img
        XYOUTS,3,5,basename(originalfile)+STRING(FORMAT=("' img ",I4.4," of ",I4.4)',j+1,number),/DEVICE
    ENDIF ELSE BEGIN
        WSET,0
        TV,BYTE(pict(*,*,jj)+meanlights2(j)),0,20
        TV,erase_img
        XYOUTS,3,5,basename(originalfile)+STRING(FORMAT=("' img ",I4.4," of ",I4.4)',j+1,number),/DEVICE
    ENDELSE
    hist = HISTOGRAM(pict(*,*,jj),REVERSE_INDICES=r,MAX=255.0,MIN=-255.0);
    s = SIZE(hist)
    r = r - r(0)

;hist = HISTOGRAM(BYTE(pict(*,*,jj)),REVERSE_INDICES=r )

```



```

ENDIF
ENDIF ELSE BEGIN
WDELETE,0 & WDELETE,1 & WDELETE,9 & WDELETE,4
WDELETE,5 & WDELETE,6 & WDELETE,7 & WDELETE,8
IF ( KEYWORD_SET(back_sub) OR KEYWORD_SET(back_div) ) THEN BEGIN
WDELETE,2 & WDELETE,3
ENDIF
ENDELSE
ENDIF
END

FUNCTION tif_gif_hed_read,originalfile,size,ysize

pict = FLTARR(size,ysize)
filewithoutext = basename(originalfile,/NO_EXTENSION)
extension = basename(originalfile,/EXTENSION)
CASE extension OF
".tif": BEGIN
;; React on changing image size
query_ok = QUERY_TIFF(originalfile,query_info)
xs = query_info.DIMENSIONS(0)
ys = query_info.DIMENSIONS(1)
IF ( xs LT size ) THEN BEGIN
pict( (size-xs)/2 : xs + (size-xs)/2 - 1, $
(sizey-ys)/2 : ys + (sizey-ys)/2 - 1) $
= REVERSE(READ_TIFF(originalfile),2)
ENDIF
IF ( xs GT size ) THEN BEGIN
abcd = REVERSE(READ_TIFF(originalfile),2)
pict(*,*) = abcd( (xs-size)/2 : size+(xs-size)/2 - 1,*)
ENDIF
IF ( xs EQ size ) THEN BEGIN
pict(*,*) = REVERSE(READ_TIFF(originalfile),2)
ENDIF
END
".gif": BEGIN
READ_GIF,originalfile,abcd
pict(*,*) = abcd
END
".hed": BEGIN
pict(*,*) = read_hed(originalfile,0)
END
ELSE:
ENDCASE
RETURN,pict
END

```

## References

- [1] Ball, P. (2001) *The Self-Made Tapestry: Pattern Formation in Nature*. Oxford University Press, New York.
- [2] Goldbeter, A. (1996) *Biochemical Oscillations and Cellular Rhythms*. Cambridge University Press, Cambridge.
- [3] Kapral, R. and Showalter, K. (1995) *Chemical Waves and Patterns*. Kluwer Academic Publishers, Dordrecht.
- [4] Li, Y.J., Oslovitch, J., Mazouz, N., Plenge, F., Krischer, K., and Ertl, G. (2001) Turing-type patterns on electrode surfaces. *Science*, **291**, 2395-2398.
- [5] Murray, J.D. (1989) *Mathematical Biology*. Springer, Berlin.
- [6] Suchorski, Y., Drachsel, W., Gorodetskii, V.V., Medvedev, V.K., and Weiss, H. (2006) Lifted reconstruction as a feedback mechanism in the oscillating CO oxidation on Pt nanofacets: Microscopic evidences. *Surf. Sci.*, **600**, 1579-1585.
- [7] Umbanhowar, P.B., Melo, F., and Swinney, H.L. (1996) Localized excitations in a vertically vibrated granular layer. *Nature*, **382**, 793-796.
- [8] Walgraef, D. (1997) *Spatio-Temporal Pattern Formation*. Springer, New York.
- [9] Nicolis, G. and Prigogine, I. (1977) *Self-Organization in Nonequilibrium Systems*. John Wiley & Sons, New York.
- [10] Keener, J.P. and Tyson, J.J. (1986) Spiral waves in the Belousov-Zhabotinskii reaction. *Physica D*, **21**, 307-324.
- [11] Turing, A.M. (1952) Chemical basis of morphogenesis. *Philos. Trans. Roy. Soc. (London)*, **B237**, 37-72.
- [12] Belousov, B.P. (1958) A periodic reaction and its mechanism, In Sbornik Referatov po Radiatsionnoi Meditsine. *Moscow: Medgiz.*, 145-147.
- [13] Zaikin, A.N. and Zhabotinsky, A.M. (1970) Concentration wave propagation in two-dimensional liquid-phase self-oscillating system. *Nature*, **225**, 535-537.
- [14] Zhabotinskii, A.M. (1964) Periodic process of the oxidation of malonic acid in solution (study of kinetics of Belousov's reaction). *Biofizika*, **9**, 306-311.
- [15] Lechleiter, J., Girard, S., Peralta, E., and Clapham, D. (1991) Spiral calcium wave propagation and annihilation in *Xenopus laevis* oocytes. *Science*, **252**, 123-126.

- [16] Basarsky, T.A., Duffy, S.N., Andrew, R.D., and MacVicar, B.A. (1998) Imaging spreading depression and associated intracellular calcium waves in brain slices. *J. Neurosci.*, **18**, 7189-7199.
- [17] Dahlem, M.A. and Müller, S.C. (1997) Self-induced splitting of spiral-shaped spreading depression waves in chicken retina. *Exp. Brain Res.*, **115**, 319-324.
- [18] Hilgardt, C., Cejková, J., Hauser, M.J.B., and Sevciková, H. (2008) Streamless aggregation of *Dictyostelium* in the presence of isopropyladenosin. *Biophys. Chem.*, **132**, 9-17.
- [19] Tomchik, K.J. and Devreotes, P.N. (1981) Adenosine 3',5'-monophosphate waves in *Dictyostelium discoideum*: a demonstration by isotope dilution-fluorography. *Science*, **212**, 443-446.
- [20] Mair, T. and Müller, S.C. (1996) Traveling NADH and proton waves during oscillatory glycolysis in vitro. *J. Biol. Chem.*, **271**, 627-630.
- [21] Mair, T., Warnke, C., and Müller, S.C. (2001) Spatio-temporal dynamics in glycolysis. *Faraday Discuss.*, **120**, 249-259.
- [22] Petty, H.R., Worth, R.G., and Kindzelskii, A.L. (2000) Imaging sustained dissipative patterns in the metabolism of individual living cells. *Phys. Rev. Lett.*, **84**, 2754-2757.
- [23] Ebeling, W. (1991) *Chaos, Ordnung, Information*. Harri Deutsch, Frankfurt am Main/ Thun.
- [24] Mair, T. and Müller, S.C. (2000) Propagating waves of biological activity. *Recent Res. Devel. Biophys. Chem.*, **1**, 105-121.
- [25] Petty, H.R. (2001) Neutrophil oscillations: temporal and spatiotemporal aspects of cell behavior. *Immunol. Res.*, **23**, 85-94.
- [26] Betz, A. and Chance, B. (1965) Phase relation of glycolytic intermediates in yeast cells with oscillatory metabolic control. *Arch. Biochem. Biophys.*, **109**, 585-594.
- [27] Chance, B., Estabrook, R.W., and Ghosh, A. (1964) Damped sinusoidal oscillations of cytoplasmic reduced pyridine nucleotide in yeast cells. *Proc. Natl. Acad. Sci. USA*, **51**, 1244-1251.
- [28] Ghosh, A. and Chance, B. (1964) Oscillations of glycolytic intermediates in yeast cells. *Biochem. Biophys. Res. Commun.*, **16**, 174-181.
- [29] Chance, B., Hess, B., and Betz, A. (1964) DPNH oscillations in a cell-free extract of *S. carlsbergensis*. *Biochem. Biophys. Res. Commun.*, **16**, 182-187.
- [30] Hess, B., Brand, K., and Pye, K. (1966) Continuous oscillations in a cell-free extract of *S. carlsbergensis*. *Biochem. Biophys. Res. Commun.*, **23**, 102-108.

- [31] Bergsten, P., Westerlund, J., Liss, P., and Carlsson, P.O. (2002) Primary in vivo oscillations of metabolism in the pancreas. *Diabetes*, **51**, 699-703.
- [32] Chou, H.F., Berman, N., and Ipp, E. (1992) Oscillations of lactate released from islets of Langerhans: evidence for oscillatory glycolysis in beta-cells. *Am. J. Physiol.*, **262**, E800-E805.
- [33] Corkey, B.E., Tornheim, K., Deeney, J.T., Glennon, M.C., Parker, J.C., Matschinsky, F.M., Ruderman, N.B., and Prentki, M. (1988) Linked oscillations of free  $\text{Ca}^{2+}$  and the ATP/ADP ratio in permeabilized RINm5F insulinoma cells supplemented with a glycolyzing cell-free muscle extract. *J. Biol. Chem.*, **263**, 4254-4258.
- [34] Juntti-Berggren, L., Webb, D.L., Arkhammar, P.O., Schultz, V., Schweda, E.K., Tornheim, K., and Berggren, P.O. (2003) Dihydroxyacetone-induced oscillations in cytoplasmic free  $\text{Ca}^{2+}$  and the ATP/ADP ratio in pancreatic beta-cells at substimulatory glucose. *J. Biol. Chem.*, **278**, 40710-40716.
- [35] Danø, S., Sørensen, P.G., and Hynne, F. (1999) Sustained oscillations in living cells. *Nature*, **402**, 320-322.
- [36] Hocker, C.G., Epstein, I.R., Kustin, K., and Tornheim, K. (1994) Glycolytic pH oscillations in a flow reactor. *Biophys. Chem.*, **51**, 21-35.
- [37] Nielsen, K., Sørensen, P.G., Hynne, F., and Busse, H.G. (1998) Sustained oscillations in glycolysis: an experimental and theoretical study of chaotic and complex periodic behavior and of quenching of simple oscillations. *Biophys. Chem.*, **72**, 49-62.
- [38] Hervagault, J.F. and Thomas, D. (1983) Experimental evidence and theoretical discussion for long-term oscillations of phosphofructokinase in a compartmentalized system. *Eur. J. Biochem.*, **131**, 183-187.
- [39] Schellenberger, W., Eschrich, K., and Hofmann, E. (1981) Self-stabilization of the energy charge in a reconstituted enzyme system containing phosphofructokinase. *Eur. J. Biochem.*, **118**, 309-314.
- [40] Dulos, E., Boissonade, J., and De Kepper, P. (1991) Excyclon dynamics. In *Nonlinear Wave Processes in Excitable Media* (Holden, A.V., Markus, M., & Othmer, H.G., eds), pp. 423-434. Plenum, New York.
- [41] Tam, W.Y., Horsthemke, W., Noszticzius, Z., and Swinney, H.L. (1988) Sustained spiral waves in a continuously fed unstirred chemical reactor. *J. Chem. Phys.*, **88**, 3395-3396.
- [42] Castets, V., Dulos, E., Boissonade, J., and De Kepper, P. (1990) Experimental evidence of a sustained standing Turing-type nonequilibrium chemical pattern. *Phys. Rev. Lett.*, **64**, 2953-2956.

- [43] Ouyang, Q. and Swinney, H.L. (1991) Transition from a uniform state to hexagonal and striped Turing patterns. *Nature*, **352**, 610-612.
- [44] Rudovics, B., Barillot, E., Davies, P.W., Dulos, E., Boissonade, J., and De Kepper, P. (1999) Experimental Studies and Quantitative Modeling of Turing Patterns in the (Chlorine Dioxide, Iodine, Malonic Acid) Reaction. *J. Phys. Chem. A*, **103**, 1790-1800.
- [45] Mikhailov, A.S. (1994) *Foundations of Synergetics I*, 2nd edn., Springer, Berlin.
- [46] Kheowan, O.-U. (2001) *Dynamics of spiral waves under feedback control in the light-sensitive Belousov-Zhabotinsky reaction*. Dissertation, Mahidol University, Bangkok.
- [47] Luengviriyaya, C. (2008) *Dynamics of three-dimensional excitation waves*. Dissertation, Otto-von-Guericke Universität Magdeburg.
- [48] Belmonte, A. and Flesselles, J.M. (1996) Experimental Determination of the Dispersion Relation for Spiral Waves. *Phys. Rev. Lett.*, **77**, 1174-1177.
- [49] Flesselles, J.M., Belmonte, A., and Gaspar, V. (1998) Dispersion relation for waves in the Belousov-Zhabotinsky reaction. *J. Chem. Soc., Faraday Trans.*, **94**, 851-855.
- [50] Pagola, A., Ross, J., and Vidal, C. (1988) Measurement of dispersion relation of chemical waves in an oscillatory reacting medium. *J. Phys. Chem.*, **92**, 163-166.
- [51] Hamik, C.T., Manz, N., and Steinbock, O. (2001) Anomalous dispersion and attractive pulse interaction in the 1,4-cyclohexanedione Belousov-Zhabotinsky reaction. *J. Phys. Chem. A*, **105**, 6144-6153.
- [52] Manz, N., Müller, S.C., and Steinbock, O. (2000) Anomalous dispersion of chemical waves in a homogeneously catalyzed reaction system. *J. Phys. Chem. A*, **104**, 5895-5897.
- [53] Zykov, V.S. (1980) Analytical estimation of dependence of excitation wave velocity in two-dimensional excitable medium on curvature of its front. *Biofizika*, **25**, 888-892.
- [54] Foerster, P., Müller, S.C., and Hess, B. (1988) Curvature and Propagation Velocity of Chemical Waves. *Science*, **241**, 685-687.
- [55] Reusser, E.J. and Field, R.J. (1979) The transition from phase waves to trigger waves in a model of the Zhabotinskii reaction. *J. Amer. Chem. Soc.*, **101**, 1063-1071.
- [56] Bodet, J.M., Ross, J., and Vidal, C. (1987) Experiments on phase diffusion waves. *J. Chem. Phys.*, **86**, 4418-4424.

- [57] Winfree, A.T. (1974) Two kinds of wave in an oscillating chemical solution. *Farad. Symp. Chem. Soc.*, **9**, 38-46.
- [58] Aliev, R.R. and Biktashev, V.N. (1994) Dynamics of the oscillation phase distribution in the BZ reaction. *J. Phys. Chem.*, **98**, 9676-9681.
- [59] Bordiougov, G. and Engel, H. (2006) From trigger to phase waves and back again. *Physica D*, **215**, 25-37.
- [60] Vanag, V.K. and Epstein, I.R. (2001) Inwardly rotating spiral waves in a reaction-diffusion system. *Science*, **294**, 835-837.
- [61] Gong, Y. and Christini, D.J. (2003) Antispiral waves in reaction-diffusion systems. *Phys. Rev. Lett.*, **90**, 088302.
- [62] Wang, H.L. and Ou-Yang, Q. (2004) Transition to antispirals in the complex Ginzburg-Landau equation. *Chin. Phys. Lett.*, **21**, 1437-1440.
- [63] Nicola, E.M., Bruschi, L., and Bär, M. (2004) Antispiral waves as sources in oscillatory reaction-diffusion media. *J. Phys. Chem. B*, **108**, 14733-14740.
- [64] Stich, M. (2003) *Target patterns and pacemakers in reaction-diffusion systems*. Dissertation, Technische Universität Berlin.
- [65] Wang, C., Zhang, C., and Ouyang, Q. (2006) Propagation of wave modes and antispiral waves in a reaction-diffusion system. *Phys. Rev. E*, **74**, 036208.
- [66] Danø, S. (1999) *Glycolytic oscillations in yeast yeasts. The nonlinear dynamics of metabolism studied in living cells*. Dissertation, University of Copenhagen.
- [67] Duysens, L.N. and Amesz, J. (1957) Fluorescence spectrophotometry of reduced phosphopyridine nucleotide in intact cells in the near-ultraviolet and visible region. *Biochim. Biophys. Acta*, **24**, 19-26.
- [68] Poulsen, A.K., Petersen, M.Ø., and Olsen, L.F. (2007) Single cell studies and simulation of cell-cell interactions using oscillating glycolysis in yeast cells. *Biophys. Chem.*, **125**, 275-280.
- [69] Frenkel, R. (1966) Reduced diphosphopyridine nucleotide oscillations in cell-free extracts from beef heart. *Arch. Biochem. Biophys.*, **115**, 112-121.
- [70] Tornheim, K. and Lowenstein, J.M. (1973) The purine nucleotide cycle. 3. Oscillations in metabolite concentrations during the operation of the cycle in muscle extracts. *J. Biol. Chem.*, **248**, 2670-2677.
- [71] O'Rourke, B., Ramza, B.M., Romashko, D.N., and Marban, E. (1995) Metabolic oscillations in heart cells. *Adv. Exp. Med. Biol.*, **382**, 165-174.



- [72] Ibsen, K.H. and Schiller, K.W. (1967) Oscillations of nucleotides and glycolytic intermediates in aerobic suspensions of Ehrlich ascites tumor cells. *Biochim. Biophys. Acta*, **131**, 405-407.
- [73] Hess, B. and Boiteux, A. (1968) Control of glycolysis. In *Regulatory Functions of Biological Membranes* (Jarnefelt, J., ed), pp. 148-162. Elsevier, Amsterdam.
- [74] Pye, K. and Chance, B. (1966) Sustained sinusoidal oscillations of reduced pyridine nucleotide in a cell-free extract of *Saccharomyces carlsbergensis*. *Proc. Natl. Acad. Sci. USA*, **55**, 888-894.
- [75] Hess, B., Boiteux, A., and Krüger, J. (1969) Cooperation of glycolytic enzymes. *Adv. Enzyme Regul.*, **7**, 149-167.
- [76] Das, J. and Busse, H.G. (1985) Long term oscillation in glycolysis. *J. Biochem.*, **97**, 719-727.
- [77] Mair, T., Warnke, C., Tsuji, K., and Müller, S.C. (2005) Control of glycolytic oscillations by temperature. *Biophys. J.*, **88**, 639-646.
- [78] Warnke, C. (2003) *Externe Kontrolle räumlich-zeitlicher Muster des Energiestoffwechsels von Bierhefe mittels Temperaturegradienten*. Diploma thesis, Otto-von-Guericke Universität Magdeburg.
- [79] Goldbeter, A. and Lefever, R. (1972) Dissipative structures for an allosteric model. Application to glycolytic oscillations. *Biophys. J.*, **12**, 1302-1315.
- [80] Atkinson, D.E. (1977) *Cellular Energy Metabolism and its Regulation*. Academic Press, New York.
- [81] Koshland, D.E.Jr., Nemethy, G., and Filmer, D. (1966) Comparison of experimental binding data and theoretical models in proteins containing subunits. *Biochemistry*, **5**, 365-385.
- [82] Monod, J., Wyman, J., and Changeux, J.P. (1965) On the nature of allosteric transitions: a plausible model. *J. Mol. Biol.*, **12**, 88-118.
- [83] Hervé, G. (1989) *Allosteric enzymes*. CRC Press, Boca Raton, Florida.
- [84] Gilbert, H.F. (2000) *Basic concepts in Biochemistry: A student's survival guide*, 2nd edn., McGraw-Hill.
- [85] Higgins, J. (1964) A chemical mechanism for oscillation of glycolytic intermediates in yeast cells. *Proc. Natl. Acad. Sci. USA*, **51**, 989-994.
- [86] Sel'kov, E.E. (1968) Self-oscillations in glycolysis. 1. A simple kinetic model. *Eur. J. Biochem.*, **4**, 79-86.

- [87] Termonia, Y. and Ross, J. (1981) Oscillations and control features in glycolysis: numerical analysis of a comprehensive model. *Proc. Natl. Acad. Sci. USA*, **78**, 2952-2956.
- [88] Goldbeter, A. and Dupont, G. (1990) Allosteric regulation, cooperativity, and biochemical oscillations. *Biophys. Chem.*, **37**, 341-353.
- [89] Goldbeter, A. (1973) Patterns of spatiotemporal organization in an allosteric enzyme model. *Proc. Natl. Acad. Sci. USA*, **70**, 3255-3259.
- [90] Hess, B. and Boiteux, A. (1968) Mechanism of glycolytic oscillation in yeast. I. Aerobic and anaerobic growth conditions for obtaining glycolytic oscillation. *Hoppe Seyler. Z. Physiol. Chem.*, **349**, 1567-1574.
- [91] [http://www.columbia.edu/cu/biology/courses/c2005/lectures/lec1\\_07.html](http://www.columbia.edu/cu/biology/courses/c2005/lectures/lec1_07.html).
- [92] Warburg, O. and Christian, W. (1942) Isolation and crystallization of enolase. *Biochem. Z.*, **310**, 384-421.
- [93] Lowry, O.H., Rosebrough, N.J., Farr, A.L., and Randall, R.J. (1951) Protein measurement with the Folin phenol reagent. *J. Biol. Chem.*, **193**, 265-275.
- [94] Bergmeyer, H.U. (1974) *Methods of Enzymatic Analysis*. Vol. III, Verlag Chemie Weinheim/Academic Press, New York.
- [95] Jolliffe, I.T. (2002) *Principal Component Analysis*, 2nd edn., Springer, New York.
- [96] Suchorski, Y., Beben, J., and Imbihl, R. (2000) Spatiotemporal dynamics of fluctuations in a surface reaction by Karhunen-Loève decomposition of field emission images. *Surf. Sci.*, **454**, 331-336.
- [97] Meixner, M., Zoldi, S.M., Bose, S., and Schöll, E. (2000) Karhunen-Loève local characterization of spatiotemporal chaos in a reaction-diffusion system. *Phys. Rev. E*, **61**, 1382-1385.
- [98] Schröter, M. (2003) *Die Fingermorphologie in der Elektrodeposition, ein komplexes Grenzflächenphänomen*. Dissertation, Otto-von-Guericke Universität Magdeburg.
- [99] Naknaimueang S. (2006) *Control of spiral wave dynamics by feedback mechanism via triangular sensory domain*. Dissertation, Otto-von-Guericke Universität Magdeburg.
- [100] Shinjyo, T., Nakagawa, Y., and Ueda, T. (1995) Hierarchical Spatiotemporal Dynamics in Glycolysis. *Physica D*, **84**, 212-219.
- [101] Aranson, I.S. and Kramer, L. (2002) The world of the complex Ginzburg-Landau equation. *Rev. Mod. Phys.*, **74**, 99-143.

- [102] Battogtokh, D. (2002) Front instabilities in a forced oscillatory medium with global coupling. *Phys. Rev. E*, **66**, 066202.
- [103] Battogtokh, D. and Tyson, J.J. (2004) Turbulence near cyclic fold bifurcations in birhythmic media. *Phys. Rev. E*, **70**, 026212.
- [104] Zhan, M. and Kapral, R. (2006) Destruction of spiral waves in chaotic media. *Phys. Rev. E*, **73**, 026224.
- [105] Hofmann, E., Eschrich, K., and Schellenberger, W. (1985) Temporal organization of the phosphofructokinase/fructose-1,6-biphosphatase cycle. *Adv. Enzyme Regul.*, **23**, 331-362.
- [106] Koebmann, B.J., Westerhoff, H.V., Snoep, J.L., Nilsson, D., and Jensen, P.R. (2002) The glycolytic flux in *Escherichia coli* is controlled by the demand for ATP. *J. Bacteriol.*, **184**, 3909-3916.
- [107] Kroukamp, O., Rohwer, J.M., Hofmeyr, J.H., and Snoep, J.L. (2002) Experimental supply-demand analysis of anaerobic yeast energy metabolism. *Mol. Biol. Rep.*, **29**, 203-209.
- [108] Thomas, S. and Fell, D.A. (1998) A control analysis exploration of the role of ATP utilisation in glycolytic-flux control and glycolytic-metabolite-concentration regulation. *Eur. J. Biochem.*, **258**, 956-967.
- [109] Larsson, C., Pahlman, I.L., and Gustafsson, L. (2000) The importance of ATP as a regulator of glycolytic flux in *Saccharomyces cerevisiae*. *Yeast*, **16**, 797-809.
- [110] Eschrich, K., Schellenberger, W., and Hofmann, E. (1982) Transitions between alternate ATP-producing and ATP-consuming stationary states in a reconstituted enzyme system containing phosphofructokinase. *Acta Biol. Med. Ger.*, **41**, 415-424.
- [111] Aon, M.A., Cortassa, S., Westerhoff, H.V., Berden, J.A., Van Spronsen, E., and van Dam, K. (1991) Dynamic regulation of yeast glycolytic oscillations by mitochondrial functions. *J. Cell Sci.*, **99**, 325-334.
- [112] Reijenga, K.A., Snoep, J.L., Diderich, J.A., van Verseveld, H.W., Westerhoff, H.V., and Teusink, B. (2001) Control of glycolytic dynamics by hexose transport in *Saccharomyces cerevisiae*. *Biophys. J.*, **80**, 626-634.
- [113] Teusink, B., Bakker, B.M., and Westerhoff, H.V. (1996) Control of frequency and amplitudes is shared by all enzymes in three models for yeast glycolytic oscillations. *Biochim. Biophys. Acta*, **1275**, 204-212.
- [114] Teusink, B., Passarge, J., Reijenga, C.A., Esgalhado, E., van der Weijden, C.C., Schepper, M., Walsh, M.C., Bakker, B.M., van Dam, K., Westerhoff, H.V., and Snoep, J.L. (2000) Can yeast glycolysis be understood in terms of in

- vitro kinetics of the constituent enzymes? Testing biochemistry. *Eur. J. Biochem.*, **267**, 5313-5329.
- [115] Berleth, T., Burri, M., Thoma, G., Bopp, D., Richstein, S., Frigerio, G., Noll, M., and Nusslein-Volhard, C. (1988) The role of localization of bicoid RNA in organizing the anterior pattern of the *Drosophila embryo*. *EMBO J.*, **7**, 1749-1756.
- [116] Singer, R.H. (1992) The cytoskeleton and mRNA localization. *Curr. Biol.*, **4**, 15-19.
- [117] St Johnston, D., Driever, W., Berleth, T., Richstein, S., and Nusslein-Volhard, C. (1989) Multiple steps in the localization of bicoid RNA to the anterior pole of the *Drosophila oocyte*. *Development*, **107**, 13-19.
- [118] Wang, S. and Hazelrigg, T. (1994) Implications for bcd mRNA localization from spatial distribution of exu protein in *Drosophila oogenesis*. *Nature*, **369**, 400-403.
- [119] Wilhelm, J.E. and Vale, R.D. (1993) RNA on the move: the mRNA localization pathway. *J. Cell Biol.*, **123**, 269-274.
- [120] Lavrova, A.I. (2008) Humboldt University, Group of Theoretical Biophysics. *Personal communication*.
- [121] Mair, T., Zimanyi, L., Khoroshyy, P., Müller, A., and Müller, S.C. (2006) Analysis of the oscillatory kinetics of glycolytic intermediates in a yeast extract by FT-IR spectroscopy. *Biosystems*, **83**, 188-194.
- [122] Vanag, V.K. and Epstein, I.R. (2002) Comparative analysis of packet and trigger waves originating from a finite wavelength instability. *J. Phys. Chem. A*, **106**, 11394-11399.
- [123] Vanag, V.K. and Epstein, I.R. (2003) Dash waves in a reaction-diffusion system. *Phys. Rev. Lett.*, **90**, 098301.
- [124] Vanag, V.K. and Epstein, I.R. (2003) Segmented spiral waves in a reaction-diffusion system. *PNAS*, **100**, 14635-14638.
- [125] Horvath, D., Petrov, V., Scott, S.K., and Showalter, K. (1993) Instabilities in propagating reaction-diffusion fronts. *J. Chem. Phys.*, **98**, 6332-6343.
- [126] Zykov, V.S., Mikhailov, A.S., and Müller, S.C. (1998) Wave instabilities in excitable media with fast inhibitor diffusion. *Phys. Rev. Lett.*, **81**, 2811-2814.
- [127] Mihaliuk, E., Sakurai, T., Chirila, F., and Showalter, K. (2001) Experimental and theoretical studies of feedback stabilization of propagating wave segments. *Faraday Discuss.*, **120**, 383-394.

- 
- [128] Rotermund, H.H., Jakubith, S., von Oertzen, A., and Ertl, G. (1991) Solitons in a surface reaction. *Phys. Rev. Lett.*, **66**, 3083-3086.
- [129] Vanag, V.K. and Epstein, I.R. (2007) Localized patterns in reaction-diffusion systems. *Chaos*, **17**, 037110.
- [130] Epstein, I.R. and Pojman, J.A. (1998) *An Introduction to Nonlinear Chemical Dynamics: Oscillations, Waves, Patterns, and Chaos*. Oxford University Press, New York.
- [131] Strier, D.E. and Ponce, D.S. (2007) Turing patterns inside cells. *PLoS. ONE.*, **2**, e1053.

## Acknowledgement

I would like to thank Prof. S. C. Müller for giving me this great opportunity to perform my PhD study in the Biophysics Group, Otto-von-Guericke University of Magdeburg.

Further, I wish to express my sincere gratitude and appreciation to my supervisor Dr. Thomas Mair for his excellent guidance and supervision throughout this work. He was always available and willing to answer all questions concerning this work.

I am also very grateful to Prof. Marcus J. B. Hauser for his support, helpful discussions, and valuable criticism during my study.

I would like to express my special gratitude to Prof. Helmut Weiß for giving me the possibility to defend my PhD thesis in his department.

My special thanks go to Dr. Ronny Straube for his great suggestions and excellent cooperation.

I would like to thank Prof. Y. Suchorski for his fruitful discussions and suggestions regarding the Karhunen-Loève decomposition.

I am also very thankful to Dr. Wolfgang Jantsoß for his kind advice and help in solving the computer problems; Christian Warnke for a lot of interesting and helpful discussions; Uli Storb, Chaiya Luengviriya, and Frank Rietz for valuable software support and help with computer programming.

To all members and former members of the Biophysics Group I offer my great appreciation for their support, guidance, help, advice, smiles and pleasant atmosphere throughout my PhD study. Special thanks to my good colleagues and friends: Dr. Lenka Šebestíková, Katja Guttmann, Uta Lehmann, Jiraporn Luengviriya, Kristin Wegner, and Dr. Lama Naji.

Many thanks to Ramona Bengsch, Dorothea Erndt, Erika Matthies, Petra Hünerbein, Gregor Nuglisch, and Jürgen Weissenborn for their helpful assistance.

I am greatly thankful to Frau Böhning and the International Office for the excellent help and the financial support during the last years of my study.

Furthermore, I would like to thank Prof. Quistoff (Department of Medical Biochemistry and Genetics, University of Copenhagen, Denmark) for giving me the possibility to perform a scientific project for 3 months in his lab.

I will never forget the warm-heart support from Dr. Thomas Mair, Christian, Ariane, Lutz, and Annegret, who took care of me when I came to Magdeburg.

My heartfelt gratitude goes to my former supervisors and “second parents” Prof. Anahit Tonoyan and Prof. Sevan Davtyan (Department of Chemical Technologies and Environmental Engineering, State Engineering University of Armenia), who

encouraged and supported me to do my PhD in Germany. Their love and care accompanied me throughout my study. Without them I would never have become a scientist!

I am deeply thankful to my boyfriend Benjamin for his love, understanding, great help, and support throughout all these years. Finally, I would like to thank my parents and my brother for giving me power and moral support. My special gratitude goes to my lovely mother for her patience, love, and care, without I would never have been able to finish this work: “Շնորհակալություն իմ սիրելի Մայրիկ”.

## Curriculum Vitae

**Name** Satenik Bagyan  
**Address** Gartenstraße 7, 39114 Magdeburg, Germany  
**Date of birth** 26 February 1979  
**Marital status** Not married  
**Nationality** Armenian

**School** 1985-1995  
Isakov's school number 132, Yerevan, Armenia  
Final degree: **High School**

**Study** 1995-1999  
**Chemical Technology** at the Department of Chemical Technology of Synthetic Medicine, State Engineering University of Armenia, Yerevan, Armenia  
Thesis "Synthesis of Fubromeganum"  
Final degree: **Bachelor of Science (B.Sc.)**

1999-2001  
**Chemical Technology** at the Department of Technology of Organic Synthesis, State Engineering University of Armenia, Yerevan, Armenia  
Thesis "Autowave polymerization of metalcomplex monomers and observation of their properties"  
Final degree: **Master of Science (M.Sc.)**

Since December 2001  
**PhD** at the Institute of Experimental Physics, Biophysics Group, Otto-von-Guericke University, Magdeburg, Germany  
Thesis "Spatio-temporal dynamics of glycolysis in an open spatial reactor"



April 2005-June 2005

Within the scope of the study, research stay at the  
Department of Medical Biochemistry and Genetics,  
Panum Institute, University of Copenhagen, Denmark

Magdeburg, June 27, 2008

---

Satenik Bagyan